Dissertation zur Erlangung des Doktorgrades

der Fakultät für Chemie und Pharmazie

der Ludwig-Maximilians-Universität München

Targeting endolysosomal cation channels to modulate cancer cell death

Franz Florian Sebastian Geißlinger

aus Bamberg, Deutschland

2023

Erklärung

Diese Dissertation wurde im Sinne von §7 der Promotionsordnung vom 28. November 2011 von Frau Prof. Dr. Angelika M. Vollmar betreut.

Eidesstattliche Versicherung

Diese Dissertation wurde eigenständig und ohne unerlaubte Hilfe erarbeitet.

München, den 06.02.2023 _____
(Franz Geißlinger)

Dissertation eingereicht am: 09.02.2023

1. Gutachterin: Prof. Dr. Angelika M. Vollmar

2. Gutachter: Prof. Dr. Stefan Zahler

Mündliche Prüfung am: 21.03.2023

Meinen Eltern

Table of contents

1 Abstract

In the last decade, manipulating lysosomal function emerged as a promising anticancer strategy. Prominently, endolysosomal cation channels, for instance the sodium- and calcium-selective two-pore channel 2 (TPC2) and the broad-range cation-specific transient receptor potential mucolipin 1 (TRPML1), have been connected to several cancer hallmarks and are investigated as potential anticancer targets. Yet, their role in chemoresistance and cell death signaling remains unidentified despite the crucial implication of the endolysosomal system and especially of lysosomes in both processes.

Given the important role of lysosomes in chemoresistance and cancer cell death, we hypothesized that the endolysosomal cation channel TPC2 might be a promising therapeutic target for chemosensitization of cancer cells. This project focuses on leukemic cells, which are prone to develop chemoresistance. Interestingly, we found that interfering with TPC2 function either by genetic knockout (ko) or pharmacological inhibition sensitized chemo-resistant as well as drug-naïve cell lines and patient-derived xenograft acute lymphoblastic leukemia cells to treatment with cytostatics. This chemosensitizing effect by loss-of-TPC2-function was mediated by a dual mechanism of action. On the one hand, TPC2 ko impaired sequestration of weak base cytostatics inside the lysosomes owing to increased lysosomal pH, resulting in increased drug concentrations at the site of action. Concurrently, TPC2 ko favored lysosomal damage, initiating lysosomal cell death (LCD) signaling, a special form of cell death which was capable of circumventing resistance to mitochondrial apoptosis (Fig. 1A).

To shed more light on the implications of lysosomal cation channels in cancer cell death, we furthermore focused on the role of TPC2 and TRPML1 in ferroptosis, as this novel form of cell death depending on iron accumulation and lipid peroxidation, is intriguingly influenced by lysosomal function. Recent reports underline that ferroptosis bears promising potential for novel treatment strategies. Interestingly, we found that TPC2 ko and TRPML1 ko differentially affected ferroptosis sensitivity in hepatocellular carcinoma (HCC), a cancer type often lacking sufficient response to current treatment regimens. Loss-of-TPC2-function led to ferroptosis resistance mediated by depletion of labile ferrous iron and of phospholipids carrying polyunsaturated fatty acids. In contrast, TRPML1 ko sensitized HCC cells to ferroptosis owing to increased oxidative and latent endoplasmic reticulum stress (Fig. 1B).

Taken together, this thesis highlights TPC2 as a promising and druggable target that can be exploited in combination therapy regimens to improve chemotherapy response in leukemia and concurrently provides valuable mechanistic insights into lysosomal cell death signaling in chemo-resistant cancer cells. Furthermore, this study identifies TPC2 and TRPML1 as novel, differential modulators of ferroptosis sensitivity, emphasizing hitherto unknown implications of

these endolysosomal cation channels in ferroptosis. Hence, these findings provide a basis for new therapeutic approaches for HCC.

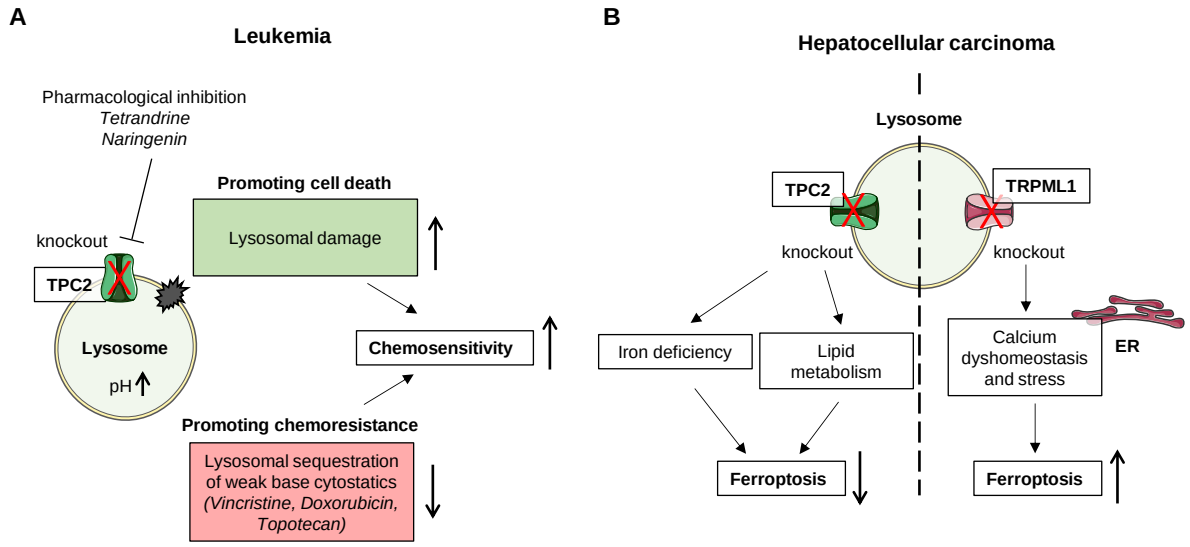

Figure 1. Graphical abstract – major findings.
A Interfering with TPC2 function sensitizes leukemic cells to chemotherapy by a dual mechanism of action. Importantly, TPC2 ko causes impaired lysosomal drug sequestration and promoted lysosomal cell death signaling owing to increased susceptibility to lysosomal damage, increasing sensitivity to chemotherapeutics. **B** TPC2 and TRPML1 differentially regulate ferroptosis sensitivity. Loss-of-TPC2-function renders hepatocellular carcinoma cells resistant to ferroptosis mediated by intracellular iron deficiency and alterations in lipid metabolism, whereas TRPML1 ko has a ferroptosis-sensitizing effect as a result of endoplasmic reticulum stress.

2 Introduction

2.1 Chemoresistance – a challenge in cancer therapy

Cancer is still one of the leading causes of death worldwide with increasing incidence. In 2020, there were approximately 20 million new cancer diagnoses. Even though the survival rates of cancer patients improved over the past decades due to improved diagnostic and therapy strategies, there were still approximately 10 million cancer-related fatalities worldwide in 2020 [1]. Besides novel targeted therapy strategies, such as pharmacological inhibition of cancer-specific kinases, immunotherapy, or CAR-T-cell therapy, classic cytostatics are still important components of many therapy regimens. Unfortunately, drug resistance against these chemotherapeutic agents frequently occurs [2]. This is exceptionally true for acute lymphoblastic leukemia (ALL) which is commonly treated with a combination of chemotherapeutics, including vincristine, doxorubicin, or cytarabine for example together with corticosteroids [3, 4]. While initially, 80-90 % of patients show remission of the disease under these treatment strategies, about 50% suffer from a later relapse [5]. If the leukemia is refractory or relapses, the response to renewed chemotherapy is poor [6]. Consequently, the underlying mechanisms of chemoresistance have been studied with extensive effort in the past and many possible mechanisms contributing to chemoresistance have been identified. These are mainly connected to decreased drug uptake, increased drug efflux, and mutation of drug targets [7]. Unfortunately, the vast majority of approaches targeting these mechanisms have not turned out to be successful in the past. A prominent example is the drug efflux pump P-glycoprotein (P-gp). By actively transporting xenobiotics, including cytostatics, out of the cell, high P-gp expression causes low intracellular drug concentrations. Despite the development of many different inhibitors, P-gp inhibition could not be proven to be beneficial in the clinical setting [8, 9]. This example illustrates that development of chemoresistance still lacks appropriate treatment strategies and is therefore strongly associated with poor patient outcomes [6, 10], emphasizing that novel targets are required to overcome chemoresistance and thus improve chemotherapy response.

2.2 The endolysosomal system and its cation channels are promising anti-cancer targets

One organelle which has come into the focus of cancer research and might provide a promising target to overcome chemoresistance, is the endolysosomal system. The endolysosomal system consists of early, late, and recycling endosomes as well as lysosomes. They are distinguished by their intraluminal composition, pH value, and expression of surface and

transmembrane proteins, e.g. ion channels [11, 12]. Lysosomes contain various degrading enzymes, such as proteases and lipases, and are characterized by an acidic lumen. Lysosomes are indispensable for the degradation of several types of macromolecules, such as proteins and lipids [13]. Accordingly, the endolysosomal system, first identified in 1955 [14], has mainly been considered as “trash can” of cells due to its high implication in macromolecule digestion. In the past decades, the endolysosomal system became known as an interesting signaling hub, being involved in nutrient homeostasis [15, 16], autophagy [17], or the regulation of cell death [18, 19]. It is furthermore associated with many physiological and pathophysiological processes, such as cellular homeostasis [20], lipid metabolism [21], and immune defense [22] as well as lysosomal storage diseases [23], neurodegenerative disorders [23], and tumor growth and metastasis [24].

2.2.1 Lysosome-driven mechanisms in chemoresistance

Owing to the constant unraveling of additional functions of lysosomes within the cell, it has become evident now, that their function and characteristics can enormously influence response to chemotherapy [25]. There are two major, recently identified mechanisms connected to chemoresistance, including lysosomal drug sequestration, and lysosomal cell death (LCD).

The characteristic acidity of lysosomes facilitates the intraluminal accumulation of weak base drugs, occurring by passive diffusion as a result of the cytosolic-lysosomal pH gradient [25]. Additionally, it has been repeatedly reported that cytostatics are actively transported from the cytosol into lysosomes via the drug efflux transporter P-gp which is thought to be localized within lysosomal membranes in chemo-resistant cells [26-28]. Regardless of the mode of entering, weak base cytostatics are protonated in the lysosomal lumen due to the acidic lysosomal pH. As a result of their positive charge, these molecules are now poorly membrane permeable and thus unable to diffuse back into the cytosol, leading to lysosomal trapping [29]. By this mechanism, lysosomes might prevent the accumulation of cytostatics at their sites of action, which are commonly located in the cytosol or nucleus, promoting chemoresistance (Fig. 2A). The capability of lysosomal sequestration greatly depends on the physicochemical features of the compounds on the one hand, and on lysosomal properties, including lysosomal pH and volume on the other hand [29, 30]. Therefore, interfering with lysosomal function might be an appropriate opportunity to overcome chemoresistance.

Secondly, it is by now well-known that lysosomes are the main driver of a regulated cell death pathway, called lysosomal cell death (LCD). LCD is initiated by defects in the lysosomal membrane which cause lysosomal contents, e.g. proteolytic enzymes, to leak into the cytosol

[18]. The abundance of lysosomal cathepsins, the main family of lysosomal proteolytic enzymes, in the cytosol leads to activating cleavage of pro-apoptotic signaling proteins, such as Bid or caspase-8 and eventually caspase-3/7, and to degradation of anti-apoptotic signaling proteins, such as Bcl-2 and Mcl-1 [31]. Therefore, lysosomal damage is deeply associated with the intrinsic apoptosis pathway, creating a pro-apoptotic milieu. Besides, cathepsin release through damaged lysosomes can directly lead to cell death by degradation of proteins essential for cellular survival (Fig. 2B) [32]. Importantly, LCD is thought to preferentially target cancer cells since they are more susceptible to lysosomal damage as a result of reduced acid sphingomyelinase activity upon oncogenic transformation [33]. Hence, triggering LCD might be a suitable strategy for cancer therapy, employing lysosomal damage inducers either as monotherapy or in combination with already approved cytostatics.

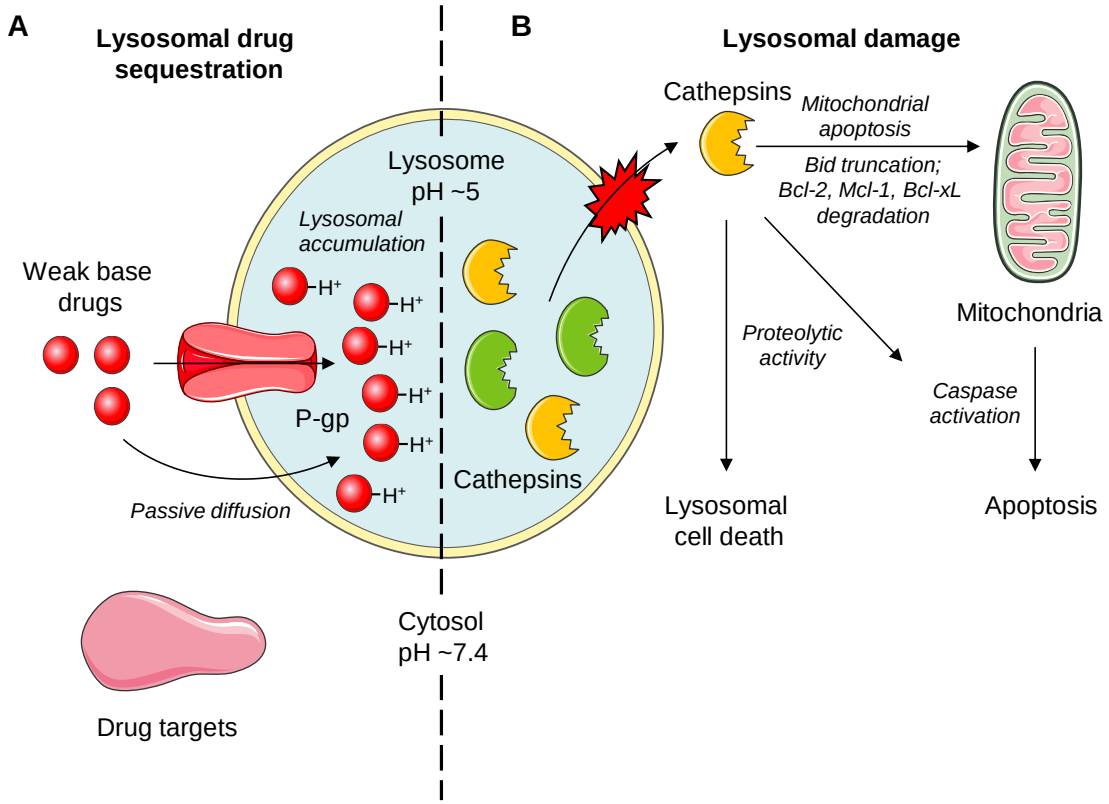

Figure 2. The role of lysosomes in chemoresistance.
A Lysosomes sequester weak base cytostatics due to their protonation inside the lysosomal lumen. This process might either occur by passive diffusion or by active transport via lysosome-abundant P-glycoprotein (P-gp). Thereby, lysosomes hinder weak base drugs from reaching their intracellular targets. **B** Lysosomal damage causes release of intraluminal components, such as cathepsins into the cytosol. Cathepsins promote pro-apoptotic signaling pathways, for example by activating Bid or degrading Bcl-2 family proteins. Besides, abundance of cathepsins in the cytosol leads to activation of initiator or effector caspases or directly causes so-called lysosomal cell death (LCD) due to their proteolytic activity. Schemes were created using building blocks of cellular structures from Servier Medical Art (smart.servier.com, Servier, Suresnes, France).

2.2.2 Lysosomal cation channels

Lysosomes harbor a broad variety of surface and transmembrane proteins, such as ion channels of different subgroups. As they are deeply connected to lysosomal function and signaling, lysosomal surface proteins provide a reasonable strategy to make lysosomes druggable [34]. Hence, many of those are in the focus of current cell biological and pharmacological research. Nowadays, endolysosomal ion channels gained huge interest, especially the endolysosomal cation channels from the two-pore channel (TPC) and transient receptor potential mucolipin (TRPML) subfamily [12, 35].

2.2.2.1 Two-Pore channel 2 (TPC2)

TPCs are a group of cation channels localized to membranes within the endolysosomal system. Activation of two-pore channels leads to the release of sodium and calcium ions from the lysosomal store into the cytosol. TPCs are subdivided into two isoforms, namely TPC1 which is mainly abundant at endosomal membranes, and TPC2 which can be found in late endosomes and lysosomes [12, 36].

Despite their diverse roles in disease, especially that of TPC2, the structure of mammalian TPCs was unknown for a long time. Recently, She et al. elucidated the structure of human TPC2 by cryo-electron microscopy [37]. Similar to TPC1 [38], they identified TPC2 as a dimer of two homologous domains which consist of six transmembrane domains, 6-TM I and 6-TM II. Pore opening is facilitated by structural changes in the inner helix IS6 at the ion conduction pore. This conformational change is a result of the binding of the endolysosome-specific signaling lipid phosphatidylinositol 3,5-bisphosphate [$PI(3,5)P_2$] to arginine residues at 6-TM I [37]. In contrast to TPC1 whose activation is voltage-dependent, TPC2 can be activated by the sole binding of its activators [39].

Pore opening of TPC2 upon $PI(3,5)P_2$ activation predominantly leads to the release of sodium into the cytosol [40]. Besides, TPC2 is also activated by the calcium release-inducing second messenger nicotinic acid adenine dinucleotide phosphate (NAADP) at a different binding site, causing calcium permeability of TPC2 [41]. These different activation modes led to a controversial debate about the ion selectivity of TPC2. However, it is meanwhile accepted that TPC2 is permeable for sodium and calcium ions in dependence on its activation mode [39, 42, 43]. On the other hand, both, sodium and calcium TPC2 currents, are endogenously inhibited by ATP in an mTORC1-dependent manner [44]. Due to the high interest in the cellular function of TPC2, extensive efforts were put into the development of novel, drug-like TPC2 inhibitors.

As a result, promising natural product-derived inhibitors from different scaffolds which block activation of TPC2 are now available [45, 46].

These pharmacological, as well as genetic tools revealed an important role of TPC2 in many physiological and pathophysiological processes, such as autophagy [47], phagocytosis [48], viral infection [49, 50], fatty liver disease [51], and neurodegenerative diseases [52, 53]. Interestingly, TPC2 was further found to play an important role in cancer and is suggested to be a novel oncogene that sustains cancer-promoting hallmarks [54-56]. High TPC2 expression, for example, correlates with a poor survival probability of prostate cancer patients [57]. Hence, TPC2 emerged as a promising anti-cancer target in several different pre-clinical cancer models, including hepatocellular carcinoma (HCC), melanoma, or urinary bladder cancer. Loss-of-TPC2-function leads to reduced cancer cell proliferation *in vitro* and inhibits tumor growth *in vivo* by shifting energy metabolism from glycolysis to oxidative phosphorylation in HCC [45]. Furthermore, knockout (ko) or knockdown of TPC2 hampers cancer cell migration and formation of metastases, mediated by impaired β1-integrin trafficking to the cell membrane [58]. Concurrently, there is evidence that TPC2 is in general an important regulator of intracellular trafficking, for example of EGF/EGFR trafficking in a murine non-cancerous liver mouse model [51]. Similar functional effects of TPC2 ko or pharmacological inhibition were found in melanoma, including reduced proliferation, migration and invasion, mechanistically attributed to increased melanin production and increased MITF degradation upon loss-of-TPC2-function [46].

Although many cancer hallmarks regulated by TPC2 were identified in the past, there are no data available dealing with the involvement of TPC2 in chemoresistance and modulation of cell death. Given the critical involvement of lysosomes in these processes, the role of TPC2 in chemoresistance and cancer cell death was investigated as part of this thesis.

2.2.2.2 Transient receptor potential mucolipin 1 (TRPML1)

TRPML cation channels include three different subtypes – TRPML1, TRPML2, and TRPML3. TRPML2 and TRPML3 are predominantly expressed in specialized cells and are for example important for proper function of macrophages [59] or lung health [60]. In contrast, TRPML1 is ubiquitously expressed in late endosomes and lysosomes [61]. It consists of four subunits with each subunit containing 6 transmembrane domains [62, 63]. Similar to TPC2, TRPML1 is activated by binding of $PI(3,5)P_2$ to TRPML1 at the S5 and S6 domains, leading to conformational changes and pore opening [63]. Besides $PI(3,5P)_2$, reactive oxygen species have also been reported to activate the channel [64]. Pore opening enables conduction of different cations, including calcium, sodium, ferrous iron, zinc, magnesium and potassium ions

[61]. Therefore, TRPML1 is a cation channel with comparably low ion selectivity, regulating for example calcium [65, 66] and iron homeostasis [67, 68]. In a physiological context, TRPML1 promotes autophagy and is an important activating regulator of the transcription factor EB (TFEB), the master regulator of lysosomal biogenesis. TRPML1-mediated calcium release from lysosomes activates calcineurin which subsequently dephosphorylates TFEB, facilitating its nuclear translocation [69]. In the past years, loss-of-function mutations in the TRPML1 gene were identified as the cause of the inherited lysosomal storage disease mucolipidosis type IV [70] which causes neurodevelopmental disorders [71]. Furthermore, it was recently discovered that downregulation of TRPML1 results in motor neuron cell death, whereas TRPML1 expression facilitates survival in an ALS mouse model [72].

Interestingly, TRPML1 plays an ambiguous role in cancer progression. Similar to TPC2, functional effects upon TRPML1 knockout, silencing, or pharmacological inhibition include impaired cancer cell proliferation [73, 74] and migration [75]. In this context, Jung et al. found that especially HRAS-driven cancer cells are susceptible to TRPML1 inhibition [76]. Furthermore, high TRPML1 expression correlates with poor survival in glioblastoma [77] and pancreatic cancer [78]. A recent study from our lab suggests that loss-of-TRPML1-function exerts its anti-cancer activity by impairing mitochondrial renewal and thereby hampering mitochondrial function [74]. In addition, TRPML1 is important for autophagic clearance of damaged mitochondria as result of oxidative stress [64]. Besides, TRPML1 knockout causes alterations in protein homeostasis, resulting in the aggregation of misfolded proteins [73]. On the other hand, hyperactivation of TRPML1 was found to have anti-cancer effects as well, as shown in glioblastoma [77] and hepatocellular carcinoma [74] using pharmacological activators. This is mediated by calcium overloading of mitochondria which causes depletion of the mitochondrial membrane potential, resulting in induction of apoptosis [74]. These data suggest an important role of TRPML1 in tumor progression, however, the detailed mechanistic implications need further investigation, as it is not clear whether the channel activity predominantly exerts pro- or anti-cancer function. Due to its role in iron homeostasis and oxidative stress, we investigated the influence of TRPML1 on ferroptosis induction as a potential anti-cancer mechanism in this study.

2.3 Ferroptosis as novel anticancer strategy and implication of lysosomes

Ferroptosis is a form of regulated cell death that is distinct from other types of cell death, such as apoptosis. In the past decade, the knowledge about ferroptosis rapidly increased, shedding light on mechanistic backgrounds and clinical implications of this mode of cell death. The main hallmark of ferroptosis is iron-dependent formation and accumulation of phospholipid

peroxides which cause damage to cellular and organellar membranes, resulting in cell death (Fig. 3) [79]. Recently, ferroptotic cell death has been connected to a broad variety of pathomechanisms, for instance in neurodegenerative diseases [80, 81], hemorrhagic brain injury [82] as well as cardiotoxicity upon doxorubicin treatment [83]. Notably, accumulating evidence suggests that ferroptosis is an important anti-tumor mechanism. Hence, inducing ferroptosis in cancer cells emerged as a promising anti-cancer strategy [84], especially for chemo-resistant tumors [84, 85] or cancer entities that mostly lack effective therapy regimens, such as hepatocellular carcinoma [86, 87]. Therefore, current research aims at developing novel, ferroptosis-based treatment strategies.

Although oxidative cell death mechanisms have been known for a long time, ferroptosis was first named in 2012 by Dixon and co-workers based on their observation that its induction is dependent on an excessive accumulation of labile ferrous iron [88]. Iron is in general extremely important for proper cellular function, for example for cellular redox processes, as it can readily accept and donate electrons [89]. On the other hand, this feature makes iron, especially when it is abundant at high levels, potentially toxic to cells, necessitating strict regulation of the cellular labile iron pool. Importantly, ferrous iron promotes the formation of peroxyl radicals from hydrogen peroxide via Fenton chemistry, causing cellular damage and ultimately ferroptotic cell death (Fig. 3) [90].

As cells are regularly challenged by reactive oxygen species (ROS) as a result of cellular metabolism and environmental stress, they contain antioxidant systems that are able to detoxify ROS by utilizing reducing equivalents. Accordingly, these antioxidant systems, most importantly the system xc-/GPX4 axis, protect cells from ferroptotic cell death [79]. System xc- facilitates cellular uptake of cystine, the oxidized form of cysteine, in exchange for glutamate [91]. Cysteine itself is the rate-limiting building block of glutathione, a reducing equivalent many antioxidant systems depend on [92]. GPX4 converts highly reactive phospholipid peroxides which are built upon ferroptosis induction into unharmful lipid alcohols by utilizing glutathione [93]. Therefore, pharmacological inhibitors of system xc- and GPX4 are the most widely used ferroptosis inducers, namely erastin and RSL3, respectively. Inhibition of either component of this antioxidant axis induces lipid peroxidation and subsequently causes cell death (Fig. 3) [79, 88].

Due to their chemical structure, especially polyunsaturated fatty acids (PUFAs) are prone to lipid peroxidation. This lipid peroxidation propagates in a radical chain reaction, leading to a rapid expansion and accumulation of lipid peroxides (Fig. 3) [79]. In contrast, monounsaturated fatty acids (MUFAs) protect cells from ferroptosis, suggesting that the fraction of PUFA- and MUFA-containing phospholipids is a decisive regulator of ferroptosis sensitivity [94, 95]. How

cells exactly die upon ferroptosis induction is still a matter of debate. It is assumed that cell death is caused by oxidative damage of the cell membrane, but also of organellar membranes [79]. It has been proposed, for example, that lipid peroxidation upon ferroptosis induction causes lysosomal damage which eventually segues into LCD [96].

Intriguingly, the aforementioned ferroptosis-associated homeostasis systems, i.e. iron homeostasis, redox balance, and lipid composition, are influenced by lysosomal function [97]. For instance, the endolysosomal system is involved in the regulation of intracellular iron homeostasis, as lysosomal acidity enables the dissociation of transferrin-iron complexes to release free iron [98]. Furthermore, the reduction of ferric iron to ferrous iron takes place in the endolysosomal system [99]. In addition, the degradation of the iron storage protein ferritin by a selective autophagy pathway called ferritinophagy, regulates the availability of labile ferrous iron [100]. Similarly, the regulation of protein levels of GPX4 is controlled by degradation via chaperone-mediated autophagy [101]. Another autophagic process called lipophagy is furthermore involved in the regulation of cellular lipid metabolism (Fig. 3) [102]. Notably, it has been recently shown that lipid composition is also influenced by manipulation of intracellular calcium homeostasis and distribution [103]. As lysosomes and especially their associated ion channels are regulators of calcium homeostasis, the question arises of whether they influence ferroptosis sensitivity. Given the implications of lysosomes in the regulation of ferroptosis and the role of TRPML1 and TPC2 in calcium homeostasis, we investigated whether or not TRPML1 and TPC2 regulate ferroptosis sensitivity and if so, how this can be mechanistically explained.

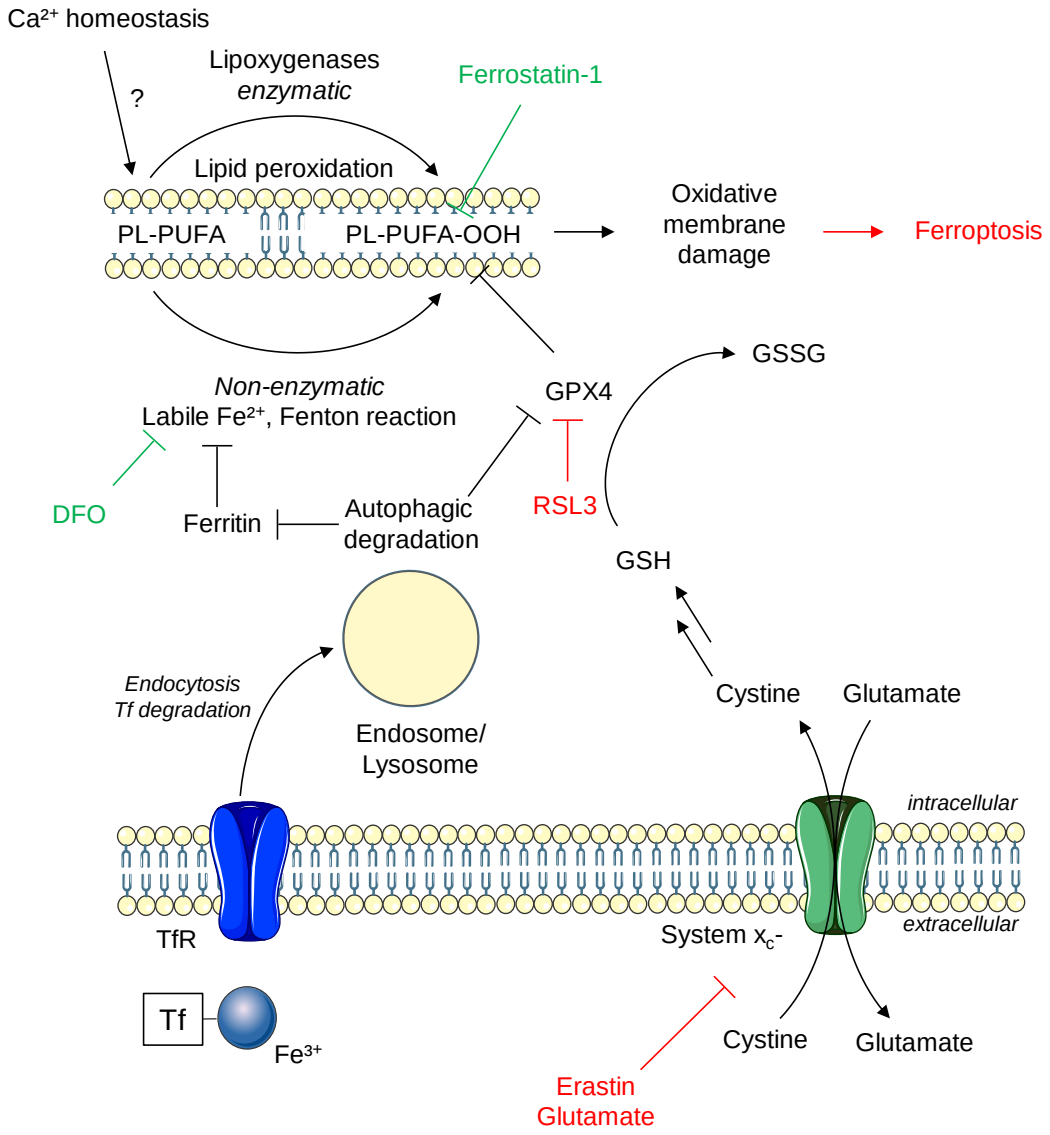

Figure 3. Molecular mechanism of ferroptosis induction.
Ferroptosis is characterized by iron-dependent lipid peroxidation of phospholipid-(PL)-bound polyunsaturated fatty acids (PUFA). Abundance of lipid peroxides causes oxidative membrane damage, resulting in ferroptotic cell death. Under physiological conditions, ferroptosis is prevented by GPX4 which detoxifies highly reactive peroxidized lipids to lipid alcohols by utilizing glutathione. Glutathione is mainly built from cysteine which is taken up into the cell in its oxidized form cystine. The labile iron pool which facilitates ferroptosis induction, is highly regulated, for example by the iron storage protein ferritin. The endolysosomal system plays an important role in these processes, by influencing intracellular ferrous iron levels, GPX4 abundance as well as lipid availability. Schemes were created using building blocks of cellular structures from Servier Medical Art (smart.servier.com, Servier, Suresnes, France).

2.4 Aims of the study

Chemoresistance remains a challenge in cancer therapy, negatively influencing patient outcomes. Interestingly, recent research identified lysosomes as important regulators of chemoresistance. This led us to the hypothesis that manipulation of lysosomal function, i.e. by targeting the endolysosomal cation channel TPC2 which was recently associated with cancer progression, is a suitable approach to increase sensitivity towards chemotherapy which has to be analyzed in this study.

In the second part, we focused on the involvement of the endolysosomal cation channels TPC2 and TPRML1 in ferroptosis, as recent research emphasizes an important role of lysosomes in this process. This part aims at gaining mechanistic insights into ferroptosis-related mechanisms upon knockout of the endolysosomal cation channels and might provide therapeutical approaches for future anti-cancer strategies.

In detail, the objectives of this thesis were as follows:

Part I: The role of TPC2 in chemoresistance

1. Elucidation of TPC2 as a suitable target to re-sensitize chemo-resistant leukemia cells to chemotherapeutic agents in a TPC2 ko model.
2. Verification of chemosensitization by targeting TPC2 using established pharmacological inhibitors.
3. Adaption of this combination approach to other leukemic cell lines, other cancer types, and patient-derived ALL cells with respect to its therapeutic margin.
4. Elucidation of the underlying mechanism of action with regard to the recently identified implications of lysosomes in chemoresistance and cell death.

Part II: The role of TPC2 and TRPML1 in ferroptosis

1. Analysis of susceptibility to ferroptosis upon TPC2 ko or TRPML1 ko.
2. Verification with available TPC2 and TPRML1 inhibitors.
3. Gaining mechanistic insights into the modulation of ferroptosis sensitivity by TPC2 and TRPML1 based on previously known ferroptosis-regulating pathways.

3 Materials and Methods

3.1 Materials

3.1.1 Compounds

Compound	Function/description	Producer
4-phenylbutyric acid	ER stress inhibitor	Sigma-Aldrich, Taufkirchen, Germany
5-fluorouracil	Chemotherapeutic	Sigma-Aldrich, Taufkirchen, Germany
Ammonium chloride	Lysosomotropic agent	Sigma-Aldrich, Taufkirchen, Germany
Brefeldin A	ER stress inducer	Cayman Chemical, Ann Arbor, MI, USA
CA-074Me	Cathepsin B inhibitor	Selleckchem, Houston, TX, USA
Calcimycin (A23187)	Ionophore	Sigma-Aldrich, Taufkirchen, Germany
CCCP	Uncoupler of oxidative phosphorylation	Sigma-Aldrich, Taufkirchen, Germany
CDN1163	SERCA activator	Sigma-Aldrich, Taufkirchen, Germany
Chloroquine	Lysosomotropic agent	Sigma-Aldrich, Taufkirchen, Germany
Deferoxamine	Ferrous iron chelator	Cayman Chemical, Ann Arbor, MI, USA
Doxorubicin	Chemotherapeutic	Sigma-Aldrich, Taufkirchen, Germany
EDME	TRPML1 inhibitor	Bracher Lab, Department Pharmacy, LMU Munich, Germany
Elacridar	P-gp inhibitor	Selleckchem, Houston, TX, USA
Erastin	System x_c- inhibitor	Cayman Chemical, Ann Arbor, MI, USA
Ferrostatin-1	Lipid peroxidation inhibitor	Cayman Chemical, Ann Arbor, MI, USA
Glutamate	System x_c- inhibitor	Sigma-Aldrich, Taufkirchen, Germany
Ketoconazole	P-gp inhibitor	Sigma-Aldrich, Taufkirchen, Germany
LLOMe	Lysosomal damage inducer	Santa Cruz Biotechnology, Dallas, TX, USA
Naringenin	TPC2 inhibitor	Sigma-Aldrich, Taufkirchen, Germany
Paclitaxel	Chemotherapeutic	Sigma-Aldrich, Taufkirchen, Germany
Pepstatin A	Cathepsin D inhibitor	Selleckchem, Houston, TX, USA
RSL3	GPX4 inhibitor	Cayman Chemical, Ann Arbor, MI, USA

Sg094	TPC2 inhibitor	Bracher Lab, Department Pharmacy, LMU Munich
Siramesine	Functional ASM inhibitor	Selleckchem, Houston, TX, USA
Tetrandrine	TPC2 inhibitor	Sigma-Aldrich, Taufkirchen, Germany
Thapsigargin	SERCA inhibitor	Santa Cruz Biotechnology, Dallas, TX, USA
Topotecan	Chemotherapeutic	Sigma-Aldrich, Taufkirchen, Germany
Tunicamycin	ER stress inducer	Cayman Chemical, Ann Arbor, MI, USA
Verapamil	P-gp inhibitor	Sigma-Aldrich, Taufkirchen, Germany
Vincristine	Chemotherapeutic	Adipogen, Füllinsdorf, Switzerland
Z-VAD-FMK	Pan-caspase inhibitor	Selleckchem, Houston, TX, USA

Table 1. Compounds used in this study.

3.1.2 Reagents

Reagent	Producer
Acridine orange	Invitrogen, Waltham, MA, USA
Bodipy™ C11 581/591	Invitrogen, Waltham, MA, USA
Bovine serum albumin (BSA)	Anprotec, Bruckberg, Germany
Bradford reagent Roti® Quant	Carl Roth, Karlsruhe, Germany
Cal-520 AM	Cayman Chemical, Ann Arbor, MI, USA
Calcein-AM	Cayman Chemical, Ann Arbor, MI, USA
Cathepsin B Activity Assay Kit	PromoKine, Heidelberg, Germany
CellTiter-Bue® reagent	Promega, Mannheim, Germany
Collagen G	Biochrom AG, Berlin, Germany
Complete®	Roche Diagnostics, Penzberg, Germany
Dimethyl sulfoxide (DMSO)	Carl Roth, Karlsruhe, Germany
DiOC6(3)	Enzo Life Sciences, Lörrach, Germany
Dithiothreitol (DTT)	AppliChem, Darmstadt, Germany
Dulbecco's Modified Eagle Medium (DMEM)	PAN Biotech, Aidenbach, Germany; Anprotec, Bruckberg, Germany
FerroOrange	Dojindo Laboratories, Kumamoto, Japan
Fetal calf serum (FCS)	PAN Biotech, Aidenbach, Germany; Anprotec, Bruckberg, Germany
FluorSave mounting medium	Merck Millipore, Darmstadt, Germany
Formaldehyde	Polysciences, Eppelheim, Germany
GlutaMAX Supplement	Life Technologies, Eugene, OR, USA

GSH/GSSG Glo Assay	Promega, Mannheim, Germany
GSH/GSSG-Glo™ Assay Kit	Promega, Mannheim, Germany
High-Capacity cDNA Reverse Transcription Kit	Applied Biosystems, Foster City, CA, USA
Hoechst 33342	Sigma-Aldrich, Taufkirchen, Germany
LysoSensor Green™ DND-189	Invitrogen, Waltham, MA, USA
LysoTracker Green™ DND-26	Invitrogen, Waltham, MA, USA
LysoTracker Red™ DND-99	Invitrogen, Waltham, MA, USA
Methyl cellulose	Sigma-Aldrich, Taufkirchen, Germany
MitoTracker™ Green FM	Invitrogen, Waltham, MA, USA
MTT	VWR, Radnor, PA, USA
Page Ruler™ Prestained Protein Ladder	Fermentas, St. Leon-Rot, Germany
Penicillin/Streptomycin 100x	PAA Laboratories, Pasching, Austria
Phenylmethylsulfonyl fluoride (PMSF)	Sigma-Aldrich, Taufkirchen, Germany
Polyacrylamide	Carl Roth, Karlsruhe, Germany
PowerUp™ SYBR® Green Master Mix	Applied Biosystems, Foster City, CA, USA
Primers	Metabion, Planegg, Germany
Propidium iodide	Sigma-Aldrich, Taufkirchen, Germany
RNeasy® Mini Kit	Qiagen, Hilden, Germany
Rotiphorese® Gel 30	Carl Roth, Karlsruhe, Germany
RPMI 1640	PAN Biotech, Aidenbach, Germany
Sodium chloride	Sigma-Aldrich, Taufkirchen, Germany
Sodium dodecyl sulfate	Carl Roth, Karlsruhe, Germany
Sodium fluoride	Merck, Dermstadt, Germany
TCE	Sigma-Aldrich, Taufkirchen, Germany
Tris Base/HCl	Sigma-Aldrich, Taufkirchen, Germany
Trypsin	PAN Biotech, Aidenbach, Germany
Tween 20	Bio-Rad, Munich, Germany

Table 2. Reagents used in this study.

3.1.3 Technical equipment

Device	Producer
Acquity UPLC BEH C8 column (1.7 µm, 2.1 × 100 mm)	Waters, Milford, MA, USA
BD FACS Canto II	BD Biosciences, Heidelberg, Germany
ChemiDoc™ Touch Imaging System	Bio-Rad, Munich, Germany
ExionLC™ AD UHPLC system	Sciex, Darmstadt, Germany
Leica DMi1 microscope	Leica, Wetzlar, Germany
Leica TCS SP8 confocal laser scanning microscope	Leica, Wetzlar, Germany
Nanodrop® Spectrophotometer	PEQLAB Biotechnologie GmbH, Erlangen, Germany
Orion II microplate luminometer	Berthold Detection Systems GmbH, Bad Wildbad, Germany
Primus 25 advanced® Thermocycler	PEQLAB Biotechnologie GmbH, Erlangen, Germany
QTRAP 6500+ Mass Spectrometer	Sciex, Darmstadt, Germany
QuantStudio™ 3 Real-Time PCR System	Applied Biosystems, Foster City, CA, USA
Rotational Vacuum Concentrator RVC 2-18	Martin Christ Gefriertrocknungsanlagen GmbH, Osterode am Harz, Germany
SpectraFluor Plus	Tecan, Männedorf, Switzerland
Ultra Clear TP	Evoqua Water Technologies, Günzburg, Germany
Vi-Cell™ XR cell counter	Beckman Coulter, Brea, CA, USA

Table 3. Technical equipment used in this study.

3.2 Cell culture

3.2.1 Buffers and solutions

PBS (pH 7.4)		Trypsin EDTA		HBSS (pH 7.2)	
NaCl	132.2 mM	Trypsin	0.05 %	$CaCl_2$	1.26 mM
Na_2HPO_4	10.4 mM	EDTA	0.02 %	D-glucose	5.56 mM
KH_2PO_4	3.2 mM			KCl	5.33 mM
				$MgCl_2$	0.49 mM
				KH_2PO_4	0.44 mM
				$MgSO_4$	0.41 mM
				Na_2HPO_4	0.34 mM
				NaCl	137.9 mM
				$NaHCO_3$	4.17 mM
in H_2O		in PBS		in H_2O	

Table 4. Cell culture buffers and solutions.

3.2.2 Cell models

VCR-R CEM TPC2 wt and CCRF-CEM cells were kindly provided by Prof. Maria Kavallaris (University of New South Wales, Sydney, Australia). VCR-R CEM cells were generated by exposition to increasing concentrations of vincristine and have been characterized in the literature [104, 105]. VCR-R CEM TPC2 ko cells were generated from VCR-R CEM TPC2 wt cells during my master thesis and are described in my master thesis and Martin Müller's doctoral thesis [106]. VCR-R CEM TPC2 wt, VCR-R CEM TPC2 ko and CCRF-CEM cells were cultivated in RPMI-1640 (PAN Biotech) supplemented with 10% FCS (PAN Biotech). Jurkat cells were purchased from DSMZ and cultivated in RPMI-1640 supplemented with 10% FCS and 1% pyruvate. HeLa cells were purchased from DSMZ. HepG2 cells were purchased from ATCC (Manassas, Virginia, USA). RIL-175 wt cells were a kind gift from Prof. Dr. Simon Rothenfußer (Center of Integrated Protein Science Munich (CIPS-M) and Division of Clinical Pharmacology, Department of Internal Medicine IV, Klinikum der Universität München). RIL-175 TPC2 ko cells were generated by Dr. Martin Müller and RIL-175 TRPML1 ko cells were generated by Dr. Wei-Xiong Siow (both Pharmaceutical Biology, Prof. Dr. Angelika Vollmar, LMU Munich). HeLa, HepG2 and all RIL-175 cells were cultivated in DMEM (Anprotec) supplemented with 10% FCS (Anprotec).

Patient-derived xenograft acute lymphoblastic leukemia (PDX ALL) cells were kindly provided by Dr. Binje Vick (Prof. Dr. Irmela Jeremias, Research Unit Apoptosis in Hematopoietic Stem Cells, Helmholtz Munich). The model of ALL patients' leukemia cells growing in mice has been

described previously [107]. In the present study, PDX cells were engrafted and freshly isolated from the bone marrow or spleen of NSG mice (The Jackson Laboratory, Bar Harbour, ME, USA). They were cultivated in RPMI-1640 supplemented with 20% FCS, glutamine and P/S. PBMCs were purchased from ATCC and cultivated in RPMI-1640 supplemented with 20% FCS, glutamine and P/S (PAN Biotech).

All cells were cultured at 37°C at constant humidity with 5% CO_2. For HepG2 cells, cell culture flasks and multi well plates were coated with collagen G (0.001% in PBS) before cell seeding.

3.2.3 Passaging

Cell lines were passaged twice to thrice a week and sub-cultivated in a 1:3 to 1:10 ratio in 75cm² cell culture flasks or seeded in multi well plates for experimental use. Adherent cells were washed twice with PBS and detached with trypsin/ethylenediaminetetraacetic acid (T/E, PAN Biotech) at 37°C for about 5 min. When cells were fully detached, reaction was stopped by addition of growth medium. Suspension cell lines were sub-cultivated by dilution of the cell suspension in the respective culture medium. Cells were counted using a ViCell XR cell viability analyzer (Beckmann Coulter).

3.2.4 Freezing and thawing

Cell suspensions were centrifuged (1,000 rpm, 5 min, RT) and resuspended in ice-cold freezing medium (growth medium supplemented with 20% FCS and 10% DMSO) and transferred to cryovials (3×10^6 cells per vial in 1.5 ml) and frozen at -80°C for short-term storage or at -196°C (liquid nitrogen vapor phase) for long-term storage.

For thawing of cells, the frozen cell suspension was mixed with pre-warmed growth medium. Excessive DMSO was removed by centrifugation (1,000 rpm, 5 min, RT) followed by resuspension of the cells in culture medium. Cells were seeded in 25 cm² flasks and later on re-seeded in 75 cm² flasks.

3.3 CellTiter-Blue cell viability assay

Cells were seeded into 96 well plates (VCR-R CEM TPC wt, TPC2 ko, CCRF-CEM, Jurkat: 20×10^3 cells/well; HeLa, HepG2: 5×10^3 cells/well, RIL-175 wt, TPC2 ko, TRPML1 ko: 2×10^3 cells/well) and treated as indicated. Thereafter, 20 µl of CellTiter-Blue reagent (Promega) were added and incubated for 2-4 h at 37°C and 5% CO_2. 2 hours after seeding, zero values were

determined by incubation with CellTiter-Blue reagent as described above. Fluorescence intensity was determined using a SpectraFluor Plus™ plate reader (Tecan) at 550 nm excitation and 595 nm emission wavelength. Relative proliferation was calculated as follows:

$$relative\ proliferation = \frac{intensity\ (treated) - intensity\ (zero\ value)}{intensity\ (control) - intensity\ (zero\ value)}.$$

Concentration-response curves were fitted using GraphPad Prism 9 and significance of differences between dose-response curves were determined using the comparison of fits function of GraphPad Prism 9.

3.4 MTT assay

HepG2 cells were seeded into 96 well plates (5 × 10^3 cells/well) and treated as indicated. Thereafter, 10 µl of MTT reagent (5 mg/ml in PBS, VWR) were added and incubated for 2 h at 37°C and 5% CO_2. MTT-containing medium was discarded and plates were frozen at -80°C. After 1 h, the formed formazan was dissolved in DMSO (Carl Roth) and plates were thawed under constant agitation. Absorbance was determined using a SpectraFluor Plus™ plate reader (Tecan) at 550 nm absorbance wavelength. Relative proliferation values were obtained by normalization to absorbance of control cells.

3.5 Colony formation assay

Cells were seeded at a density of 2 × 10^5 cells per well in 12 well plates and incubated overnight. Afterwards, cells were treated for 4 h. Cells were then transferred to falcon tubes, centrifuged, washed with PBS, resuspended in culture medium, put through a cell strainer (20 µm) and subsequently counted. Cell suspensions were diluted to 65 × 10^3 cells/ml. 500 µl of cell suspensions were added to 3 ml colony formation medium (RPMI-1640 containing 40% FCS and 0.52% methyl cellulose) and reseeded in 12 well plates (1 ml, 5 × 10^3 cells/well). After 5 days of incubation viable colonies were stained with MTT reagent (VWR) and colonies were analyzed by light microscopy. Relative colony area was evaluated using ImageJ.

3.6 Flow cytometry

All flow cytometry experiments were conducted on a BD FACS Canto II (BD Biosciences) and obtained results were evaluated using FlowJo 10 (BD Biosciences). Before analysis, cell debris was excluded.

3.6.1 Determination of apoptosis

Apoptosis was either analyzed by propidium iodide staining according to Nicoletti et al. [108] or by using the forward and sideward scatter method described by Ehrhardt et al. [109].

125 × 10^3 VCR-R CEM TPC2 wt and TPC2 ko cells per well were seeded in 24 well plates. 24h or 48h after stimulation, cells were transferred to pre-cooled FACS tubes, centrifuged (400g, 5 min, 4°C) and washed with ice-cold PBS. For propidium iodide staining, the cell pellet obtained after another centrifugation step was resuspended in hypotonic fluorochrome solution (50 µg/ml propidium iodide, 0.1% sodium citrate, 0.1% Triton-X 100 in H_2O). After at least 30 min incubation at 4°C in the dark, apoptosis was determined by quantification of the subG1 population using the PI filter setting.

For apoptosis analysis using the FSC/SSC method, cells were resuspended in ice-cold PBS and apoptosis was immediately determined by quantification of the dead cell population in the FSC/SSC dot plot. The FSC/SSC method was used for DXR-treated cells and for PDX ALL cells and PBMCs. For that, 1 × 10^5 PDX ALL cells or 4 × 10^5 PBMCs per well were seeded in 24 well plates and stimulated for 48h directly after cell seeding and further handled as described above. Specific apoptosis was calculated as follows:

$$specific\ apoptosis\ [\%] = \frac{\%\ apoptotic\ cells\ (treated) - \%\ apoptotic\ cells\ (ctrl)}{100\% - apoptotic\ cells\ (ctrl)} \times 100.$$

3.6.2 Determination of cell death

To determine overall cell death, PI exclusion assays were performed. Upon loss of membrane integrity of dead cells, DNA of dead cells can be stained with PI. 20 × 10^3 RIL-175 wt, RIL-175 TPC2 ko or RIL-175 TPRML1 ko cells were seeded into 24 well plates and treated as indicated. After stimulation, cells were detached by trypsinization and transferred to FACS tubes together with the respective supernatants. Cells were centrifuged (400 g, 5 min, 4°C), washed once with ice-cold PBS and resuspended in PBS containing 5 µg/ml propidium iodide (PI, Carl Roth). Cells were immediately analyzed by flow cytometry using the PI filter settings. Cell populations were gated according to PI fluorescence intensity and cells with high intensity were considered dead. Specific cell death was calculated as follows:

$$specific\ cell\ death\ [\%] = \frac{\%\ dead\ cells\ (treated) - \%\ dead\ cells\ (ctrl)}{100\% - dead\ cells\ (ctrl)} \times 100.$$

3.6.3 Lysosomal volume and lysosomal damage

Lysosomal volume was determined by LysoTracker Green DND-26 (Invitrogen) staining. LysoTracker probes accumulate in acidic cellular compartments where they are highly fluorescent. 2×10^5 VCR-R CEM TPC2 wt or TPC2 ko cells per well were seeded in 12 well plates and stimulated as indicated. Cells were transferred to pre-cooled FACS tubes, centrifuged (400g, 5 min, 4°C) and washed with ice-cold PBS. Afterwards cells were resuspended in PBS containing 200 nM LysoTracker Green DND-26 and incubated for 30 minutes at 4°C in the dark. Cells were washed again and resuspended in ice-cold PBS and analyzed by flow cytometry using the FITC filter setting. In order to determine lysosomal volume, relative geometric mean fluorescence intensity (gMFI) was evaluated. In order to determine lysosomal damage, the LysoTracker negative population was quantified and considered as cell population with damaged lysosomes according to Zhong et al. [110].

3.6.4 Lysosomal pH

Lysosomal pH was determined by LysoSensor Green DND-189 (Invitrogen) staining. LysoSensor Green DND-189 accumulates in acidic cellular compartments and its fluorescence intensity is dependent on the pH of the lysosomal compartment, being more fluorescent in acidic compartments. 2×10^5 VCR-R CEM TPC2 wt or TPC2 ko cells per well were seeded in 12 well plates. Cells were transferred to pre-cooled FACS tubes, centrifuged (400g, 5 min, 4°C) and washed with ice-cold PBS. Afterwards cells were resuspended in PBS containing 1 µM LysoSensor Green DND-189 and incubated for 30 minutes at 4°C in the dark. Cells were washed again and resuspended in ice-cold PBS and analyzed by flow cytometry using the FITC filter setting. Semi-quantitative comparison of lysosomal pH was facilitated by comparison of LysoSensor gMFI.

3.6.5 Intracellular doxorubicin

Due to its autofluorescence, intracellular doxorubicin can be quantified semi-quantitatively by flow cytometry. 2×10^5 VCR-R CEM TPC2 wt or TPC2 ko cells per well were seeded in 12 well plates and treated as indicated for 24h. Cells were transferred to pre-cooled FACS tubes, centrifuged (400g, 5 min, 4°C) and washed with ice-cold PBS. Cells were resuspended in ice-cold PBS and intracellular doxorubicin was analyzed using the PI filter setting and evaluated by calculation of gMFI.

3.6.6 Calcein-AM retention assay and doxorubicin retention assay

Calcein-AM (Cayman Chemical) is a fluorescent model substrate to analyze P-gp activity. Calcein-AM is a P-gp substrate which becomes membrane impermeable when the acetoxy methyl ester is cleaved. Hence, calcein fluorescence negatively correlates with P-gp activity. Calcein-AM retention assay was conducted according to Robey et al. [111]. 3×10^5 VCR-R CEM TPC2 wt cells per well were seeded in 12 well plates. 200 nM calcein-AM (Biomol) and the respective P-gp inhibitor or compound of interest were added and incubated for 30 min at 37°C. Cells were transferred to FACS tubes, centrifuged (400g, 5 min, RT), washed with PBS and resuspended in RPMI-1640 without phenol red (PAN Biotech) containing 10% FCS and the respective compound of interest. After 60 minutes of incubation at 37°C calcein fluorescence was analyzed using the FITC filter settings and results are expressed as gMFI. Doxorubicin retention assays were performed accordingly using 5 µM doxorubicin. Fluorescence intensity was analyzed using the PI filter setting.

3.6.7 P-glycoprotein staining

300,000 cells were transferred to pre-cooled FACS tubes, centrifuged (400 g, 5 min, 4°C) and washed with ice-cold 1% BSA in PBS. After aspiration, pelleted cells were resuspended in 20 µl of FITC Anti P-gp antibody (Catalog No. 557002, BD Biosciences) diluted with 80 µl PBS per test. Cells were incubated for 30 min at 4°C under light exclusion. To determine unspecific antibody binding, FITC Mouse IgG2b κ Isotype Control (Catalog No. 555742, BD Biosciences) was used (20 µl, diluted in 80 µl PBS). Thereafter, cells were washed once with ice-cold 1% BSA (Anprotec) in PBS and twice with 0,5% (v/v) Tween 20 (Carl Roth) in PBS and resuspended in ice-cold PBS. Subsequently, cells were analyzed by flow cytometry, using the FITC channel and results are expressed as geometric mean fluorescence intensity. These experiments were conducted as part of my master thesis under supervision of Dr. Martin Müller (Pharmaceutical Biology, Prof. Dr. Angelika Vollmar, LMU Munich).

3.6.8 Mitochondrial mass

Mitochondrial mass was assessed using MitoTracker Green FM (Invitrogen). 2×10^5 VCR-R CEM TPC2 wt or TPC2 ko cells per well were seeded in 12 well plates. Cells were transferred to pre-cooled FACS tubes, centrifuged (400g, 5 min, 4°C) and washed with ice-cold PBS. Afterwards cells were resuspended in PBS containing 100 nM MitoTracker Green FM and incubated for 30 minutes at 4°C in the dark. Cells were washed again and resuspended in ice-cold PBS and mitochondrial mass was analyzed by flow cytometry using the FITC filter setting.

3.6.9 Mitochondrial membrane potential

Mitochondrial membrane potential was assessed by DiOC6(3) iodide (Enzo Life Sciences) staining. DiOC6(3) iodide accumulates in mitochondria in dependence of mitochondrial membrane potential. Hence, cells with disrupted mitochondrial membrane potential (damaged mitochondria) have lower DiOC(6)3 fluorescence. 2×10^5 VCR-R CEM TPC2 wt or TPC2 ko cells per well were seeded in 12 well plates. Cells were transferred to FACS tubes, centrifuged (400g, 5 min, RT) and washed with HBSS. Cells were resuspended in 100 nM DiOC6(3) iodide in growth medium and incubated for 30 min at 37°C. Subsequently, cells were centrifuged, washed again and resuspended in HBSS. DiOC(6)3 iodide fluorescence was analyzed using the FITC filter setting and events were gated for the DiOC(6)3-positive cell population.

3.6.10 Lipid ROS

Lipid ROS was quantified by Bodipy-C11 (Invitrogen) staining. Due to oxidation of Bodipy-C11 upon lipid peroxidation, its emission wavelength shifts from ~590 nm to ~510 nm. RIL-175 wt, TPC2 ko or TRPML1 ko cells were seeded in 24 well plates and treated as indicated. 30 min prior to the end of stimulation time 2 µM Bodipy-C11 was added. After 30 min of incubation, cells were detached by trypsinization, collected in FACS tubes, centrifuged (400g, 5 min, 4°C), washed with ice-cold PBS, again centrifuged and resuspended in ice-cold PBS. Bodipy-C11 green fluorescence was analyzed using the FITC filter settings and the Bodipy-C11/lipid ROS-positive cell population was quantified.

3.6.11 Endoplasmic reticulum calcium levels

Endoplasmic reticulum calcium levels were determined by quantification of intracellular calcium using Cal-520 AM (Cayman Chemical) upon induction of ER calcium release. For that, cells were seeded in 6 well plates (3×10^5/well) and incubated overnight. 1 µM of Cal-520 AM was added and cells were incubated for 90 min at 37°C followed by 30 min at room temperature. Cells were detached by trypsinization, collected in FACS tubes, centrifuged (400g, 5 min, RT), washed with PBS, again centrifuged and resuspended in PBS. Cal-520 fluorescence was analyzed using the FITC filter settings. Basal Cal-520 fluorescence was recorded for 30 sec. Thereafter, 10 µM thapsigargin or 10 µM calcimycin were added and Cal-520 fluorescence was recorded for further 150 sec or 90 sec, respectively. Results are expressed as relative median fluorescence and normalized to each cell line.

3.7 Immunoblotting

3.7.1 Cell lysis

For whole cell lysates, cells were washed twice with ice-cold PBS, resuspended in RIPA lysis buffer (1% NP-40, 0.1% SDS, 0.25% deoxycholate, 150 mM NaCl, 50 mM Tris-HCl in deionized water; pH 7.5) supplemented with the protease inhibitor Complete® (Roche Diagnostics) and frozen at -80°C for at least 30 min. Thereafter, cell lysates were thawed at 4°C under agitation and centrifuged again (18,000 rpm, 4°C, 5 min) to remove cell debris.

3.7.2 Isolation of lysosomes

Lysosomes were isolated as described previously [112]. Cells were treated as indicated, washed twice with ice-cold PBS and resuspended in pre-cooled homogenization buffer (250mM sucrose, 10 mM Tris in H_2O, pH 7.4; 1x Complete protease inhibitor was added directly prior to use). Cells were homogenized with a potter homogenizer with 12 strokes at 900 rpm. The suspension was then centrifuged (14,000g, 15 min, 4°C) and supernatant was collected. It was mixed with an equal volume of 16 mM $CaCl_2$ and shaken (15 min, 150 rpm, 4°C) to precipitate lysosomes. The mixture was centrifuged (14,000g, 15 min, 4°C). The supernatant contains the cytosolic fraction and lysosomes are pelleted. The pellet was washed with ice-cold washing buffer (150 mM KCl, 10 mM Tris in H_2O, pH 7.4; 1x Complete protease inhibitor was added directly prior to use) and centrifuged (25,000g, 15 min, 4°C). Supernatant was removed and lysosomes were resuspended in RIPA lysis buffer.

3.7.3 Isolation of mitochondria

Mitochondria cytosol fractionation was conducted following the protocol provided by abcam (Cambridge, UK). Cells were treated as indicated, washed twice with ice-cold PBS and resuspended in pre-cooled fractionation buffer (250 mM sucrose, 20 mM HEPES, 10 mM KCl, 1.5 mM $MgCl_2$, 1 mM EDTA, 1 mM EGTA in H_2O, pH 7.4; 1x Complete protease inhibitor and 1 mM DTT were added directly prior to use). The suspension was homogenized using syringe and needle (25 Ga needle, 12 times) and subsequently incubated on ice for 20 min. Afterwards, the suspension was centrifuged (720g, 5 min, 4°C) and the post-nuclear supernatant was again centrifuged (10,000g, 5 min, 4°C). The supernatant containing the cytosolic fraction was saved and the mitochondrial pellet was washed twice with fractionation buffer (centrifugation

at 10,000g, 5 min, 4°C). The mitochondrial pellet was subsequently resuspended in RIPA lysis buffer.

3.7.4 Protein quantification and sample preparation

To ensure equal protein loading, protein yield was determined by Bradford protein assay. For that, samples were diluted adequately and applied to a 96 well plate (10 µl) in triplicates. BSA (Anprotec) in different concentrations served as protein standard. 190 µl of Bradford reagent (Carl Roth, Karlsruhe, Germany; 1:5 diluted in Milli-Q® water) were added and absorbance at 592 nm was directly measured using the SpectraFluor Plus™ plate reader (Tecan). Protein concentrations were calculated by linear regression.

Subsequently, an adequate amount of 5x SDS sample buffer (3.125 M Tris-HCl, 50% Glycerol, 5% SDS, 2% DTT, 0.025% Pyronin Y in deionized water; pH 6.8) was added to the samples and samples were diluted with 1x SDS sample buffer in order to adjust protein concentrations.

3.7.5 SDS-PAGE, tank blotting and protein detection

Proteins were separated by sodium dodecyl sulfate polyacrylamide gel electrophoresis (SDS-PAGE) using appropriate gels (Table 5) to separate proteins of interest. SDS-PAGE was conducted at 100 V for 21 min followed by 200 V for 40 min in electrophoresis buffer (4.9 mM Tris base, 38 mM glycine, 0.1% SDS in deionized water). Equal protein loading and subsequent normalization to the total protein amount, proteins on the gels were stained and imaged utilizing the stain-free technology. Thereafter, proteins were transferred to polyvinylidene difluoride (PVDF, 0.2 µm, Amersham Bioscience) membranes by tank blotting. Membranes were equilibrated in methanol, deionized water and ice-cold tank buffer (48 mM Tris base, 39 mM glycine, 20% methanol in deionized water), blotting sandwiches were assembled and transferred to tank blotting systems filled with ice-cold tank buffer. Proteins were transferred at 100 V for 1.5 h at 4°C or at 25 V overnight at 4°C.

For protein detection, membranes were blocked with 5% BSA in TBS-T (50 mM Tris/HCl pH 8.0, 138 mM NaCl, 2.7 mM KCl, 0.1% Tween-20) overnight at 4°C under agitation. Membranes were then washed thrice (5 min, RT, agitation) with TBS-T and incubated in primary antibody solutions (Table 6) in 5% BSA in TBS-T overnight (4°C, agitation). After three more washing steps with TBS-T, membranes were incubated with appropriate HRP-coupled secondary antibodies (Table 7) in 5% BSA in TBS-T for 2 h at RT. Membranes were washed thrice with TBS-T and ECL solution (100 mM Tris/HCl pH 8.5, 2.5 mM luminol, 1 mM cumaric acid, 17 µM H_2O_2 in deionized water) was added and membranes were imaged using a ChemiDoc™

Touch Imaging System (Bio-Rad). Data processing was conducted with the ImageLab (Bio-Rad) software and results were normalized to the protein amount on the gel (stain-free detection).

Ingredient	Stacking gel	4-20% Separation gel		15% Separation Gel
		4%	20%	
Rotiphorese® Gel 30	13.3%	13.3%	66.7%	50%
Tris-HCl pH 6.8	125 mM	-	-	-
Tris-HCl pH 8.8	-	375 mM	375 mM	375 mM
TCE	-	0.05%	0.05%	0.05%
SDS	0.1%	0.1%	0.1%	0.1%
TEMED	0.2%	0.1%	0.1%	0.1%
APS	0.1%	0.05%	0.05%	0.05%
in H_2O				

Table 5. Recipes for Western blot gels. 4-20% gradient gels were produced by mixing of 4% and 20% gels in a pipette by aspirating air bubbles.

Antigen	Catalogue	Species	Producer	Dilution
PARP	9542	rabbit	Cell Signaling	1:1000
Active caspase 3	C8487	rabbit	Sigma-Aldrich	1:1000
γ-H2AX (Ser139)	2577	rabbit	Cell Signaling	1:1000
Hsp70	sc-1060	goat	Santa Cruz	1:200
Bcl-xL	2726	rabbit	Cell Signaling	1:1000
Bcl-2	2872	rabbit	Cell Signaling	1:1000
Bax	sc-493	rabbit	Santa Cruz	1:200
LAMP1	H4A3	mouse	Developmental Studies Hybridoma Bank	1:200
Vinculin	sc-225336	mouse	Santa Cruz	1:200
Cathepsin B	31718	rabbit	Cell Signaling	1:1000
VDAC	4866	rabbit	Cell Signaling	1:1000
Bid	2002	rabbit	Cell Signaling	1:1000
Cytochrome c	4272	rabbit	Cell Signaling	1:1000
Caspase 9	9502	rabbit	Cell Signaling	1:1000
ATM	A1106	mouse	Sigma-Aldrich	1:2000
p-ATM (Ser1981)	5883	rabbit	Cell Signaling	1:1000

FTH1	3998	rabbit	Cell Signaling	1:1000
p-eIF2alpha (Ser51)	9721	rabbit	Cell Signaling	1:1000
eIF2alpha	sc-133132	mouse	Santa Cruz	1:1000
ACSL4	sc-271800	mouse	Santa Cruz	1:200
BiP/GRP78	610978	mouse	BD Biosciences	1:1000
p53	9282	rabbit	Cell Signaling	1:1000
p-p53 (Ser15)	9284	rabbit	Cell Signaling	1:1000

Table 6. Primary antibodies used in this study.

Description	Catalogue	Species	Producer	Dilution
Goat IgG anti-Rabbit IgG (H+L)- HRPO, MinX Hu,Ms,Rt	111-035-144	goat	dianova	1:10000
Goat Anti-Rabbit IgG (H+L)-HRP Conjugate	172-1019	goat	Bio-Rad	1:5000
Goat Anti-Mouse IgG1 (HRP)	ab97240	goat	abcam	1:5000
Donkey Anti-Goat IgG H&L (HRP) preadsorbed	ab97120	donkey	abcam	1:20000
Goat Anti-Mouse IgG2a, Human ads-HRP	1080-05	goat	Southern Biotech	1:5000
Goat anti-mouse IgG-HRP	sc-2005	goat	Santa Cruz	1:2000

Table 7. Secondary antibodies used in this study.

3.8 Quantitative real-time PCR (RT-qPCR)

Total mRNA was isolated using the RNeasy Mini Kit (Qiagen) according to the manufacturer's protocol including the on-column digestion step of DNA impurifications. Lysis Buffer RLT was supplemented with 40 µM DTT directly prior to use. To improve cell lysis, cells resuspended in buffer RLT were frozen at -80°C for at least 30 min. mRNA yield was quantified with a Nanodrop ND-100 spectrophotometer (PEQLAB Biotechnologie GmbH). Reverse transcription into cDNA was conducted using the High-Capacity cDNA Reverse Transcription Kit (Applied Biosystems) as described by the manufacturer. RT-qPCR analysis was performed using the PowerUp SYBR Green Master Mix (Applied Biosystems) on a QuantStudio 3 Real-Time PCR System (Applied Biosystems). Primers for qPCR (Table 8) were purchased from Metabion and validated by calculating primer efficiency and analyzing the melt curves of the resulting PCR product. Results were evaluated employing the $\Delta\Delta C_T$ method as described previously [113]. Actin served as housekeeping gene.

Target	Forward primer (5'-3')	Reverse primer (5'-3')
hABCB1	CAG CTG TTG TCT TTG GTG CC	GTC TGG CCC TTC TTG ACC TC
hACTB	CCA ACC GCC AGA AGA TGA	CCA GAG GCG TAC AGG GAT AG
hATP6V0C	ATG CTT CGT TTT TCG CCG TC	ATG ACA GAC ATG GCC GCA A
hCTSB	CTG GCA GGT TGA AGT AGG GG	CCG CTA ATA ACG GCA GTT GC
hCTSD	GAC ATC CAC TAT GGC TCG GG	AGC ACG TTG TTG ACG GAG AT
hLAMP1	CGT CCT TGG GCG TCT CTA AT	CAC AGC GCA GAA CAG GAT CA
hNPC1	TTC GGC AGC TTC AGA CAC TA	TTC AGT AGG TTA TAA AAA CAG GAT GG
hTFEB	CAA GGC CAA TGA CCT GGA C	AGC TCC CTG GAC TTT TGC AG
hTPC1	GGA GCC CTT CTA TTT CAT CGT	CGG TAG CGC TCC TTC AAC T
hTPC2	TGC ATT GAT CAG GCT GTG GT	GAA GCT CAA AGT CCG TTG GC
hTRPML1	TCT TCC AGC ACG GAG ACA AC	GCC ACA TGA ACC CCA CAA AC
hTRPML2	AAC GGT GTT TCC TGT TCC GA	GCC ATT GCA TTT CTG ACG GTT A
hTRPML3	TGC TTC TGT GGA TGG ATC G	GAG ACC ATG TTC AGA GAAA CGA A
mACTB	CCA CCA TGT ACC CAG GCA TT	AGG GTG TAA AAC GGA GCT CA
mSLC7A11	AAT ACG GAG CCT TCC ACG AG	ACT GTT CGG TCG TGA CTT CC
mGCLC	GAC TGT TGC CAG GTG GAT GA	ACC CTC TCT CTC TCT GCT GG
mGSS	GGA CAT GGG TGA AGA AGG GG	ACC CAG CTC CGA GAT ACA CT
mGPX4	AGC TAG TCG ATC TGC ATG CC	CCC TTG GGC TGG ACT TTC AT
mTFRC	CGG GGT TGG ACC TAC ACT TC	CTA CCA CGT TGA CCC TCC AC
mTF	GGA AGT GCT CAA CCT CAC GA	CAC CAG TTA GTC CCA ACC CC
mFTH1	GCC AGA ACT ACC ACC AGG AC	TCT CCC AGT CAT CAC GGT CT
mFTL1	CGG ATC AGC CAT GAC CTC TC	AGC CCA GAG AGA GGT AGG TG
mSLC11A2	TAT CCC AAG GTC CCA CGG AT	CGA TGG TGA TGA GGA CTC CG
mSLC40A1	GAG CCA GTG TCC CCA ACT AC	CTT GCA GCA ACT GTG TCA CC
mSTEAP3	CAG CTT CTT CTT CGC GAT GC	GAC CTG CTT CAC AGC CAG AT
mNCOA4	GGC TCT GCC CTT CCA GAA AT	GCT GAG GCT TCC CAC TTT CT

mACSL4	CCC CTT CAG ACA TGG CCA TT	TAC GTT CAC ACT GGC CTG TC
mSCD1	CAC CTG CCT CTT CGG GAT TT	CTT TGA CAG CCG GGT GTT TG

Table 8. Primers used in this study.

3.9 Confocal microscopy

Confocal microscopy was performed on a Leica TCS SP8 confocal microscope with an HC PL APO CS2 63x/1.4 oil objective, using the Las X software (Leica). According to the excitation spectra of the respective dyes, excitation lasers at 405 nm, 488 nm or 561 nm wavelength were used. Fluorescence signals were detected either with PMT or HyD detectors. Images were analyzed using ImageJ.

For confocal microscopy of fixed leukemic cells, cells were immobilized on ibiTreat µ-Slides as previously described. For that, the respective cell suspensions were centrifuged (1000 rpm, 5 min, RT), washed with PBS and thereafter resuspended in PBS. The cell suspension was transferred to the imaging slides and incubated for 30 min at RT. For confocal microscopy of adherent cells, cells were seeded, grown and stained in ibiTreat µ-Slides. Subsequently, cells were washed twice with PBS and fixed for 10 min in 4% formaldehyde in PBS. Cells were again washed twice in PBS and mounted with FluorSave reagent (Merck Millipore) and cover slips. To assess lysosomal pH, cells were incubated with 1 µM LysoSensor Green (Invitrogen) for 30 minutes in PBS and nuclei were stained with Hoechst 33342 (100 µg/ml in PBS, 30 min, Sigma-Aldrich) after fixation. To assess nuclear doxorubicin, cells were treated with doxorubicin and nuclei were stained with Hoechst 33342 after fixation. Images were analyzed by quantifying doxorubicin fluorescence at nuclear regions. To assess lysosomal diameter, cells were incubated with 200 nM LysoTracker Red (Invitrogen) for 30 minutes in PBS and nuclei were stained with Hoechst 33342 after fixation. Images were analyzed in ImageJ by defining the LysoTracker positive regions after reasonable adjustment of the threshold. Subsequently, positive particles were characterized with the “analyze particles” function.

Lysosomal damage was assessed by live cell imaging of acridine orange-loaded cells (Invitrogen). Cells were loaded with acridine orange (2 µg/ml, 30 min) in growth medium. Cells were washed twice with PBS, resuspended in growth medium without dye, transferred to ibiTreat µ-slides and covered with a cover slip. Cells were exposed to high intensity laser light (FRAP mode, 60% of maximal power of 488 nm laser) and images were acquired after every exposition cycle. Images were analyzed by quantification of red and green fluorescence in the region of acidic vacuoles and results are expressed as green to red fluorescence ratio.

3.10 Cathepsin B activity assay

Cathepsin B activity was determined using the Cathepsin B Activity Assay Kit (PK-CA577-K140, PromoKine) according to the manufacturer's instructions. Equal amounts of protein for each sample were used for each reaction. Cathepsin B-mediated cleavage of the substrate RR-AFC leads to a release of free AFC which is highly fluorescent. Fluorescence was measured in clear-bottom black 96 well plates on a Tecan plate reader (excitation wavelength: 390 nm, emission wavelength: 535 nm).

3.11 Quantification of free ferrous iron

Ferrous iron levels were quantified with FerroOrange (Dojindo). Cells were seeded in 24 well plates (4×10^4/well) and incubated for 48h. Cells were washed twice with HBSS and stained with 1 µM FerroOrange in HBSS for 30 min at 37°C. Fluorescence intensity was determined on a Tecan plate reader (excitation wavelength: 535 nm, emission wavelength 590 nm). Subsequently, the staining solution was aspirated, cells were washed twice with PBS and stained with crystal violet (0.5% crystal violet in 20% methanol) for 10 min under shaking. Excessive crystal violet was washed off with water and membrane-bound crystal violet was subsequently re-dissolved in trisodium citrate solution (14.7 g/l in 50% ethanol). Absorbance at 550 nm is proportional to the cell number and was employed to normalize FerroOrange fluorescence to the cell number.

3.12 Quantification of GSH/GSSG levels

GSH and GSSG levels were quantified using the GSH/GSSG-Glo assay kit (V6612, Promega) according to the manufacturer's instructions. Cells were seeded in 96 well plates (3×10^3/well) and treated for 24 h. Cells were washed twice in PBS and either lysed in total glutathione lysis reagent (luciferin 1 µl/well, 5X lysis buffer 10 µl/well, H_2O 39 µl/well) or oxidized glutathione lysis reagent (luciferin 1 µl/well, NEM 0.5 µl/well, 5X lysis buffer 10 µl/well, H_2O 38.5 µl/well) and incubated for 5 min while shaking. In parallel, GSH standards were prepared accordingly in concentrations ranging from 0.25 µM to 8 µM. Thereafter, luciferin generation reagent (DTT 1.25 µl/well, GSH-S-transferase 3 µl/well, glutathione reaction buffer 45.75 µl/well) were added to each sample. After 30 min of incubation, 100 µl of luciferin detection reagent were added, plate was equilibrated for 15 min and transferred to white-walled luminescence-compatible 96 well plates. Data were acquired on an Orion II microplate luminometer (Berthold Detection Systems GmbH). Total glutathione and oxidized glutathione were quantified by linear regression from the glutathione standards and GSH/GSSG ratios were calculated as follows:

$$GSH/GSSG = \frac{c\,(total\ glutathione) - 2 \times c\,(oxidized\ glutathione)}{c\,(oxidized\ glutathione)}.$$

3.13 Targeted analysis of phosphatidylethanolamines by UPLC-MS/MS

2×10^6 cells were centrifuged (270 g, 5 min, 4°C) and washed with PBS. The supernatant was removed and cell pellets were snap-frozen in liquid nitrogen. Cells were resuspended in 150 µl PBS and 365 µl standard mix [1 µl 0.2 mM 1,2-dimyristoyl-sn-glycero-3-phosphoethanolamine (DMPE) + 364 µl methanol] and 187.5 µl chloroform were added. The mixture was vortexed for 30 sec and another 187.5 µl chloroform were added. The mixture was vortexed for 30 sec and 187.5 µl 0.9% NaCl solution were added and again vortexed for 30 sec. The mixture was centrifuged (1500 g, 5 min, 4°C) and the lower phase (chloroform) was transferred into a new Eppendorf tube and the solvent was evaporated in a vacuum concentrator at 30°C for 30 min. The lipid films were dissolved in 100 µl methanol and centrifuged (14800 rpm, 5 min, 4°C), and the supernatants were appropriately diluted in methanol and again centrifuged (14800 rpm, 5 min, 4°C).

Phosphatidylethanolamines (PE) were chromatographically separated using an Acquity UPLC BEH C8 column (1.7 µm, 2.1 × 100 mm, Waters) and an ExionLC™ AD UHPLC system (Sciex). The composition of the mobile phase was A (water/acetonitrile, 90/10, 2 mM ammonium acetate) and B (acetonitrile/water, 95/5, 2 mM ammonium acetate). The flow rate was set to 0.75 ml/min. Starting with A/B = 25/75, the gradient raised to 85 % of mobile phase B within 5 min, followed by isocratic elution with 100 % mobile phase B for 2 min. The column oven kept the temperature of the column at 45 °C. Separated phospholipids were ionized in an electrospray ionization (ESI) source and detected by multiple reaction monitoring (MRM) in the negative ion mode using a QTRAP 6500+ Mass Spectrometer (Sciex) [114, 115]. To analyse the phospholipids, both fatty acid anion fragments were determined and, for quantitation, the average of both transitions was calculated. The system parameters were set to the following: curtain gas at 40 psi, collision gas set to medium and an ion spray voltage of 4500 V in the negative mode. For the analysis of PE the temperature of the heated capillary is set to 650 °C, the sheath gas pressure was set to 55 psi, and the auxiliary gas to 75 psi. Compound-specific parameters were defined as the following: declustering potential was set to -44 V, entrance potential to -10 V, collision energy was adjusted to -45 eV and the collision cell exit potential to -11 V. The total amount of PE was calculated as the sum of the individual signal intensities of the PE species analysed. Lipid species were normalized to the internal standard DMPE. The proportions of individual lipids were calculated as percentage of the summarized total intensity of PE. The targeted analysis of phosphatidylethanolamines by

UPLC-MS/MS were performed by Finja Witt from the group of Prof. Andreas Koeberle (Michael Popp Institute, University of Innsbruck, Austria).

3.14 Statistical analyses

Experiments were conducted at least three times independently unless stated otherwise. The number of replicates is stated in the figure legends. Data are displayed as mean ± standard deviation (SD) unless stated otherwise. Statistical significance and non-linear regression were performed using GraphPad Prism 9. Statistical significance between two samples was determined using two-tailed student's t test with Welch's correction if appropriate. Statistical significance between more than two samples within one group was analyzed by ordinary one-way ANOVA with Dunnett's or Tukey's post-test. Statistical significance between two groups with different samples was determined using ordinary two-way ANOVA with Sidak's or Tukey's post-test as indicated in the respective figure legend. The significance of differences in concentration-response curves was determined using the comparison of fits function of GraphPad Prism 9. Results were considered statistically significant for $p<0.05$.

4 Results

4.1 Part I: Targeting TPC2 sensitizes leukemia cells to cytostatics by impairing lysosomal function

4.1.1 Role of lysosomes in chemoresponse and chemoresistance

4.1.1.1 Lysosomal drug sequestration and damage in leukemic cells

Recent studies have shown that lysosomes and lysosome-mediated signaling are important regulators of chemoresistance [29]. Hence, we checked, in which way treatment with cytostatics alters lysosomal characteristics of acute lymphoblastic leukemia (ALL) cells. We chose vincristine-resistant CEM (VCR-R CEM) cells [105, 116] as model to investigate the role of lysosomes and TPC2 in chemoresistance. As a result of exposition to vincristine, VCR-R CEM cells are not only resistant to vincristine, but also cross-resistant to doxorubicin and topotecan (Fig. 4A). The acquired multidrug resistance phenotype is at least partly mediated by overexpression of P-gp, as membranous P-gp (Fig. 4B) and ABCB1 mRNA levels (Fig. 4B) are tremendously increased.

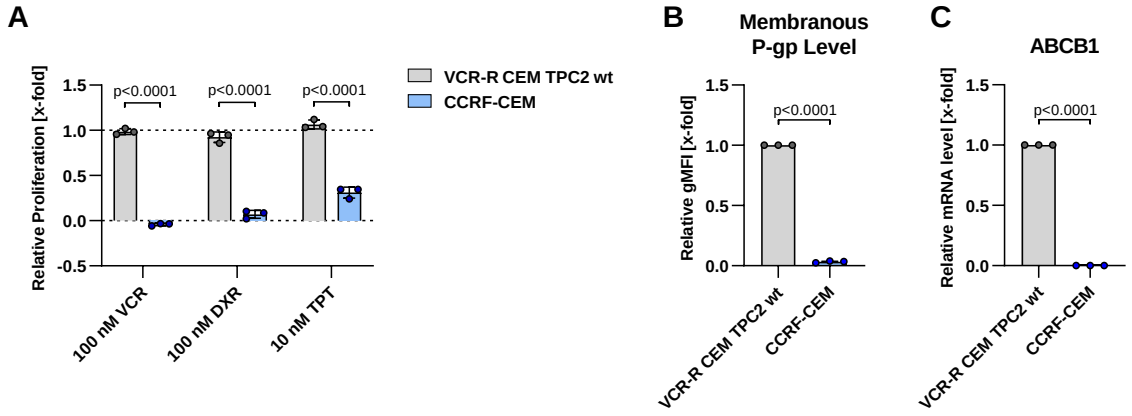

Figure 4. VCR-R CEM cells are multidrug resistant by overexpressing P-gp.
A VCR-R CEM TPC2 wt and CCRF-CEM cells were treated for 72 h and relative proliferation was assessed using CellTiter-Blue reagent. **B** Membranous P-gp levels of untreated VCR-R CEM TPC2 wt and CCRF-CEM cells were quantified by antibody staining and flow cytometry. **C** ABCB1 mRNA levels were determined by qPCR. **B**, **C** These experiments were conducted during my master thesis under supervision of Dr. Martin Müller (Pharmaceutical Biology, Prof. Dr. Angelika Vollmar, LMU Munich). Data are presented as mean ± SD from three independent experiments. Statistical significance was analyzed by two-way ANOVA with Sidak's posttest (**A**) or student's t-test with Welch's correction (**B**, **C**).

Analyzing LysoTracker intensity revealed that short-term doxorubicin treatment leads to an increase in lysosomal volume in VCR-R CEM TPC2 wt, CCRF-CEM and Jurkat cells (Fig. 5A). Similar effects were observed for topotecan in VCR-R CEM TPC2 wt cells, while there was no increase detectable upon vincristine treatment (Fig. 5B). Interestingly, this phenotype was independent of lysosomal biogenesis, as mRNA levels of the lysosomal housekeeping genes LAMP1 and ATP6V0C, a subunit of the vacuolar ATPase, as well as the master regulator of endolysosomal biogenesis TFEB were unchanged after short-term doxorubicin treatment (Fig. 5C). Overall, this could point to an induction of lysosomal stress and might be an indication for drug sequestration inside the lysosomal lumen.

Since lysosomal damage as initiator of LCD is an important pathway in chemotherapy response [18, 117], we wondered whether or not lysosomal stress upon short-term chemotherapy segues into lysosomal damage after prolonged treatment duration. Indeed, quantification of LysoTracker-negative cells which represent the cell population with highly damaged lysosomes, revealed induction of lysosomal damage after treatment with doxorubicin in all tested cell lines (Fig. 5D). This effect could also be confirmed for vincristine and topotecan in VCR-R CEM TPC2 wt cells (Fig. 5E). Furthermore, long-term doxorubicin treatment led to induction of lysosomal biogenesis, evident by upregulation of lysosomal housekeeping genes, including LAMP1, ATP6V0C, and TFEB (Fig. 5F). These results indicate an involvement of lysosomes in chemotherapy response of ALL cells; especially lysosomal volume, lysosomal stress and lysosomal damage may play a pivotal role.

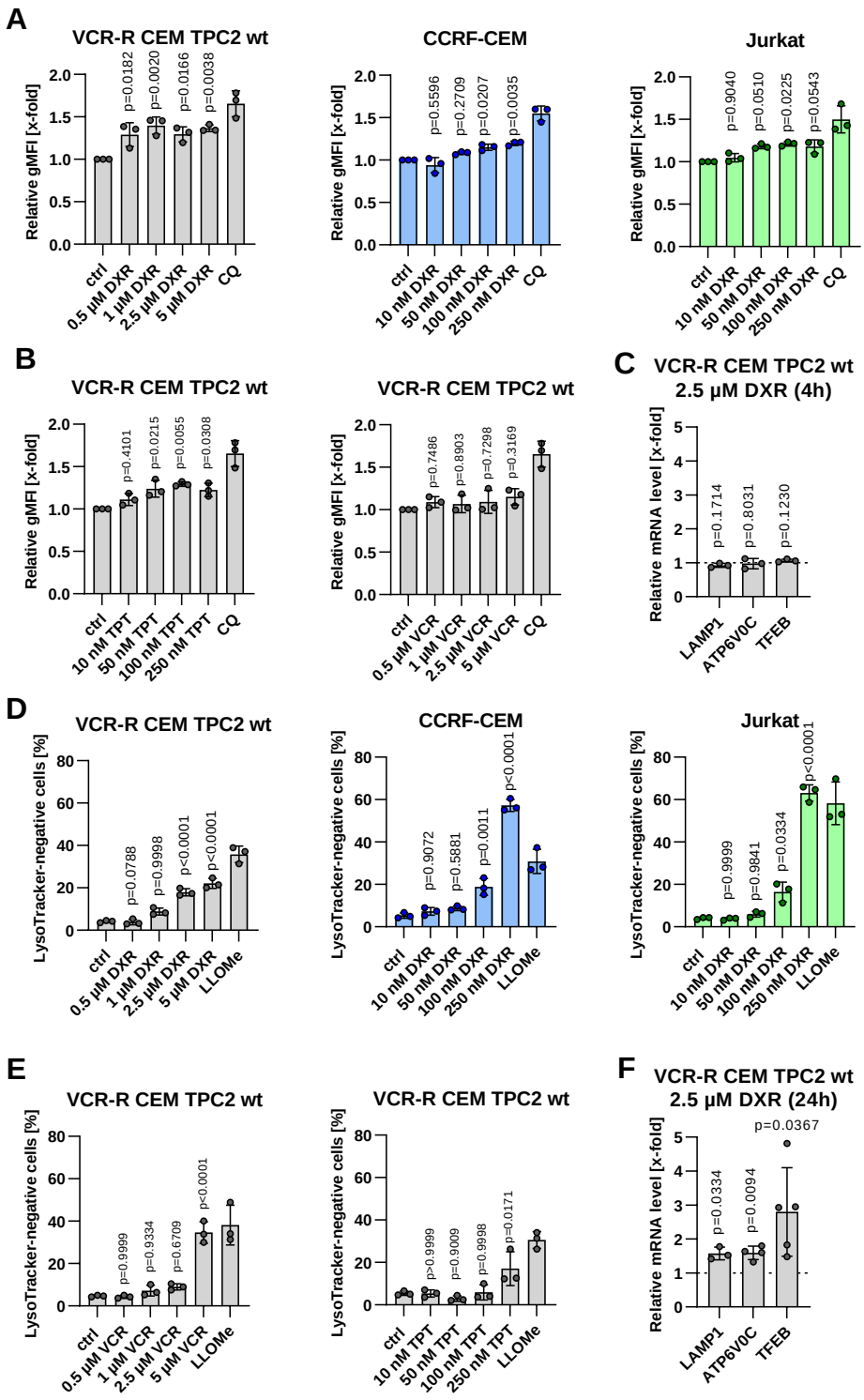

Figure 5. Lysosomal phenotype upon treatment with cytostatics.
A, **B** Cells were treated as indicated for 4 h (VCR-R CEM TPC2 wt) or 8 h (CCRF-CEM, Jurkat) and lysosomal volume was assessed by LysoTracker Green staining and flow cytometry. Chloroquine (CQ) served as positive control. **C** mRNA levels of lysosome-associated genes were analyzed by qPCR after treatment with DXR for 4 h. **D**, **E** VCR-R CEM TPC2 wt, CCRF- CEM and Jurkat cells were treated for 24 h and lysosomal damage was determined by quantifying LysoTracker Green-negative cells by flow cytometry. LLOMe served as positive control. **F** mRNA levels of lysosome-associated genes were analyzed by qPCR after treatment with DXR for 24h. Data are presented as mean ± SD from at least three independent experiments. Statistical significance was analyzed by one-way ANOVA with Dunnett's posttest (**A**, **B**, **D**, **E**) or student's t-test with Welch's correction (**C**, **F**).

4.1.1.2 Alterations in lysosomal characteristics upon development of chemoresistance

To further underline the importance of lysosomes in chemoresistance, we compared lysosomal characteristics of VCR-R CEM TPC2 wt and CCRF-CEM cells. We found that VCR-R CEM TPC2 wt cells had an increased lysosomal volume as compared to CCRF-CEM cells (Fig. 6A) and furthermore, that lysosomes of the resistant cells were more acidic as compared to their parental counterpart, as detected by LysoSensor Green staining (Fig. 6B). Therefore, we checked for expression levels of lysosomal housekeeping genes and other lysosome-abundant genes, predominantly endolysosomal cation channels. While there were no major alterations observable for most genes, TPC1 and more strikingly TPC2 were upregulated in drug-resistant cells as compared to their parental cell line (Fig. 6C). Based on these results, we hypothesized that TPC2 might promote multidrug resistance and hence might be a possible target to re-sensitize chemo-resistant cells and thereby improve chemotherapy response in leukemia.

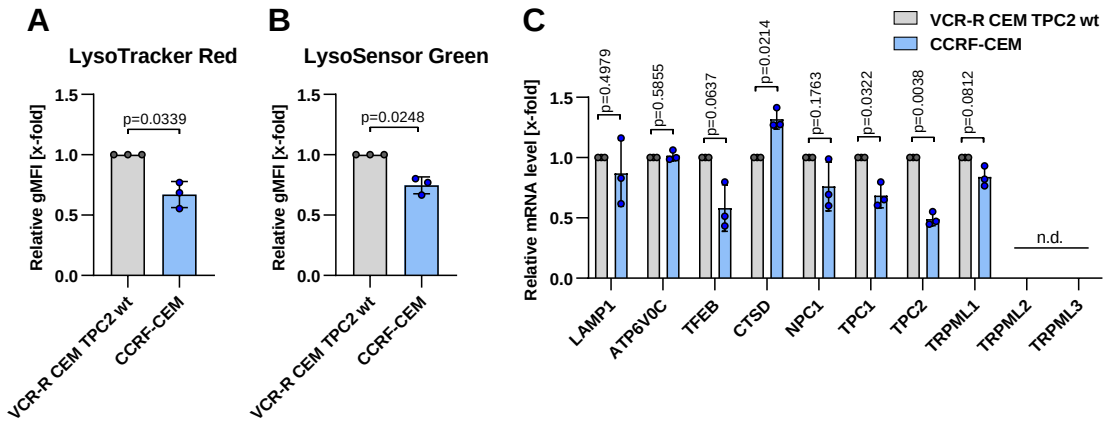

Figure 6. Lysosomal phenotype in VCR-R CEM TPC2 wt cells.
A Lysosomal volume of untreated VCR-R CEM TPC2 wt and CCRF-CEM cells was assessed by LysoTracker Red staining and flow cytometry. **B** Lysosomal pH of untreated VCR-R CEM TPC2 wt and CCRF-CEM cells was semi-quantitatively analyzed by LysoSensor Green staining and flow cytometry. Higher fluorescence intensity indicates more acidic lysosomes. **C** mRNA levels of lysosome-associated genes were analyzed by qPCR. Data are presented as mean ± SD from three independent experiments. Statistical significance was analyzed by student's t-test with Welch's correction.

4.1.2 Targeting TPC2 sensitizes leukemia cells to cytostatics

4.1.2.1 TPC2 ko sensitizes VCR-R CEM cells to weak base cytostatics

To elucidate the role of TPC2 in chemoresistance, a VCR-R CEM TPC2 ko cell line was generated using CRISPR/Cas9 as part of my master thesis (supervisors: Dr. Martin Müller, Prof. Dr. Angelika Vollmar, Pharmaceutical Biology, LMU Munich) and is described in detail in Dr. Martin Müller's doctorate thesis [106]. To verify our hypothesis, we first compared VCR-R CEM TPC2 wt and VCR-R CEM TPC2 ko cells regarding their sensitivity to weak base cytostatics, including vincristine, doxorubicin, and topotecan. Analyzing inhibition of proliferation and calculation of respective IC50 values revealed that TPC2 ko cells are around 3-fold more sensitive to vincristine, around 4-fold more sensitive to doxorubicin and around 2-fold more sensitive to topotecan (Fig. 7A). In line with proliferation experiments, TPC2 ko cells were also more sensitive to the tested cytostatics in apoptosis assays with around 2- to 3-fold lower EC50 values (Fig. 7B). Furthermore, doxorubicin treatment caused significantly increased PARP cleavage and caspase 3 activation, two prominent markers of apoptosis induction, in TPC2 ko cells as compared to TPC2 wt cells (Fig. 7C). As all tested cytostatics are known to induce cell cycle arrest in G2/M phase [118-120], we quantified the cell population in G2/M phase, showing that G2/M arrest is increased in TPC2 ko cells upon chemotherapy (Fig. 7D). Moreover, inhibition of clonogenic growth upon doxorubicin treatment was more pronounced in TPC2 ko cells (Fig. 7E). These data clearly demonstrate that loss-of-TPC2-function sensitizes VCR-R CEM cells to cytostatics and emphasize that targeting TPC2 is a promising approach to improve chemotherapy response.

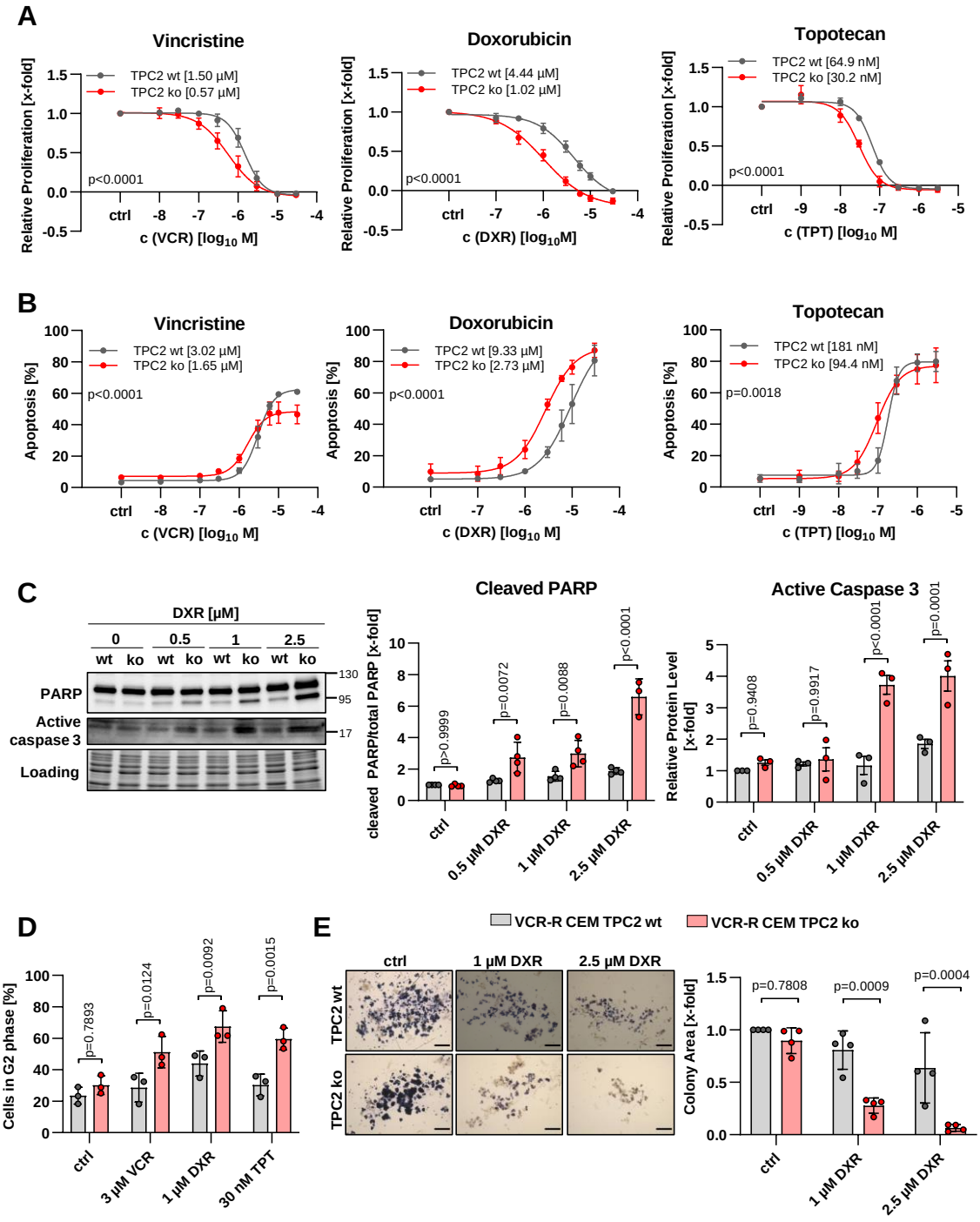

Figure 7. Loss-of-TPC2-function sensitizes VCR-R CEM cells to cytostatics.
A VCR-R CEM TPC2 wt and TPC2 ko cells were treated for 72 h and relative proliferation was assessed using CellTiter-Blue reagent. **B** Cells were treated for 48 h and apoptosis was quantified by propidium iodide staining under permeabilizing conditions and flow cytometry (VCR, TPT) or using the FSC/SSC method (DXR). **C** Cells were treated for 24 h and PARP cleavage and caspase 3 activation were analyzed by immunoblotting. **D** Cells were treated for 24 h and cells in G2 phase were quantified by propidium iodide staining under permeabilizing conditions and flow cytometry. **E** Cells were treated for 4 h, reseeded in colony formation medium and incubated for 7 d. Colonies were visualized by incubation with MTT reagent and colony area was quantified in ImageJ. Scale bar is 200 µm. Data are presented as mean ± SD from at least three independent experiments. Statistical significance was analyzed by extra sum-of-squares F test using the comparison of fits function in GraphPad Prism 9 (**A**, **B**) or two-way ANOVA with Sidak's posttest (**C**-**E**).

4.1.2.2 Chemosensitization of TPC2 ko is independent of P-gp

Due to high P-gp expression in VCR-R CEM cells (Fig. 4B) and the implication of TPC2 in trafficking of membrane proteins [121], we investigated whether chemosensitization by loss-of-TPC2-function is mechanistically connected to P-gp. Indeed, we found that P-gp is differentially regulated upon loss-of-TPC2-function. While mRNA levels of ABCB1 were increased upon TPC2 ko (Fig. 8A), membranous P-gp levels were significantly decreased (Fig. 8B), suggesting defects in membrane trafficking of P-gp. Therefore, we combined the cytostatic P-gp substrates vincristine and doxorubicin with the P-gp inhibitors verapamil and ketoconazole in TPC2 wt and TPC2 ko cells and analyzed relative proliferation. Noteworthy, there was still a difference in sensitivity detectable between TPC2 wt and TPC2 ko upon P-gp blockade (Fig. 8C), emphasizing that the observed chemosensitizing effect of TPC2 ko was not mediated by differential regulation of P-gp.

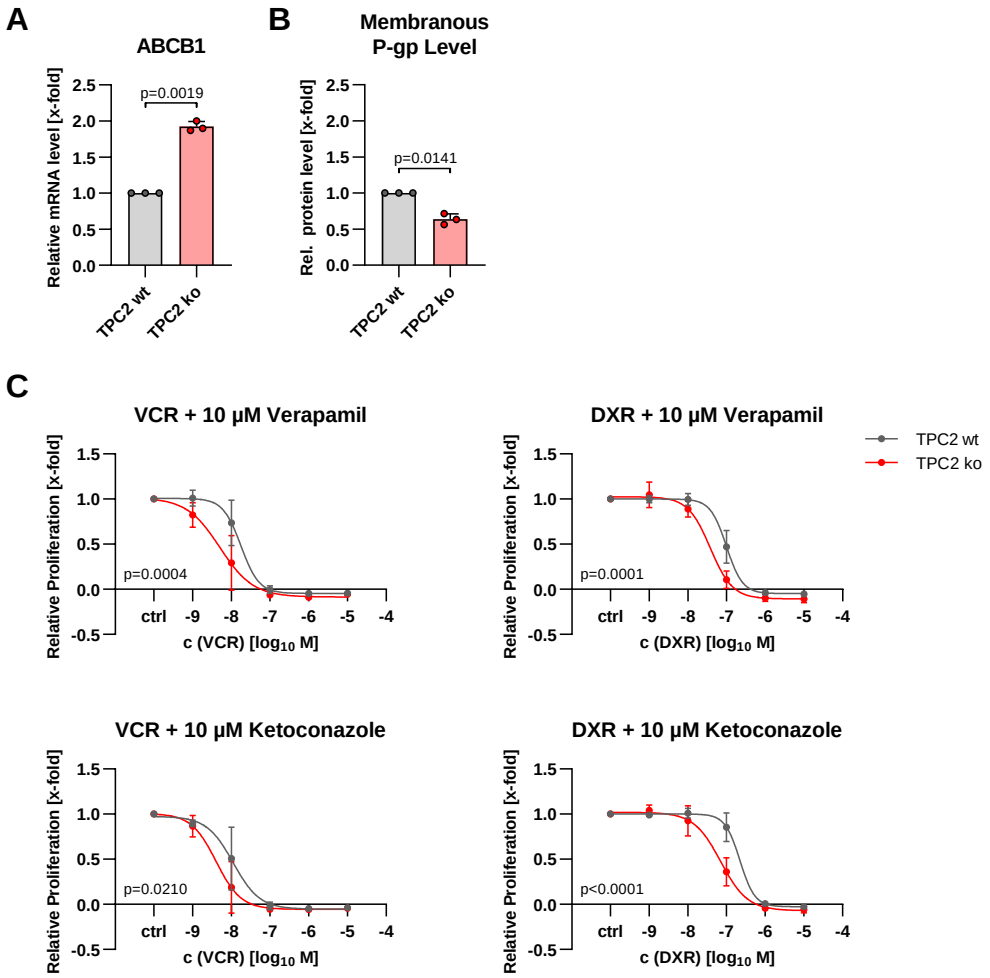

Figure 8. Chemosensitization by TPC2 ko is independent of P-gp. (Figure legend on next page)

Figure 8. Chemosensitization by TPC2 ko is independent of P-gp.
A ABCB1 mRNA levels of untreated VCR-R CEM TPC2 wt and TPC2 ko cells were analyzed by qPCR. **B** Membranous P-gp levels were analyzed by antibody staining and flow cytometry. **A**, **B** These experiments were conducted during my master thesis under supervision of Dr. Martin Müller (Pharmaceutical Biology, Prof. Dr. Angelika Vollmar, LMU Munich). **C** Cells were either treated with increasing concentrations of VCR or DXR alone, or in combination with 10 µM verapamil or 10 µM ketoconazole for 72 h and relative proliferation was assessed using CellTiter-Blue reagent. Data are presented as mean ± SD from at least three independent experiments.

4.1.2.3 Pharmacological TPC2 inhibition sensitizes leukemia cells to chemotherapy

As the next step, we aimed at verifying TPC2 as a reasonable target to achieve chemosensitization and furthermore, we investigated its druggability by using pharmacological TPC2 inhibitors. Of note, many available TPC2 inhibitors, such as tetrandrine, are substrates or inhibitors of P-gp [122]. Hence, we tested a collection of TPC2 inhibitors, including tetrandrine, naringenin, and Ned-19, for P-gp inhibition using the fluorescent P-gp substrates calcein-AM and doxorubicin. Importantly, tetrandrine and Ned-19 blocked P-gp activity evident by increased calcein-AM fluorescence intensity upon treatment, whereas naringenin treatment did not cause increased fluorescence (Supp. Fig. 1A). This was also true for doxorubicin as a model substrate, demonstrating that naringenin does not influence P-gp-mediated efflux of xenobiotics in our setting (Supp. Fig. 1B).

Therefore, we initially chose naringenin to confirm our findings in VCR-R CEM cells to avoid potential off-target effects. A combination of vincristine with naringenin led to significantly enhanced antiproliferative activity in TPC2 wt cells, while there was no further sensitization observed in TPC2 ko cells (Fig. 9A). These results indicate that TPC2 is a druggable target for chemosensitization and naringenin increases chemosensitivity by inhibiting TPC2. Hence, we were able to examine the effectiveness of this combination approach in different cell lines, demonstrating that this combination was also beneficial in drug-naïve CCRF-CEM and Jurkat cells (Fig. 9B). Synergism between TPC2 inhibitors and vincristine in leukemic cells was moreover confirmed using tetrandrine, except for Jurkat cells, in which this combination did not significantly increase vincristine sensitivity (Fig. 9C). Along the line, tetrandrine co-treatment sensitized VCR-R CEM TPC2 wt cells to doxorubicin and topotecan (Fig. 9D), whereas combination with naringenin failed to increase sensitivity to doxorubicin and topotecan (Fig. 9E). Adapting these combinations to other cell lines showed that also HeLa (Fig. 10A) and HepG2 (Fig. 10B) cells are more sensitive to vincristine and doxorubicin when combined either with naringenin or tetrandrine, emphasizing that TPC2 inhibition as chemosensitizing strategy is not only feasible in leukemia, but also in solid cancer cell lines.

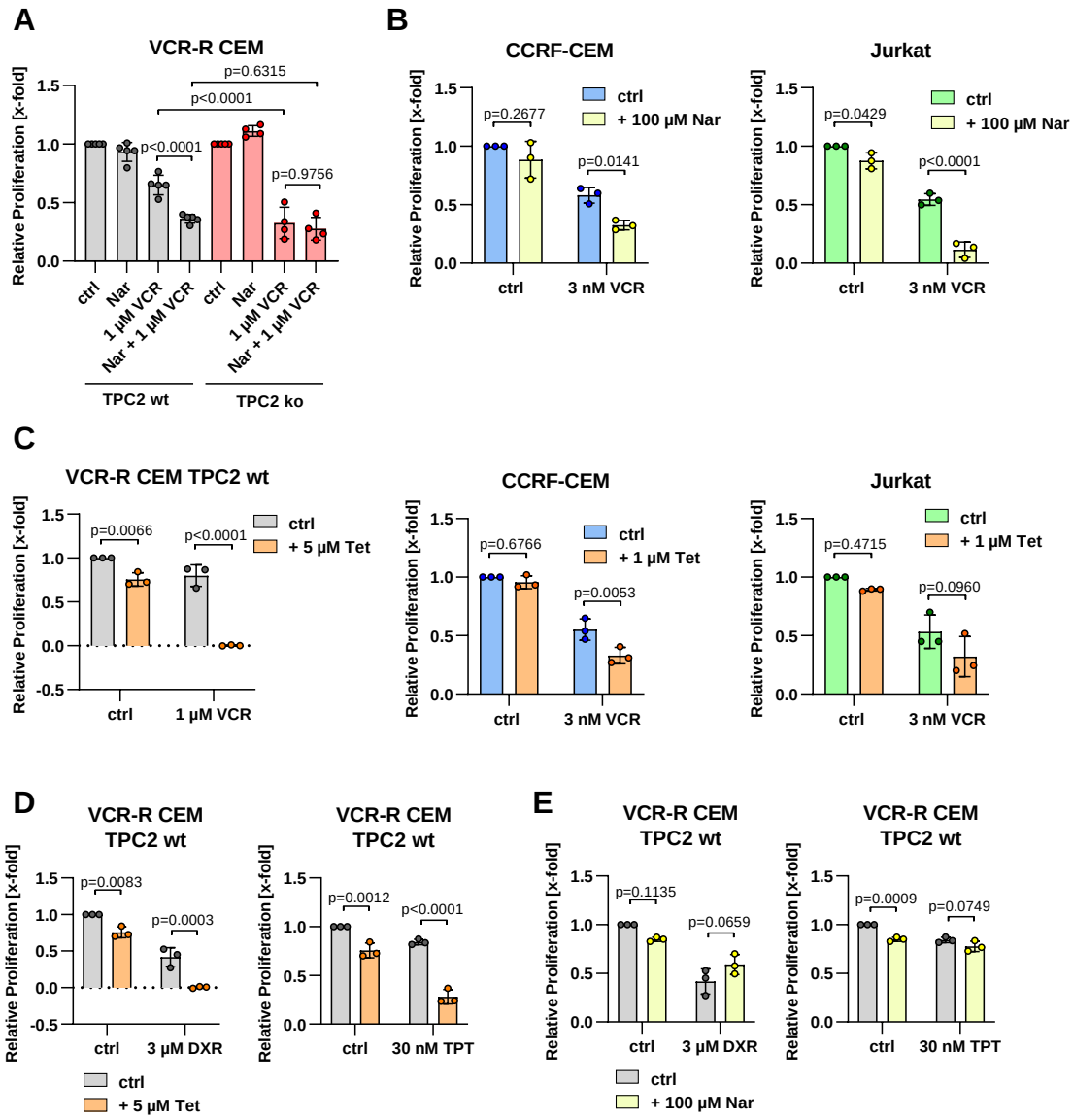

Figure 9. Pharmacological TPC2 inhibition sensitizes leukemic cells to cytostatics.
VCR-R CEM TPC2 wt and TPC2 ko cells (**A**), CCRF-CEM and Jurkat cells (**B**) were treated with VCR alone or in combination with 100 µM Nar. **C** VCR-R CEM TPC2 wt, CCRF-CEM and Jurkat cells were treated with VCR alone or in combination with Tet. **D** VCR-R CEM TPC2 wt cells were treated with DXR or TPT alone or in combination with Tet. **E** VCR-R CEM TPC2 wt cells were treated with DXR or TPT alone or in combination with Nar. **A**-**E** After 72 h of treatment, relative proliferation was assessed using CellTiter-Blue reagent. Data are presented as mean ± SD from at least three independent experiments. Statistical significance was analyzed by two-way ANOVA with Tukey's posttest (**A**) or Sidak's posttest (**B**-**E**).

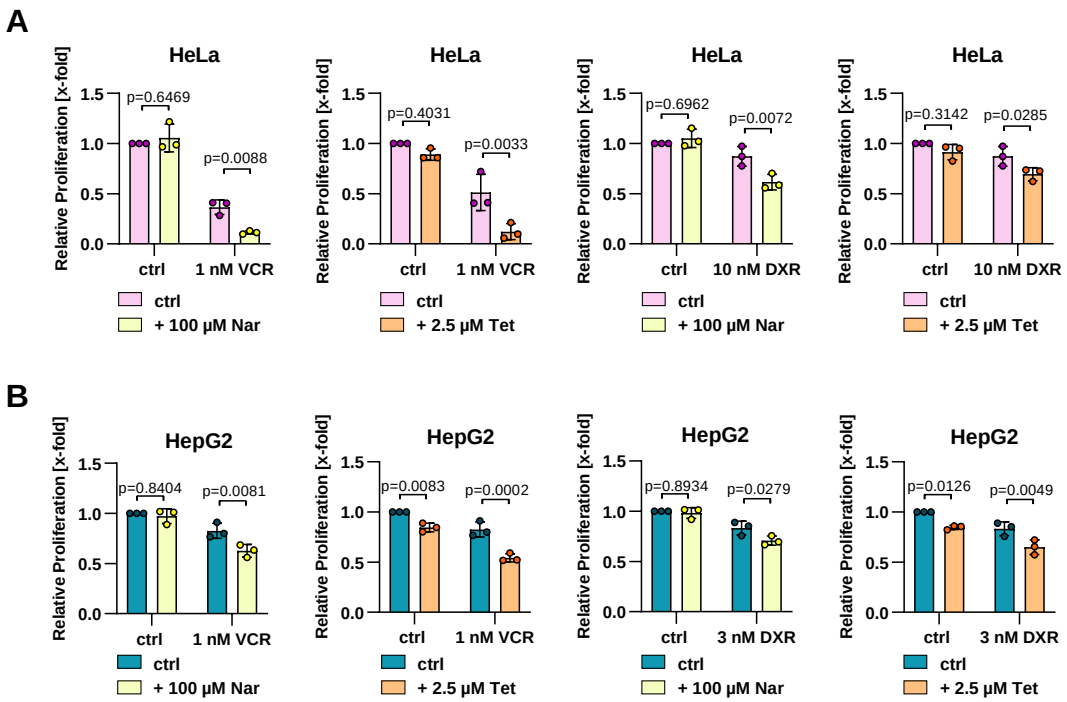

Figure 10. Pharmacological TPC2 inhibition sensitizes solid tumor cell lines to cytostatics.
HeLa cells (**A**) and HepG2 cells (**B**) were treated with VCR or DXR alone or in combination with Nar or Tet for 72h. **A** Relative proliferation was assessed using CellTiter-Blue reagent. **B** Relative proliferation was assessed using MTT. Data are presented as mean ± SD from three independent experiments. Statistical significance was analyzed by two-way ANOVA with Tukey's posttest.

To reflect ALL heterogeneity in the clinic, patient-derived xenograft ALL cells were utilized as an established *in vitro* model [123] (Supp. Fig. 2A). A combination of different vincristine concentrations and 1 or 5 µM tetrandrine significantly increased apoptosis as compared to single treatment. Importantly, tetrandrine treatment was hardly toxic for peripheral blood mononuclear cells (PBMC), neither in monotherapy nor in combination with vincristine (Fig. 11A, Supp. Fig. 2B for statistics). These results suggest that vincristine combined with TPC2 inhibition preferentially targets cancer cells, emphasizing a therapeutic margin of this approach. Of note, chemosensitization by tetrandrine was independent of P-gp, as only very low ABCB1 mRNA were detectable in PDX samples (Fig. 11B), indicating that tetrandrine sensitizes PDX ALL cells to vincristine via inhibiting TPC2. Therefore, we checked for TPC2 mRNA levels of PDX cells to correlate vincristine sensitivity expressed as area under the curve (AUC) to TPC2 expression. However, no correlation could be observed (Fig. 11C). Moreover, a comparison of TPC2 mRNA levels of PBMCs and PDX cells revealed no significant difference (Fig. 11D).

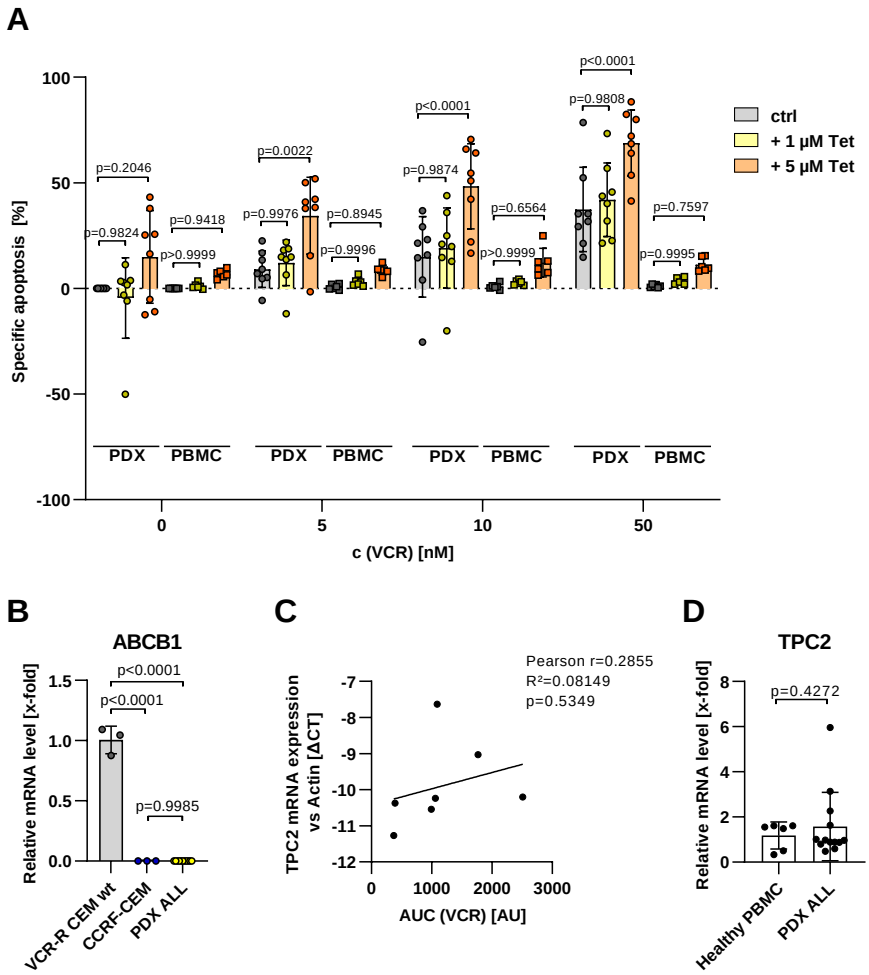

Figure 11. TPC2 inhibition sensitizes patient-derived xenograft (PDX) ALL cells to VCR.
A PDX ALL cells (circles) and peripheral blood mononuclear cells (PBMC, squares) were either treated with VCR alone or in combination with Tet for 48h and specific apoptosis was quantified by the FSC/SSC method and flow cytometry. **B** ABCB1 mRNA levels of untreated PDX ALL cells in comparison to VCR-R CEM TPC2 wt and CCRF-CEM cells were analyzed by qPCR. **C** TPC2 mRNA levels of untreated healthy PBMC and PDX ALL cells were analyzed by qPCR. **D** Correlation between sensitivity of PDX ALL cells to VCR described as area under the curve (AUC; high AUC means high sensitivity) and TPC2 mRNA levels was conducted by calculating the Pearson coefficient and R squared. Data are presented as mean ± SD from eight (PDX ALL) or six (PBMC) independent experiments. Statistical significance was analyzed by two-way ANOVA with Tukey's posttest (**A**), one-way ANOVA with Tukey's posttest (**B**), student's t-test with Welch's correction (**C**) or simple linear regression with subsequent Pearson correlation (**D**).

4.1.3 Loss-of-TPC2-function alters intracellular drug distribution

4.1.3.1 Increased lysosomal pH impedes lysosomal drug sequestration in TPC2 ko cells

As outlined in chapter 2.2.1, sequestration of weak base drugs in lysosomes is an established chemoresistance mechanism, by which cancer cells are able to prevent an excessive accumulation of cytostatics at their sites of action. The acidity of lysosomes is an important feature on this occasion, as it enables lysosomal accumulation and protonation of weak base drugs [29]. Therefore, we were curious whether loss-of-TPC2-function alters lysosomal acidity. Indeed, semi-quantitative pH measurements using LysoSensor Green revealed that lysosomes of TPC2 ko cells were less acidic, as evident by decreased fluorescence intensity in flow cytometry (Fig. 12A) as well as confocal microscopy experiments (Fig. 12B).

As a result of the accumulation of weak bases in lysosomes, the intraluminal pH increases [124]. Therefore, we analyzed lysosomal sequestration of doxorubicin in TPC2 wt and TPC2 ko cells by determining lysosomal pH after short-term doxorubicin treatment. A significant decrease of LysoSensor fluorescence and thus lysosomal sequestration of doxorubicin was only detected in TPC2 wt cells, while intraluminal pH in TPC2 ko cells remained unchanged (Fig. 12C). Along the line, only TPC2 wt cells showed induction of lysosomal stress evident by an increase in lysosomal volume (Fig. 12D). Of note, similar results were obtained upon short-term topotecan treatment (Fig. 12D). Additionally, combination with the lysosomotropic compound ammonium chloride which causes lysosomal alkalinization [125], decreased intracellular doxorubicin levels in TPC2 wt, but not in TPC2 ko cells (Fig. 12E). These results emphasize that, in contrast to TPC2 wt cells, TPC2 ko cells are not capable of sequestering weak base cytostatics inside their lysosomes.

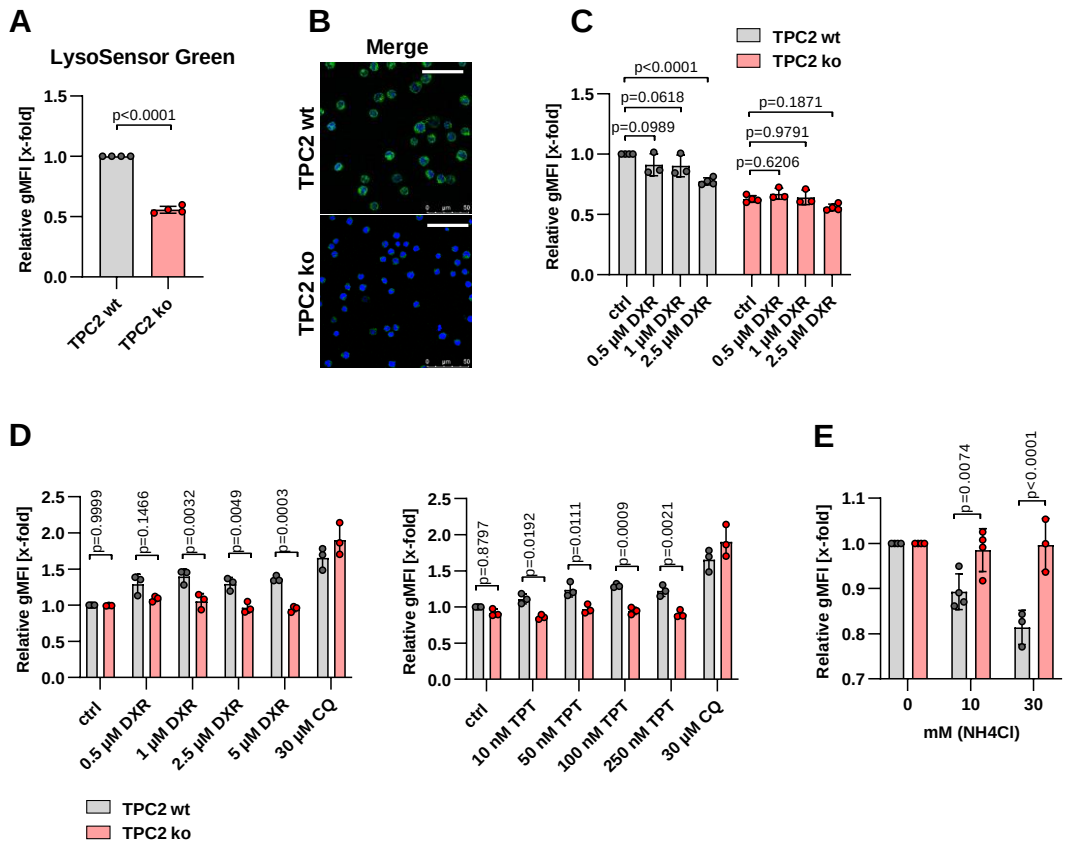

Figure 12. Decreased lysosomal acidity upon loss-of-TPC2-function impairs lysosomal drug sequestration. Lysosomal pH of untreated VCR-R CEM TPC2 wt and TPC2 ko cells was semi-quantitatively analyzed by LysoSensor Green staining and flow cytometry (**A**) or confocal microscopy (**B**, scale bar is 50 µm). **A**, **B** Higher fluorescence intensity indicates more acidic lysosomes. **C** Cells were treated for 1 h and lysosomal pH was analyzed by LysoSensor Green staining and flow cytometry. **D** Cells were treated for 4 h and lysosomal volume was quantified by LysoTracker Green staining and flow cytometry. **E** Cells were treated with 2.5 µM DXR alone or in combination with ammonium chloride for 24 h and intracellular DXR levels were assessed by flow cytometry. Note that the y-axis does not start at 0.0 and that results are normalized to the DXR control of each cell line. Data are presented as mean ± SD from at least three independent experiments. Statistical significance was analyzed by student's t-test (**A**) or two-way ANOVA with Sidak's posttest (**C**-**E**).

4.1.3.2 Increased nuclear doxorubicin abundance causes increased DNA damage in TPC2 ko cells

Having shown that loss-of-TPC2-function prevents lysosomal drug sequestration, the question arose if this affects intracellular drug distribution. Therefore, nuclear doxorubicin accumulation was quantified by confocal microscopy, showing that TPC2 ko cells have increased nuclear doxorubicin levels after 4 h of treatment (Fig. 13A). Moreover, doxorubicin fluorescence in TPC2 ko cells was almost exclusively detected inside the nucleus, while in TPC2 wt cells doxorubicin was also abundant in cytoplasmic regions (Fig. 13B, arrows).

As doxorubicin exerts its cytotoxicity by intercalating into DNA, increased nuclear accumulation of doxorubicin should lead to increased induction of DNA damage. To verify this hypothesis, γ-H2AX expression, a widely used marker for DNA damage [126], was quantified prior to

significant apoptosis induction (Fig. 13C). Quantification of DNA damage by γ-H2AX detection emphasized significantly increased DNA damage in TPC2 ko cells as compared to TPC2 wt cells after 4 h of treatment. Concurrently, cleavage of PARP was not detectable in this time range (Fig. 13D). Of note, TPC2 ko cells were not more sensitive to the non-basic cytostatics 5-fluoruracil and paclitaxel (Fig. 13E), emphasizing that chemosensitization by loss-of-TPC2-function depends on impaired lysosomal sequestration of weak base cytostatics.

Since calcium flux from two-pore channels is an important regulator of TFEB [127], whose activity was recently connected to p53-mediated DNA damage response [128], we analyzed phosphorylation of common DNA damage response proteins. However, no significant alterations in phosphorylation of the DNA damage repair-associated proteins p53 and ATM were detected (Fig. 14), suggesting that DNA damage response and repair are not affected by TPC2 ko. In summary, these data emphasize that TPC2 ko impairs lysosomal drug sequestration, leading to increased nuclear abundance of doxorubicin, increased DNA damage induction and ultimately increased apoptosis.

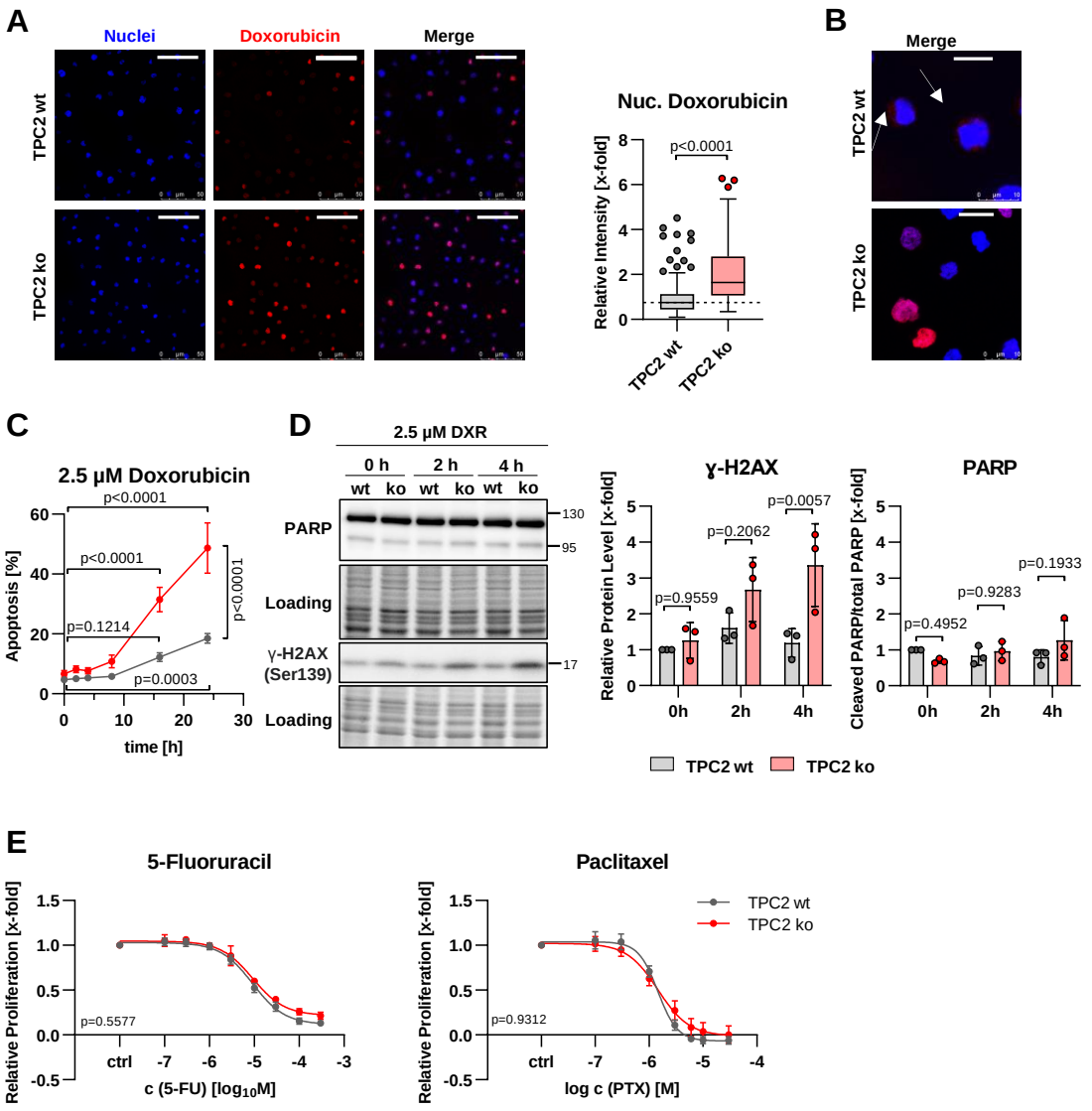

Figure 13. TPC2 ko promotes nuclear DXR accumulation and increases DXR-induced DNA damage.
A VCR-R CEM TPC2 wt and TPC2 ko cells were treated for 4 h and nuclear DXR was analyzed by confocal microscopy by simultaneous staining of nuclei using Hoechst 33342 and quantified in ImageJ. Scale bar is 50 µm. **B** Zoom from **A** showing the intracellular distribution of DXR. Arrows indicate cytoplasmic abundance. Scale bar is 10 µm. Note that brightness and contrast were adjusted to improve visibility. **C** Time-dependent apoptosis was determined using the FSC/SSC method by flow cytometry. **D** PARP cleavage and phosphorylation of H2AX at Ser139 were quantified by immunoblotting after treatment with DXR (0-4 h). **E** Cells were treated for 72 h and relative proliferation was assessed using CellTiter-Blue reagent. Data are presented as box and whiskers with Tukey depiction (**A**) or mean ± SD (**B**-**E**) from at least three independent experiments. Statistical significance was analyzed by Mann-Whitney test (**A**), two-way ANOVA with Tukey's posttest (**C**) or Sidak's posttest (**D**) or by extra sum-of-squares F test using the comparison of fits function in GraphPad Prism 9 (**E**).

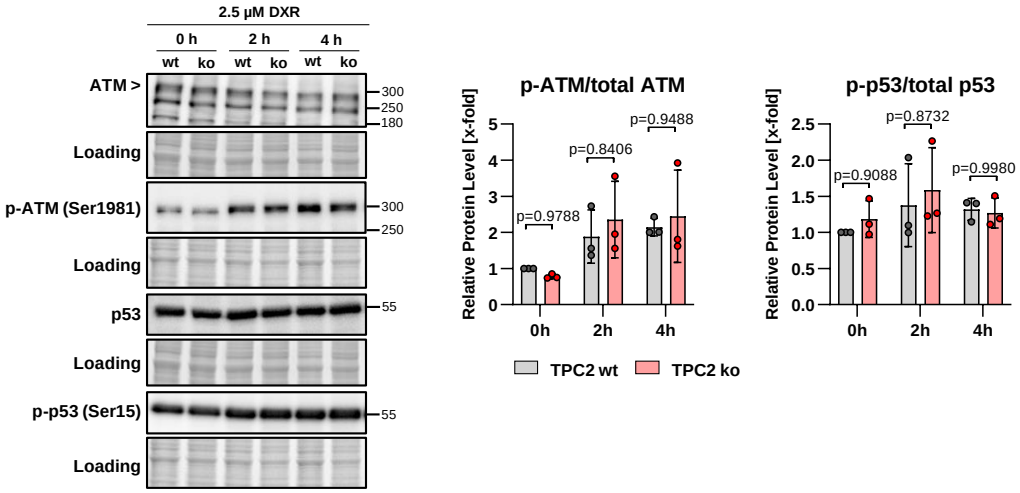

Figure 14. Chemosensitization upon TPC2 ko is not associated with impaired DNA damage response. VCR-R CEM TPC2 wt and TPC2 ko cells were treated with DXR (0-4 h) and DNA damage-associated proteins and their phosphorylated forms were quantified by immunoblotting. Data are presented as mean ± SD from three independent experiments. Statistical significance was analyzed by two-way ANOVA with Sidak's posttest.

4.1.4 Loss-of-TPC2-function promotes chemotherapy-induced lysosomal cell death

4.1.4.1 TPC2 ko cells are more prone to lysosomal damage

We further evaluated lysosomal characteristics and next focused on lysosomal size. Confocal microscopy analysis of LysoTracker-loaded cells revealed that the diameter of lysosomes of TPC2 ko cells is significantly increased (Fig. 15A). Hence, expression levels of lysosome-associated genes were analyzed to check whether this phenomenon is associated with increased lysosomal biogenesis. Notably, mRNA levels of most lysosome-associated genes were not significantly altered, except for CTSB which was increased in TPC2 ko cells (Fig. 15B). Therefore, we assumed that lysosomal biogenesis, in general, is not considerably altered, yet lysosomes of TPC2 ko cells appear to be swollen. Interestingly, this phenomenon has been previously associated with increased susceptibility to lysosomal damage and subsequently LCD induction [18, 129].

Therefore, an acridine orange-based lysosomal damage assay was employed to analyze susceptibility to lysosomal damage of TPC2 wt and TPC2 ko cells. Acridine orange accumulates in acidic compartments, and the resulting increased acridine orange concentrations lead to the formation of so-called stacks, causing a shift in emission wavelength from green (monomers) to red (stacks) [130]. Moreover, acridine orange is photosensitizing, facilitating the destruction of lysosomal membranes by exposition to high-intensity laser light [131]. Lysosomal damage then leads to leakage of acridine orange into the cytosol, leading to a shift in emission wavelength back to green fluorescence [130]. Interestingly, TPC2 ko cells loaded with acridine orange and exposed to high-intensity laser light showed a stronger increase in green-to-red fluorescence ratio as compared to TPC2 wt cells, indicating increased susceptibility to lysosomal damage (Fig. 15C). Additionally, we analyzed cytostatics-induced lysosomal damage by LysoTracker staining. Quantification of LysoTracker-negative cells after doxorubicin, vincristine, or topotecan treatment revealed a higher proportion of cells with damaged lysosomes in TPC2 ko cells as compared to TPC2 wt cells (Fig. 15D). In addition, increased lysosomal damage in TPC2 ko cells was also observed upon treatment with the widely used lysosomal damage inducer LLOMe (Fig. 15D). These results emphasize that lysosomes of TPC2 ko cells are more susceptible to lysosomal damage, either induced by phototoxicity or cytostatics.

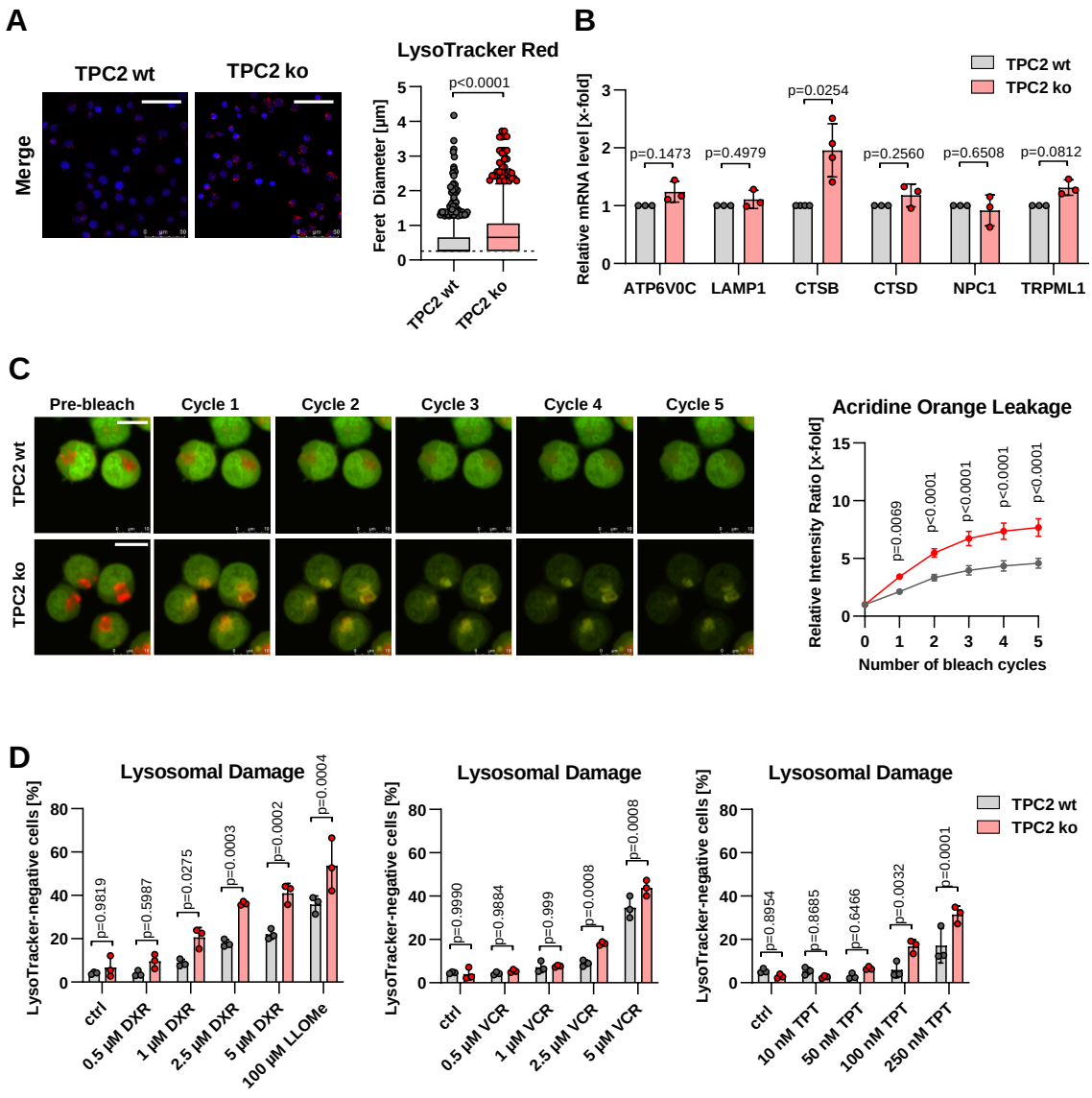

Figure 15. Lysosomes of TPC2 ko cells are more susceptible to lysosomal damage.
A Lysosomal diameter of untreated VCR-R CEM wt and TPC2 ko cells was analyzed by LysoTracker Red staining and confocal microscopy. Scale bar is 50 µm. Lysosomal diameter was quantified in ImageJ by calculation of the Feret diameter of single lysosomes. **B** mRNA levels of lysosome-associated genes were assessed by qPCR. **C** Susceptibility to lysosomal damage was assessed by acridine orange staining and exposition to high intensity laser light in 5 cycles by confocal microscopy. Scale bar is 10 µm. Note that brightness and contrast were adjusted to improve visibility. Acridine orange leakage from lysosomes into the cytosol upon lysosomal damage was quantified by calculation of the green-to-red ratio at acidic (red) spots. **D** Cells were treated for 24 h with cytostatics and lysosomal damage was determined by quantifying LysoTracker Green-negative cells by flow cytometry. LLOMe served as positive control. Data are presented as box and whiskers with Tukey depiction (**A**) or mean ± SD (**B**-**D**) from three independent experiments. Statistical significance was analyzed by Mann-Whitney test (A), student's t-test with Welch's correction (**B**) or one-way ANOVA with Sidak's posttest (**C**, **D**).

4.1.4.2 Possible mechanisms causing increased susceptibility to lysosomal damage

To get an insight into the underlying mechanism of TPC2 ko promoting lysosomal damage, several proteins were analyzed which have been previously connected to the regulation of lysosomal stability [132], revealing different expression levels upon TPC2 ko. While there were no alterations of Bcl-xL protein levels, other lysosome-stabilizing proteins, i.e. Hsp70 and Bcl-2, were downregulated in TPC2 ko cells (Fig. 16A). Furthermore, the pro-apoptotic protein Bax, which is thought to be lysosome destabilizing [132], was upregulated (Fig. 16A). Hsp70 promotes lysosomal stability by serving as a co-factor for the acid sphingomyelinase (ASMase, SMPD1) which catalyzes the reaction of sphingomyelin to ceramide and thereby creates a membrane-stabilizing milieu [133]. Therefore, we analyzed expression levels of SMPD1, and of the acid ceramidase (ASAH1) which catalyzes the reaction of membrane-stabilizing ceramide to sphingosine. Interestingly, SMPD1 was upregulated upon TPC2 ko, while ASAH1 mRNA levels were significantly downregulated (Fig. 16B), suggesting alterations in sphingolipid metabolism.

Of note, these results do neither prove differences in intracellular sphingomyelin, ceramide, and sphingosine levels nor in respective enzyme activities. Therefore, we checked how pharmacological ASMase inhibition with the model inhibitor siramesine influences doxorubicin sensitivity in TPC2 wt and TPC2 ko cells. Indeed, siramesine co-treatment led to chemosensitization, increasing doxorubicin-induced apoptosis by more than factor 3 in TPC2 wt cells (Fig. 16C). Since chemosensitization also occurred in TPC2 ko cells, albeit to a much lesser extent, and doxorubicin and siramesine co-treatment still caused significantly increased apoptosis in TPC2 ko cells as compared to TPC2 wt cells (Fig. 16C), this hypothesis was not further pursued.

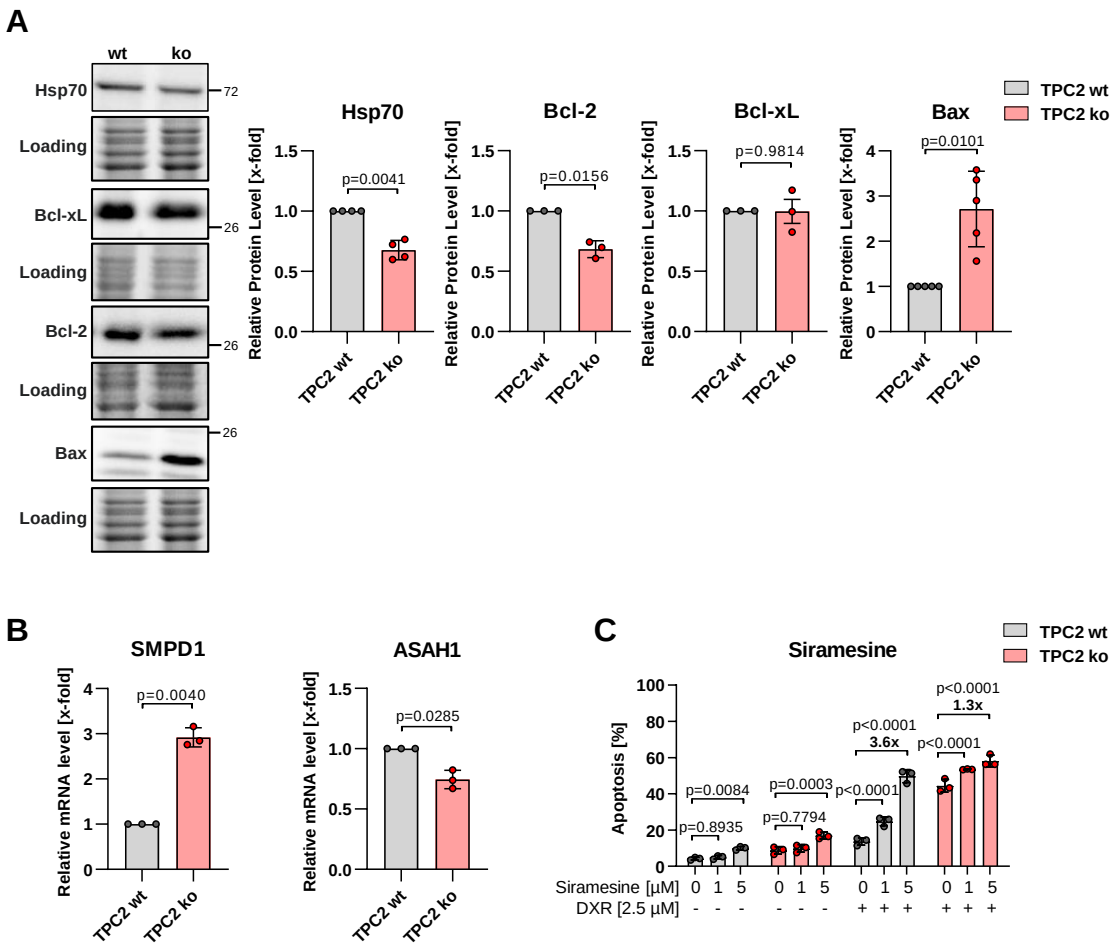

Figure 16. Mechanistic insights into increased susceptibility to lysosomal damage upon TPC2 ko.
A Protein expression levels of untreated VCR-R CEM TPC2 wt and TPC2 ko cells were quantified by immunoblotting. **B** SMPD1 and ASAH1 mRNA levels were analyzed by qPCR. **D** Cells were treated either with DXR alone or in combination with siramesine for 24 h and apoptosis was quantified using the FSC/SSC method by flow cytometry. Data are presented as mean ± SD from at least three independent experiments. Statistical significance was analyzed by student's t-test with Welch's correction (**A**, **B**) or two-way ANOVA with Tukey's posttest (**C**).

4.1.4.3 Lysosomal damage contributes to cell death

As lysosomal damage is known to initiate LCD, we analyzed relevant LCD hallmarks upon doxorubicin treatment. The main executors of LCD are cathepsins, proteases located inside the lysosomal lumen which leak into the cytosol upon lysosomal damage. Due to their proteolytic activity, cytosolic cathepsins can directly cause LCD and promote apoptotic signaling, for example by degradation or truncation of apoptosis-regulating proteins [18]. Therefore, cathepsin B levels were analyzed in lysosome-free cytosolic fractions, revealing increased levels in TPC2 ko cells (Fig. 18A). This effect was observed in untreated cells as well as in doxorubicin-treated cells, whereas doxorubicin treatment did not significantly enhance translocation of cathepsin B to the cytosol neither in TPC2 wt nor in TPC2 ko cells (Fig. 17A).

Of note, increased expression levels are not necessarily accompanied by increased enzymatic activity. Hence, cathepsin B activity was determined using a fluorescence-based enzyme activity assay relying on the cathepsin B substrate RR-AFC. While cathepsin B activity was not altered in untreated TPC2 ko cells, doxorubicin treatment led to a significant increase in cathepsin B activity in TPC2 ko cells as compared to TPC2 wt cells (Fig. 17B). The specificity of RR-AFC for cathepsin B was simultaneously confirmed by pharmacological cathepsin B inhibition which almost fully abolished AFC fluorescence (Fig. 17B). Furthermore, doxorubicin treatment led to increased expression of cathepsin B (Fig. 17C) and cathepsin D (Fig. 17D) in TPC2 ko cells, which could also be confirmed on protein level for cathepsin B (Fig. 17E). One main cytosolic target of cathepsin B is the pro-apoptotic protein Bid which is truncated by active cathepsin B [134]. Therefore, truncated Bid was analyzed in mitochondrial fractions. In line with increased expression and proteolytic activity of cathepsin B, the truncated variant of Bid was only detected in doxorubicin-treated TPC2 ko cells, whereas it was not found in TPC2 wt cells upon doxorubicin treatment (Fig. 17F).

To further verify the role of cathepsin B in cell death of TPC2 ko cells, doxorubicin was combined with the cathepsin B inhibitor CA-074Me. Interestingly, co-treatment with CA-074Me inhibited doxorubicin-induced apoptosis in TPC2 ko cells (Fig. 18A). This effect was specific for cathepsin B inhibition, as inhibition of cathepsin C with pepstatin A had no effect on doxorubicin sensitivity (Fig. 18B). Additionally, inhibition of cathepsin B inhibited doxorubicin-induced caspase 3 activation in TPC2 ko cells (Fig. 18C). These findings emphasize that activation of cathepsin B upon doxorubicin treatment leads to induction of LCD in TPC2 ko cells which probably interacts with pro-apoptotic signaling by truncation of Bid and activation of caspase 3.

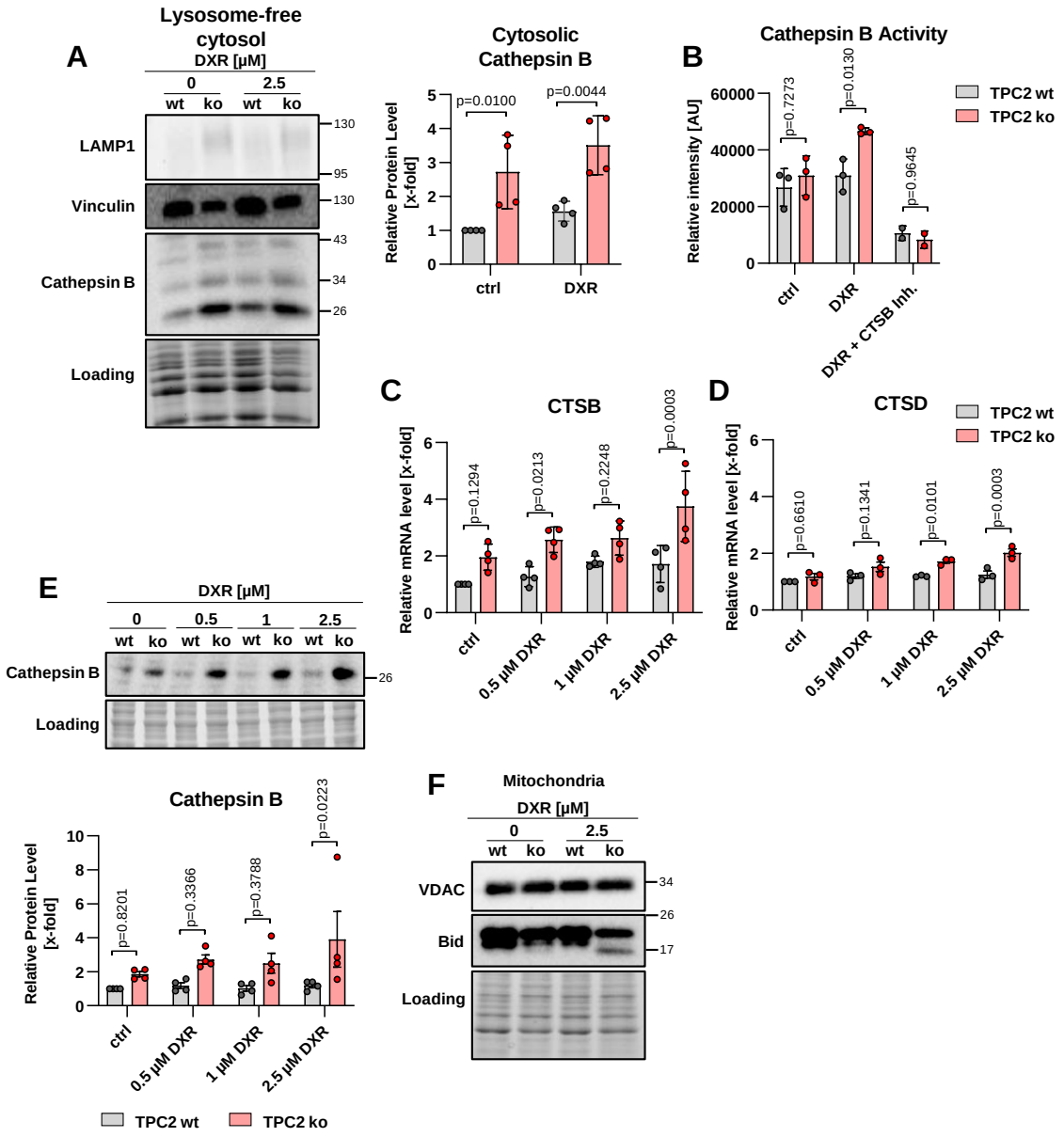

Figure 17. DXR induces LCD in TPC2 ko cells.
A VCR-R CEM TPC2 wt and TPC2 ko cells were treated for 24 h and cytosolic cathepsin B levels were analyzed by immunoblotting after separation of lysosomes from the cytosolic fraction. **B** Cathepsin B activity was assessed after 24 h of treatment using a cathepsin B-specific RR-AFC-based detection kit. Simultaneous treatment of cell lysates with a cathepsin B inhibitor served as control. CTSB (**C**) and CTSD (**D**) mRNA levels were quantified by qPCR after 24 h of treatment. **E** Cathepsin B protein levels were quantified by immunoblotting after 24 h of treatment. **F** Cells were treated for 24 h and the truncation of Bid in the mitochondrial fraction was analyzed by immunoblotting. Data are presented as mean ± SD from at least three independent experiments. Statistical significance was analyzed by two-way ANOVA with Sidak's posttest (**A**-**E**).

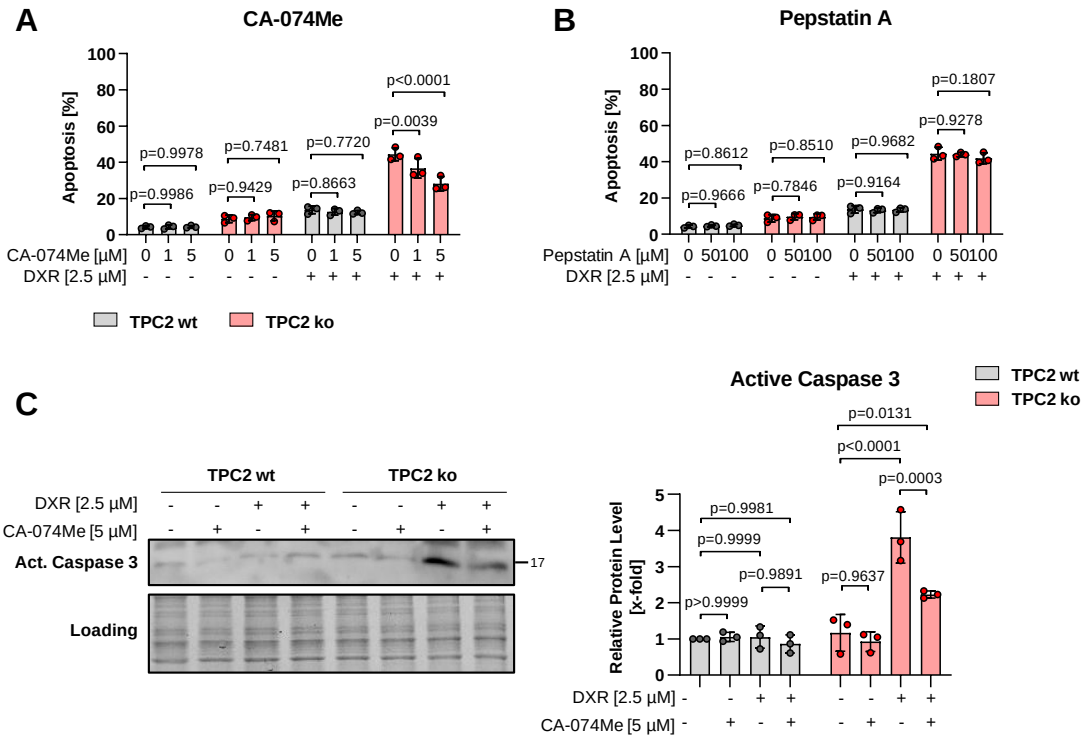

Figure 18. Cathepsin B-dependent LCD contributes to increased chemosensitivity of TPC2 ko cells.
A, **B** Cells were treated either with DXR alone or in combination with CA-074Me (**A**) or Pepstatin A (**B**) for 24 h and apoptosis was quantified using the FSC/SSC method by flow cytometry. **C** Cells were treated either with DXR alone or in combination with CA-074Me for 24 h and caspase 3 activation was analyzed by immunoblotting. Data are presented as mean ± SD from three independent experiments. Statistical significance was analyzed by two-way ANOVA with Tukey's posttest (**A**, **B**) or Sidak's posttest (**C**).

4.1.4.4 Involvement of other cell death pathways

As mentioned above, there is a deep crosstalk of LCD with mitochondria-mediated apoptosis. Having detected truncated Bid and activation of caspase 3 in dependence on cathepsin B activity, we analyzed potential alterations in the mitochondrial apoptosis pathway in TPC2 ko cells. In this context, MitoTracker staining of untreated TPC2 wt and TPC2 ko cells revealed increased mitochondrial mass (Fig. 19A) which is commonly accepted as a compensatory mechanism for mitochondrial dysfunction [135]. Therefore, we analyzed the mitochondrial abundance of Hsp70 which is important for mitochondrial integrity and function [136] and was earlier found to be downregulated in whole cell lysates of TPC2 ko cells (Fig. 17A). Supporting the mitochondrial phenotype described above, mitochondrial fractions of TPC2 ko cells contained significantly less Hsp70 (Fig. 19B). Hence, the mitochondrial membrane potential of TPC2 wt and TPC2 ko cells was analyzed. Maintaining the mitochondrial membrane potential is a very important requirement for mitochondrial function and its perturbation, for example by mitochondrial outer membrane permeabilization, can cause the initiation of apoptosis [137]. Yet, staining with DIOC6 whose accumulation in mitochondria depends on the mitochondrial membrane potential [138], displayed no alterations upon loss-of-TPC2-function (Fig. 19C). Further, the analysis of two important hallmarks of mitochondrial apoptosis, the release of cytochrome c from mitochondria into the cytosol and the activation of caspase 9 [139] were analyzed upon doxorubicin treatment. Unexpectedly, neither in TPC2 wt nor in TPC2 ko cells release of cytochrome c (Fig. 19D) or activation of caspase 9 could be observed (Fig. 19E), emphasizing that induction of apoptosis occurs independently from the intrinsic, mitochondrial apoptotic signaling pathway. Nevertheless, pan-caspase inhibition with Z-VAD-FMK reduced doxorubicin-induced apoptosis in TPC2 ko cells, indicating that caspase activation is necessary for cell death induction (Fig. 19F). As demonstrated above, this caspase activation seems to be predominantly facilitated by cytosolic cathepsin B, apparently circumventing mitochondrial apoptosis.

These data were published in Cell Death & Disease in 2022 [140].

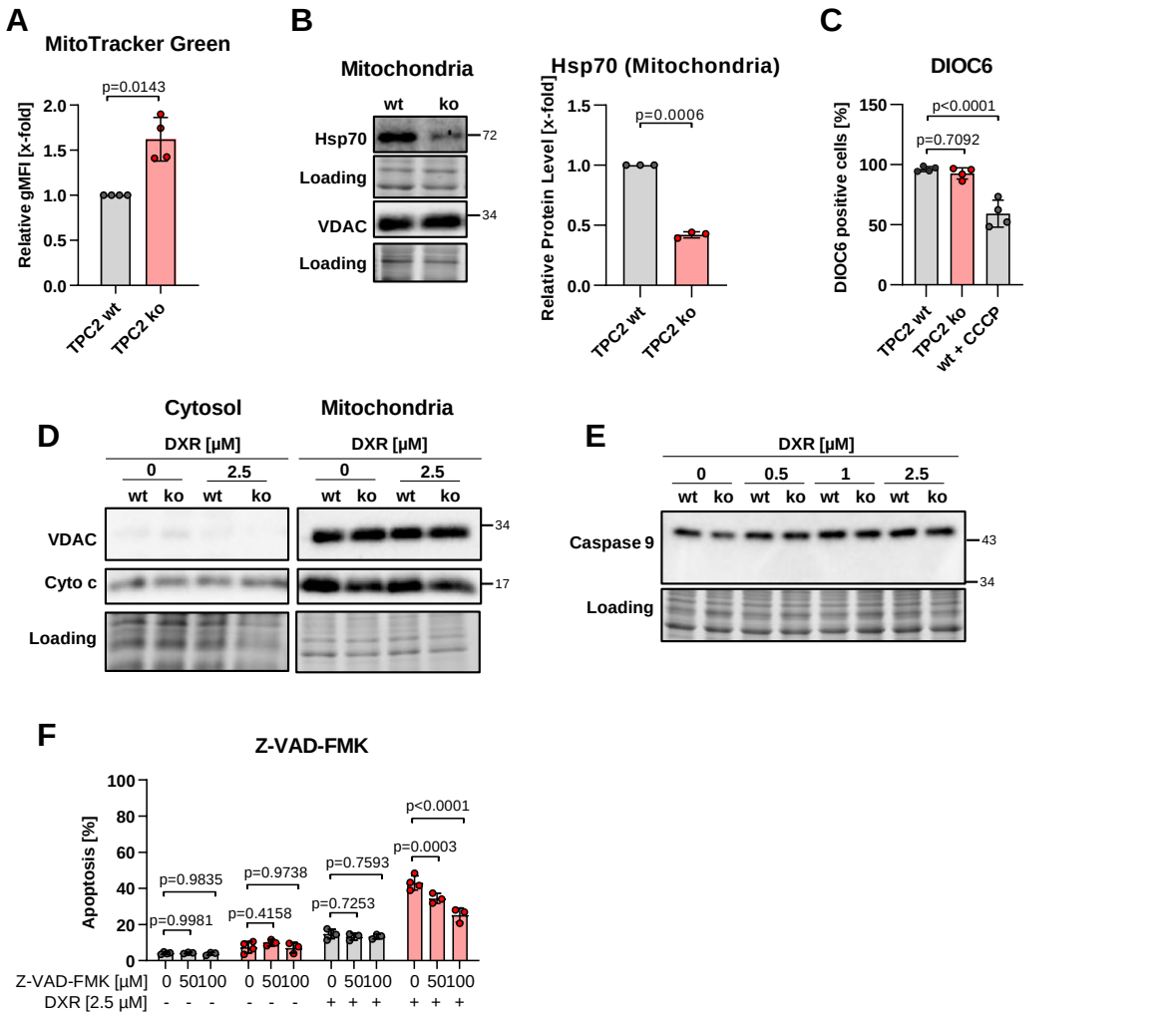

Figure 19. Doxorubicin does not induce mitochondrial apoptosis in VCR-R CEM cells.
A Mitochondrial mass of untreated VCR-R CEM TPC2 wt and TPC2 ko cells was analyzed by MitoTracker Green staining and flow cytometry. **B** Hsp70 protein levels in mitochondrial fractions were analyzed by immunoblotting. **C** Mitochondrial membrane potential was analyzed by DiOC6 staining and flow cytometry. Decreased fluorescence intensity is indicative for a depleted mitochondrial membrane potential. Carbonyl cyanide *m*-chlorophenyl hydrazone (CCCP) served as positive control. **D** Cells were treated for 24 h and cytochrome c release from mitochondria into the cytosol was analyzed by immunoblotting after subcellular fractionation. **E** Cells were treated for 24 h and activation of caspase 9 was analyzed by immunoblotting. **F** Cells were treated either with DXR alone or in combination with Z-VAD-FMK for 24 h and apoptosis was quantified using the FSC/SSC method by flow cytometry. Data are presented as mean ± SD from at least three independent experiments. Statistical significance was analyzed by student's t-test (**A**, **B**), one-way ANOVA with Dunnett's posttest or two-way ANOVA with Tukey's posttest (**F**).

4.2 Part II: TPC2 and TRPML1 regulate ferroptosis sensitivity and differentially modulate associated signaling

4.2.1 TPC2 ko and TRPML1 ko differentially modulate ferroptosis sensitivity

Ferroptosis is a recently identified form of regulated cell death which gained huge interest in the scientific community as potential anti-cancer strategy, especially in HCC [86, 87], as currently available HCC therapy regimens often lack effectiveness [141]. Besides other important ferroptosis-regulating mechanisms, recent research identified lysosomes as implicated organelle [97]. Hence, we were curious whether and how the endolysosomal cation channels TPC2 and TRPML1 modulate ferroptosis. For that, previously established RIL-175 TPC2 ko [45] and TPRML1 ko cells [74] were used. RIL-175 wt cells and the different ko cell lines were compared for their sensitivity to commonly used ferroptosis inducers, namely erastin, RSL3 and glutamate. Comparing relative proliferation upon treatment revealed that, in general, TPC2 ko cells are less sensitive to ferroptosis induction, whereas TRPML1 ko cells are more sensitive (Fig. 20A). Dependent on the ferroptosis inducer, TPC2 ko cells were almost up to 3-fold less sensitive and TPRML1 ko cells were almost up to 5-fold more sensitive to RSL3 treatment as compared to wt cells, while slightly weaker effects were observed for erastin and glutamate (Fig. 20A). These results were confirmed by quantification of cell death upon ferroptosis induction, demonstrating that TPC2 ko cells were less sensitive to all tested inducers, whereas TRPML1 ko sensitized the cells to erastin and RSL3 treatment. In contrast, alterations in cell death upon glutamate treatment were not significant (Fig. 20B). Induction of ferroptosis upon treatment was simultaneously verified by combination with the lipid peroxidation inhibitor ferrostatin-1 and the iron chelator deferoxamine (DFO) which almost completely abolished cell death (Supp. Fig. S3A). In the next step, these results were verified using established inhibitors of the cation channels. A combination of erastin or glutamate with the TPC2 inhibitor sg094 led to reduced cell death (Fig. 20C), whereas a combination with the TRPML1 inhibitor EDME sensitized RIL175 wt cells to ferroptosis (Fig. 20D).

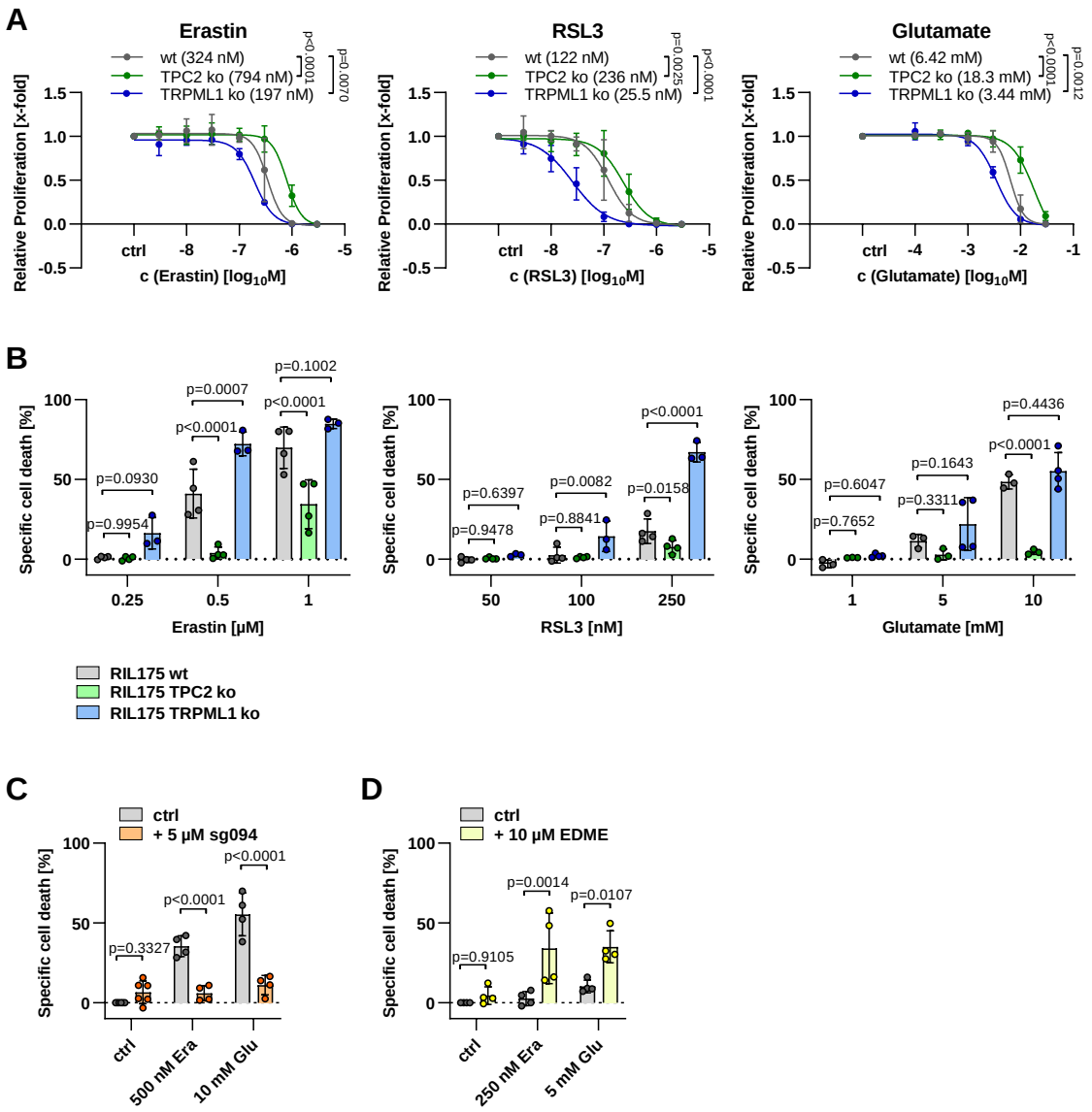

Figure 20. TPC2 and TRPML1 ko differentially modulate ferroptosis sensitivity.
A RIL175 wt, TPC2 ko and TRPML1 ko cells were treated for 72 h with ferroptosis inducers and relative proliferation was assessed using CellTiter-Blue reagent. **B** Specific cell death was assessed by propidium iodide staining and flow cytometry after 48 h of treatment. **C**, **D** RIL175 wt cells were either treated with ferroptosis inducers alone or in combination with sg094 (**C**) or EDME (**D**) for 48 h and specific cell death was assessed by propidium iodide staining and flow cytometry. Data are presented as mean ± SD from at least three independent experiments. Statistical significance was analyzed by extra sum-of-squares F test using the comparison of curve fits function in GraphPad Prism 9 (**A**), or two-way ANOVA with Dunnett's posttest (**B**) or Sidak's posttest (**C, D**).

As lipid peroxidation is a major hallmark of ferroptosis induction [79], lipid peroxides were quantified in wt, TPC2 ko, and TRPML1 ko cells to certainly link the observed effects in proliferation and cell death experiments to differential ferroptosis sensitivity. For that purpose, lipid peroxidation was quantified by Bodipy-C11 staining which is oxidized by lipid peroxides, leading to a shift in emission wavelength from red to green fluorescence. Providing proof of principle, lipid peroxides formed upon treatment with the ferroptosis inducers were abolished by combination with the ferroptosis inhibitors ferrostatin-1 or DFO (Supp. Fig. S3B). In line with

proliferation and cell death experiments, TPC2 ko cells had significantly lower levels of lipid peroxides upon treatment with all ferroptosis inducers, while it was again the other way around for TRPML1 ko cells, showing increased lipid peroxidation (Fig. 21A). Pharmacological inhibition of the cation channels in combination with ferroptosis inducers supported these results, except for glutamate and EDME (Fig. 21B, C). Taken together, loss-of-TPC2-function and pharmacological inhibition with sg094 caused ferroptosis resistance, whereas TRPML1 ko and pharmacological inhibition with EDME increased ferroptosis sensitivity. In the next step, we focused on the underlying mechanisms of differential modulation of ferroptosis sensitivity by TPC2 ko and TRPML1 ko. The main mechanistic determinants of ferroptosis sensitivity are intracellular, labile iron levels, the functionality of the cellular antioxidant defense, and membrane lipid composition [79], which were therefore analyzed in the following.

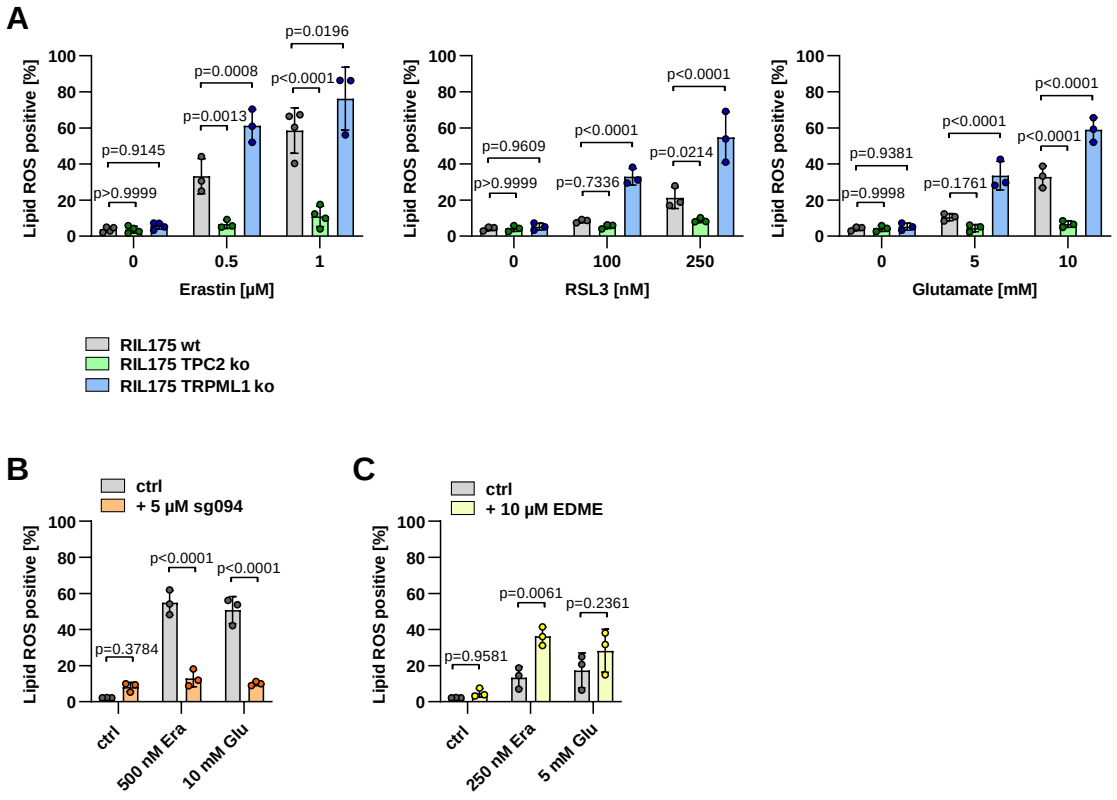

Figure 21. Loss-of-TPC2-function and loss-of-TPRML1-function affect lipid peroxidation upon ferroptosis induction.
A RIL175 wt, TPC2 ko and TRPML1 ko cells were treated for 24 h with ferroptosis inducers and lipid ROS were quantified by C11 Bodipy 581/591 staining and flow cytometry. Upon peroxidation, the emission spectrum of C11 Bodipy 581/591 shifts from red to green. **B**, **C** RIL175 wt cells were either treated with ferroptosis inducers alone or in combination with sg094 (**B**) or EDME (**C**) for 24 h and lipid peroxidation was assessed by C11 Bodipy 581/591 staining and flow cytometry. Data are presented as mean ± SD from at least three independent experiments. Statistical significance was analyzed by two-way ANOVA with Dunnett's posttest (**A**) or Sidak's posttest (**B**, **C**).

4.2.2 Loss-of-TPC2-function causes intracellular iron depletion

Importantly, labile ferrous iron promotes ROS production and subsequently lipid peroxidation, influencing ferroptotic cell death. Analyzing mRNA levels of iron-regulating genes revealed downregulation of the metalloreductase STEAP3 in TPC2 ko cells, yet, STEAP3 was upregulated in TRPML1 ko cells (Fig. 22A). Furthermore, TRPML1 ko cells had lower mRNA levels of the anti-ferroptotic iron exporter SLC40A1 [142] and an increased expression of FTH1 which was also verified by immunoblotting (Fig. 22A, B). For the other analyzed genes, including TFRC, TF, FTL1, SLC11A2, and NCOA4 no significant alterations were observed (Fig. 22A). Therefore, we wondered how these alterations might influence intracellular iron levels by quantifying free ferrous iron using FerroOrange. Upon loss-of-TPC2-function, decreased ferrous iron levels were detected as evident by reduced FerroOrange fluorescence, whereas ferrous iron levels were unchanged in TRPML1 ko cells (Fig. 22C), suggesting that intracellular iron depletion is a potential cause for ferroptosis resistance in TPC2 ko cells.

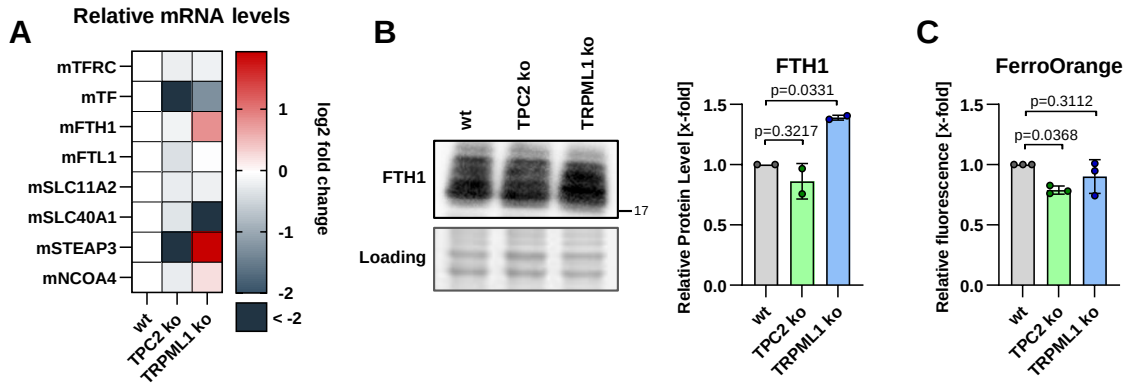

Figure 22. Free intracellular ferrous iron levels in TPC2 ko and TRPML1 ko cells.
A mRNA levels of genes associated with iron homeostasis were analyzed by qPCR. **B** Free intracellular ferrous iron levels were analyzed by FerroOrange staining on a microplate reader. **C** FTH1 levels of untreated RIL175 wt, RIL175 TPC2ko and TRPML1 ko cells were quantified by immunoblotting. Data are presented as mean (**A**), or mean ± SD (**B**, **C**) from at least three (**A**, **B**) or two (**C**) independent experiments. Statistical significance was analyzed by one-way ANOVA with Dunnett's posttest.

4.2.3 TRPML1 ko impairs antioxidant defense by induction of ER stress

The second important aspect regarding sensitivity to ferroptosis is the cellular antioxidant defense, most importantly glutathione-based antioxidant enzymes [79]. Analyzing mRNA levels of glutathione metabolism-associated genes revealed an upregulation of the system xc- component SLC7A11 in TRPML1 ko cells (Fig. 23A). Furthermore, glutathione synthetase (GSS) was upregulated and the modifying subunit of the glutamate-cysteine ligase (GCLM) was downregulated in TRPML1 ko cells, whereas other tested genes associated with glutathione metabolism were similarly expressed (Fig. 23A). To gain a better understanding of glutathione metabolism upon TPC2 ko and TRPML1 ko, intracellular reduced and oxidized

glutathione levels were analyzed. These measurements revealed a lower GSH/GSSG ratio indicative of oxidative stress in TRPML1 ko cells, while the GSH/GSSG ratio was increased in TPC2 ko cells (Fig. 23B). These alterations were mainly attributed to changes in oxidized glutathione levels which were increased in TRPML1 ko cells (Fig. 23B). Concurrently, TRPML1 ko cells showed increased total glutathione levels, probably as a result of upregulation of cystine uptake as a response to oxidative stress (Fig. 23B). Due to an earlier report about the importance of TRPML1 for proper protein homeostasis [73], we hypothesized that this phenomenon might be connected to endoplasmic reticulum (ER) stress. Providing a proof of concept, induction of ER stress with thapsigargin or tunicamycin decreased the respective GSH/GSSG ratios (Fig. 23C).

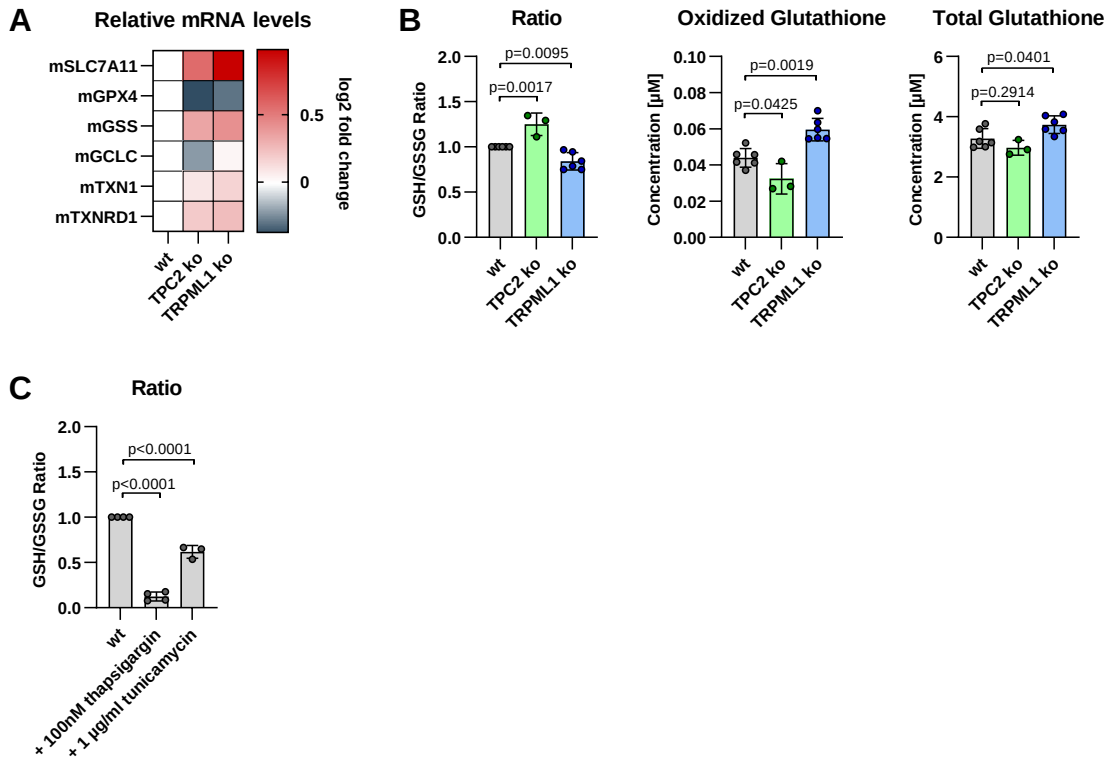

Figure 23. Glutathione-dependent antioxidant defense upon TPC2 and TRPML1 ko.
A mRNA levels of genes associated with glutathione metabolism were analyzed by qPCR. **B** GSH/GSSG ratios, oxidized GSSG levels and total glutathione levels were determined using the GSH/GSSG Glo kit. **C** RIL175 wt cells were treated for 24 h and GSH/GSSG ratios, oxidized GSSG levels and total glutathione levels were determined using the GSH/GSSG Glo kit. Data are presented as mean ± SD from at least three independent experiments. Statistical significance was analyzed by one-way ANOVA with Dunnett's posttest.

Consequently, ER calcium levels as well as the expression of mediators of the unfolded protein response were analyzed. Measuring intracellular calcium levels directly after the release of ER calcium either using the ionophore calcimycin (Fig. 24A) or the SERCA inhibitor thapsirgargin (Fig. 24B) emphasized reduced ER calcium levels in TRPML1 ko cells, whereas there were no alterations upon TPC2 ko (Fig. 24A, B).

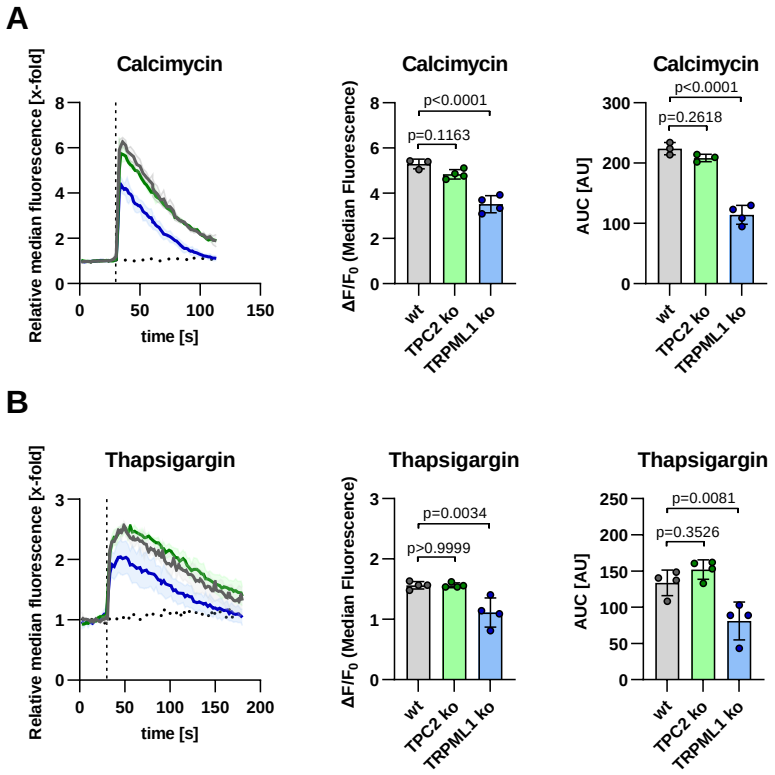

Figure 24. TRPML1 ko causes ER calcium depletion.
ER calcium levels were indirectly quantified by Cal-520 staining and flow cytometry upon release of ER calcium either using calcimycin (A23187) (**A**) or thapsigargin (**B**). $\Delta F/F_0$ and the area under the curve (AUC) were calculated from the obtained curves. Data are presented as mean ± SD from at least three independent experiments. Statistical significance was analyzed by one-way ANOVA with Dunnett's posttest.

Next, expression levels of mediators of the unfolded protein response (UPR) were analyzed, revealing increased phosphorylation of eIF2alpha and increased mRNA levels of ATF6 in TRPML1 ko cells (Fig. 25A, D). In contrast, no alterations could be observed for BiP/GRP78, ATF4, and splicing of XBP1 (Fig. 25B, C). This partial upregulation of the unfolded protein response (UPR) might be a result of latent ER stress. In line with that, TRPML1 ko cells were more sensitive to induction of ER stress with the tool compounds thapsigargin, tunicamycin, and brefeldin A, as evident by increased cell death upon treatment (Fig. 25E). Concurrently, no general alterations regarding UPR or sensitivity to induction of ER stress were detected upon TPC2 ko (Fig. 25A-E).

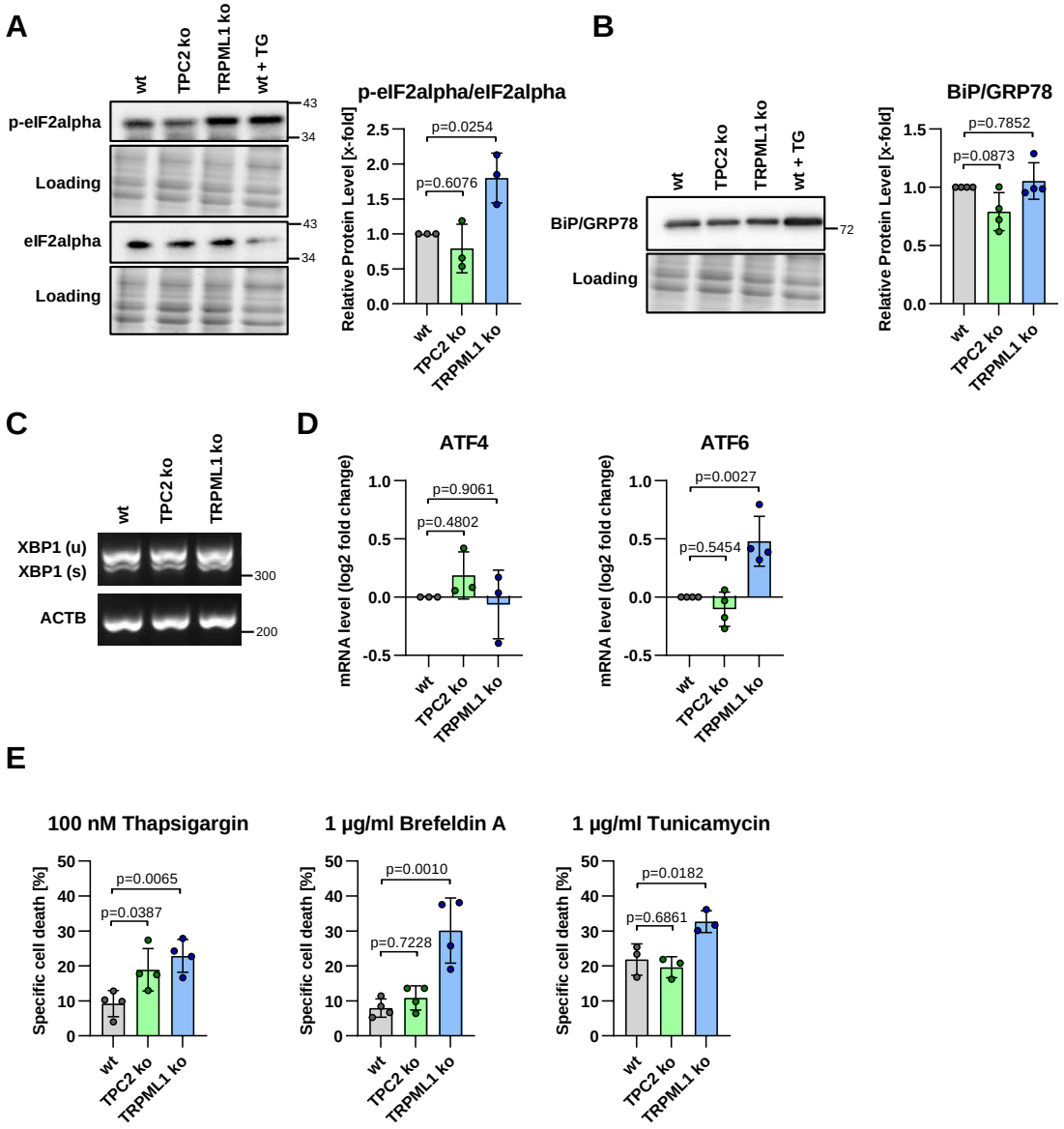

Figure 25. Loss-of-TRPML1-function causes ER stress.
A, **B** Protein expression levels of untreated RIL175 wt, TPC2 ko and TRPML1 ko cells were quantified by immunoblotting. **C** XBP1 mRNA levels were analyzed by qPCR and the unspliced and spliced form were separated by agarose gel electrophoresis. **D** mRNA levels of untreated cells were analyzed by qPCR. (E) Cell death upon treatment with ER stress inducers was quantified by propidium iodide staining and flow cytometry. Data are presented as mean ± SD from at least three independent experiments. Statistical significance was analyzed by one-way ANOVA and Dunnett's posttest.

Thus, the influence of ER stress on glutathione metabolism in TRPML1 ko cells was analyzed by inhibiting ER stress either with the chemical chaperone 4-PBA or the SERCA activator CDN1163 (Fig. 26). Indeed, inhibition of ER stress by either of them increased GSH/GSSG ratios as a result of decreased levels of oxidized glutathione (Fig. 26), suggesting that ER stress is responsible for increased oxidative stress in TRPML1 ko cells which might render them more sensitive to ferroptosis induction.

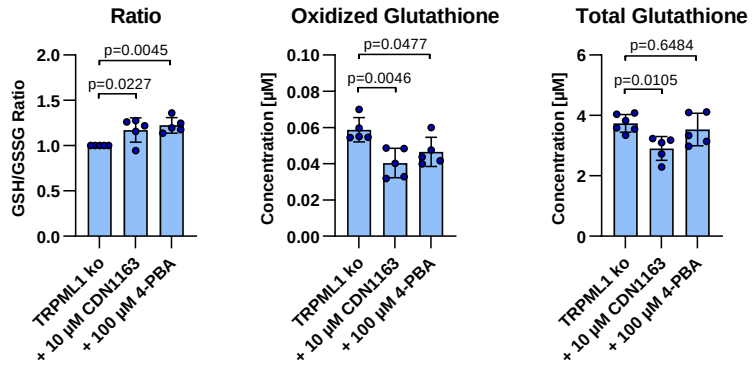

Figure 26. Inhibition of ER stress reverses altered glutathione metabolism in TRPML1 ko cells.
RIL175 TRPML1 ko cells were treated for 24 h and GSH/GSSG ratios, oxidized GSSG levels and total glutathione levels were determined using the GSH/GSSG Glo kit. Data are presented as mean ± SD from at least three independent experiments. Statistical significance was analyzed by one-way ANOVA with Dunnett's posttest.

4.2.4 Loss-of-TPC2-function shifts PUFA-PEs to MUFA-PEs

As third important mechanistic determinant, the cellular fatty acid composition, especially that of membrane lipids has been shown to be extremely important for ferroptotic cell death, as PUFAs incorporated in membrane phospholipids facilitate ferroptosis, whereas MUFAs have ferroptosis inhibiting effects [79]. Therefore, we analyzed the composition of phosphatidylethanolamines (PE) in whole cell lysates as well as lysosomal fractions of wt, TPC2 ko, and TRPML1 ko cells by tandem mass spectrometry (Fig. 27A). These experiments were carried out by Finja Witt from the group of Prof. Andreas Koeberle (Michael Popp Institute, University of Innsbruck, Austria). Interestingly, overall PUFA containing phosphatidylethanolamines were decreased in whole cell lysates of TPC2 ko cells, whereas they remained unchanged in TRPML1 ko cells (Fig. 27B). This was mainly attributed to a decreased abundance of arachidonic acid-containing PE lipids in TPC2 ko cells (Fig. 27A). In TPC2 ko cells, the lack of PUFA-containing PEs was compensated by an increase in MUFA-containing PE lipids, while in TRPML1 ko cells SFA-PEs were decreased, accompanied by increased MUFA-PE levels (Fig. 27B). In general, alterations in PE composition were less pronounced in lysosomal fractions (Fig. 27A, B). Of note, loss-of-TPC2 or loss-of-TRPML1-function did neither influence cellular PE abundance nor lysosomal PE abundance (Fig. 27C). These results emphasize decreased PUFA incorporation into phospholipids upon TPC2 ko as a mediator of ferroptosis resistance.

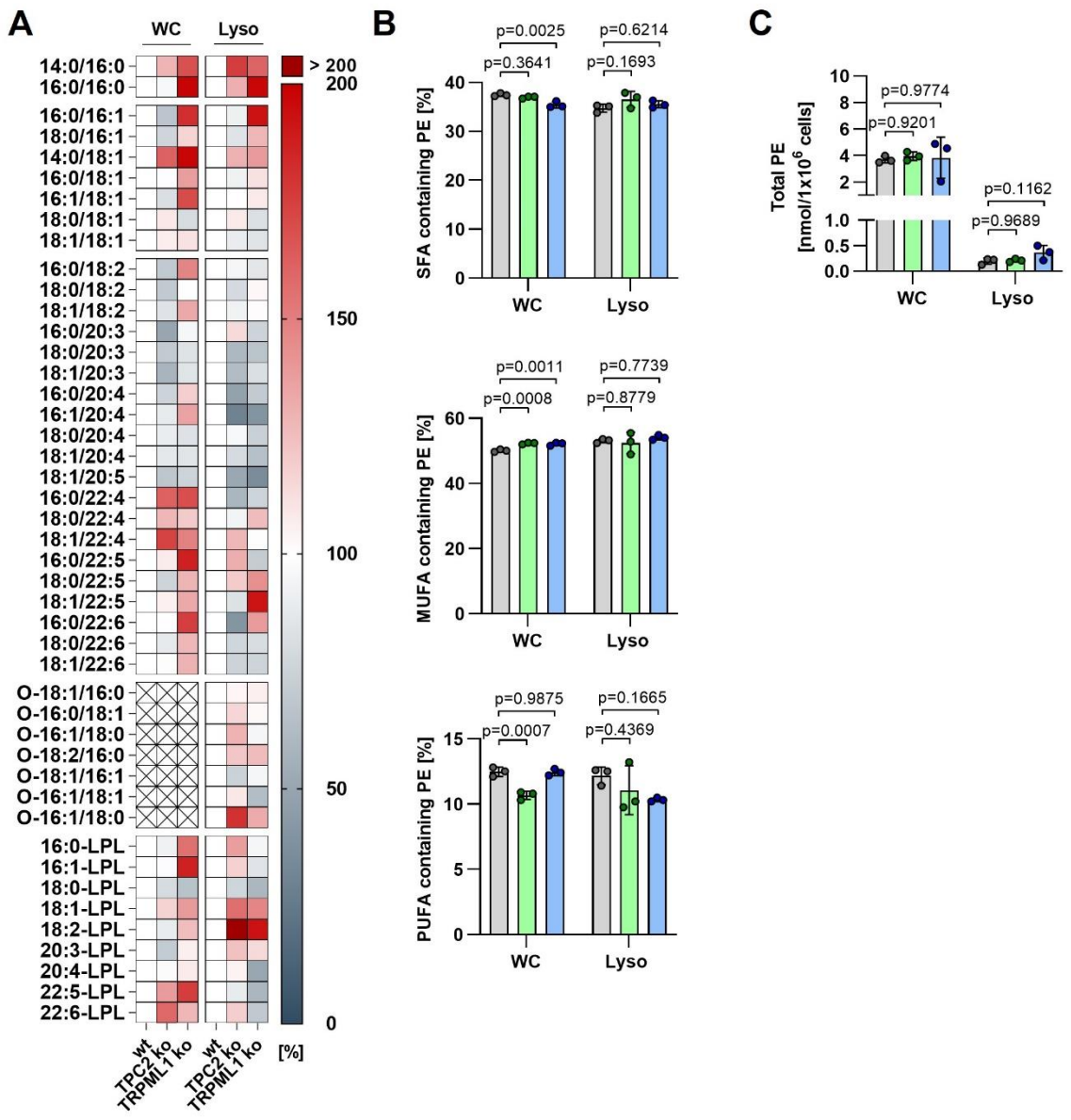

Figure 27. Loss-of-TPC2-function leads to depletion of PUFA-PEs.
A Proportions of PE species normalized to the respective wt controls of whole cells (WC) or lysosomes (Lyso). **B** Proportions of PE subfractions carrying saturated fatty acids (SFA), monounsaturated fatty acids (MUFA) or polyunsaturated fatty acids (PUFA). **C** Total amount of PE. Data are presented as mean (**A**) or mean ± SD (**B**, **C**) from three independent experiments. **B**, **C** Statistical significance was analyzed by one-way ANOVA with Dunnett's posttest. **A**-**C** These experiments were performed by Finja Witt from the group of Prof. Andreas Koeberle (Michael Popp Institute, University of Innsbruck, Austria).

To gain further mechanistic insights, the expression of important regulators of membrane lipid composition were analyzed, namely ACSL4 and LPCAT3 [143]. This revealed decreased ACSL4 expression on mRNA and protein level in TPC2 ko cells (Fig. 28A, B) which might explain the observed decrease of PUFA-containing PEs in favor of MUFA-containing PEs. Concurrently, there were no changes detectable for LPCAT3 (Fig. 28C), and loss-of-TRPML1-function did not cause any alterations (Fig. 28A-C). These data show that TPC2 ko cells have decreased levels of PUFA-PEs, which, together with decreased ferrous iron levels, and increased GSH/GSSG ratios, contribute to ferroptosis resistance. In contrast, TRPML1 ko cells are more susceptible to ferroptosis, resulting from increased oxidative stress as a consequence of ER stress.

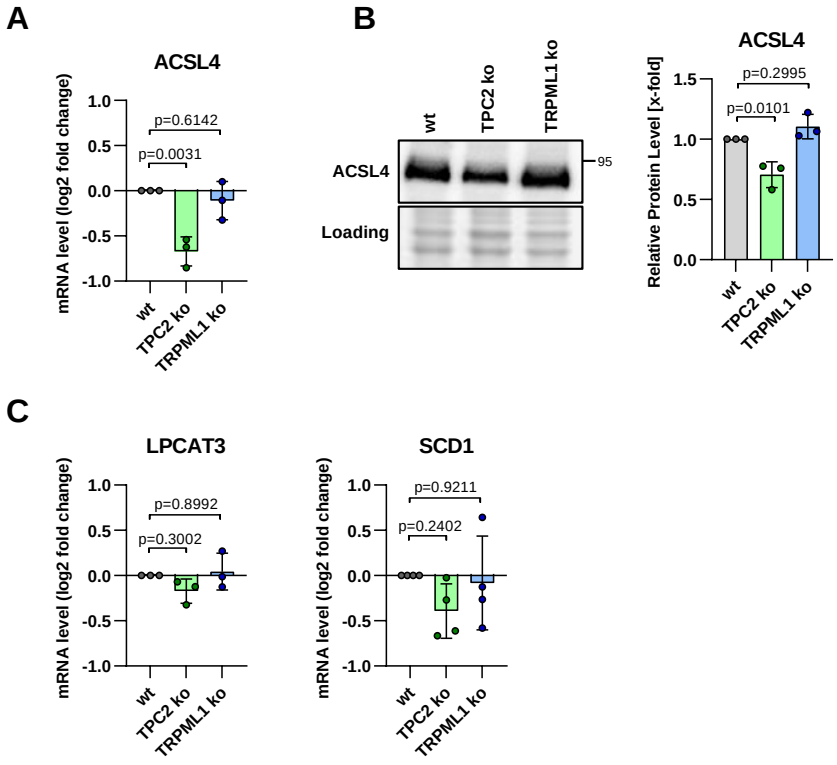

Figure 28. TPC2 ko causes downregulation of ACSL4.
A, **C** mRNA levels of untreated RIL175 wt, TPC2 ko and TRPML1 ko cells were analyzed by qPCR. **B** ACSL4 protein levels of untreated cells were analyzed by immunoblotting. Data are presented as mean ± SD from three independent experiments. Statistical significance was analyzed by one-way ANOVA with Dunnett's posttest.

5 Discussion

The data presented here highlight TPC2 as a promising target for combination therapy approaches to enhance chemoresponse in leukemia. Chemoresistance remains a therapy-limiting challenge associated with poor outcome. Recently, lysosomes emerged as intriguing modulators of chemoresistance. In this study, we show that TPC2 is a novel, druggable target to overcome this therapeutic problem. Notably, we show that TPC2 ko or pharmacological inhibition of TPC2 potentiates anti-leukemic effects of commonly used cytostatics, such as vincristine and doxorubicin. Mechanistically, chemosensitization is a result of alterations in lysosomal pH and size upon loss-of-TPC2-function, impairing sequestration of weak base cytostatics and concurrently, causing increased susceptibility to lysosomal membrane damage, resulting in increased cytostatics-induced cell death.

Furthermore, we identified TPC2 and TRPML1 as novel regulators of ferroptosis, a recently elucidated form of cell death with huge anti-tumor potential. In this context, TPC2 ko leads to ferroptosis resistance mediated by reduced intracellular iron levels and alterations in the composition of phosphatidylethanolamines. On the other hand, the ferroptosis-sensitizing effects of TRPML1 ko could be attributed to a depletion of reduced GSH as a result of latent endoplasmic reticulum stress. These data give new mechanistic insights into the role of lysosomal cation channels in ferroptosis and underline the importance of iron homeostasis, lipid composition, and antioxidant capacity for ferroptosis sensitivity.

5.1 The role of TPC2 in the regulation of lysosomal pH and size

Over the past decades, lysosomes have emerged from being regarded as simple degradation organelles to recognition as essential regulators of cellular homeostasis. Proper lysosomal function, which is closely linked to an acidic intraluminal pH, is therefore, crucial for cellular survival. For instance, a low intraluminal pH of lysosomes is required for autophagic clearance of cellular cargo – a main purpose and longest known function of the endolysosomal system – by fusion of autophagosome and lysosome and subsequent degradation [144]. Hence, modulation of lysosomal pH is of great interest and frequently analyzed upon manipulation of lysosomal targets. Lysosomal acidity is ensured by the vacuolar H^+-ATPase, a trans membranous proton pump that transports protons from the cytosol into the lysosomal lumen [145].

Importantly, ion channels have also been discussed to influence lysosomal pH. In that regard, the question of whether and how TPC2 regulates lysosomal pH remains a matter of debate. In line with our data, loss-of-TPC2-function led to lysosomal alkalinization in healthy skeletal

muscle cells [146]. However, Grimm et al. did not identify any alterations of lysosomal pH in TPC2 ko mouse embryonic fibroblasts [51]. Supporting the hypothesis that loss-of-TPC2-function leads to increased lysosomal pH, Ambrosio et al. showed that TPC2 ko causes alkalinization of melanosomes – a different type of acidic vacuoles which co-localize with TPC2 in malignant melanoma [147]. In contrast, NAADP signaling in TPC2 overexpressing HeLa cells increased lysosomal pH which functionally resulted in impaired autophagic breakdown [148]. Furthermore, the influence of different TPC2 activators, in detail a synthetic $PI(3,5)P_2$ mimic (TPC2-A1-P) and a synthetic NAADP mimic (TPC2-A1-N), was analyzed by Gerndt et al. While there were no changes observed for activation with TPC2-A1-P, TPC2-A1-N caused lysosomal alkalinization by direct proton conductance from lysosomes into the cytosol [42]. This was recently underpinned by Yuan et al., showing that TPC2-A1-P single treatment does not modify lysosomal pH, whereas it enhances the lysosome-alkalinizing properties of TPC2-A1-N [43]. Consequently, the exact implication of TPC2 in vesicular pH regulation is ambiguous and the reason for partially contradicting results in different systems is unknown so far. Our study adds novel data to this controverse debate, as we reveal that loss-of-TPC2-function causes lysosomal alkalinization in leukemia cells. One reasonable explanation for partially contradicting results in the literature is that the role of TPC2 in the regulation of lysosomal pH might be highly cell-type-dependent. On the other hand, it is noteworthy that in most cases manipulation of TPC2 no matter if knockout, overexpression or over-activation causes lysosomal alkalinization. As proper ion homeostasis is indispensable for lysosomal acidification by evoking a cation counter flux [149], it could be possible that any kind of manipulation of the cation channel TPC2 impairs lysosomal acidification owing to unbalanced ion homeostasis. However, shedding light on this controversy requires further investigations.

Besides the controversial findings on lysosomal acidity upon manipulation of TPC2, TPC2 has been reported to influence other lysosomal characteristics as well. Nguyen et al. discovered that TPC2 depletion causes swelling of lysosomes in HUH7 and T24 cancer cells and additionally confirmed these findings by pharmacological TPC2 inhibition [58]. Furthermore, lysosomal swelling was observed upon inhibition of PIKfyve, the enzyme catalyzing the formation of $PI(3,5)P_2$ [150, 151]. As $PI(3,5)P_2$ is a main endogenous activator of TPC2, these findings support the theory that insufficient channel activation is connected to lysosomal swelling [37]. These data are in line with our results, showing that TPC2 depletion leads to an increased lysosomal diameter.

An increase in luminal pH accompanied by lysosomal swelling is a phenotype which has been previously reported upon lysosomal stress [152]. Under these conditions lysosomal biogenesis was induced by nuclear translocation of TFEB, enabling the cells to cope with lysosomal stress [152, 153]. As lysosomal housekeepers, apart from cathepsins B and D, were not substantially

altered upon loss-of-TPC2-function in our model cells, our results emphasize that the alterations in lysosomal characteristics in TPC2 ko cells are not accompanied by TFEB activation. Interestingly, there are indications that proper TPC2 function might be necessary for the cells' ability to adapt lysosomal biogenesis. Along that line, it has been reported that TPC1 is involved in the activation of TFEB, as calcium efflux from lysosomes via lysosomal cation channels activates calcineurin, a phosphatase which dephosphorylates and thus activates TFEB [69, 127]. In addition, TPC2 knockout in melanoma causes decreased MITF levels [46]. MITF is, like TFEB, a member of the MiT-TFE family of transcription factors, which regulate endolysosomal biogenesis [154]. Therefore, we hypothesize that loss-of-TPC2-function causes a form of lysosomal stress to which cells are unable to adapt, resulting in lysosomal swelling and increased luminal pH.

5.2 Targeting TPC2 as promising approach to impair lysosomal drug sequestration

It is accepted in the literature that a proper function of lysosomes and especially their pH critically promote chemoresistance by enabling lysosomal sequestration of weak base chemotherapeutics. Therefore, impairing lysosomal drug sequestration is a promising approach to overcome chemoresistance in pre-clinical studies [29]. Underlining this hypothesis, it was discovered that lysosomes of chemo-resistant cells are more acidic as compared to those of drug-naïve cells [155]. Moreover, cancer cells with a high number of lysosomes are more resistant to weak base drugs as compared to cancer cells with a low number of lysosomes, resulting in a correlation between lysosomal volume and chemoresistance. In detail, lysosomal drug sequestration as a result of a high number of lysosomes facilitated resistance to palbociclib in triple-negative breast cancer [156]. We obtained similar results, showing that chemo-resistant VCR-R CEM TPC2 wt cells have an increased lysosomal volume and reduced lysosomal pH as compared to their drug-naïve counterpart.

Especially increased volume of the lysosomal compartment is commonly associated with TFEB which induces transcription of lysosomal genes of the CLEAR (coordinated lysosomal expression and regulation) network [157, 158]. Along the line, it has been stated that siRNA-mediated knockdown of TFEB sensitizes cancer cells to various antitumor agents, including doxorubicin [159], trametinib [160], and palbociclib [156] mediated by impaired autophagy or impaired lysosomal drug sequestration. Furthermore, the lysosomal housekeeper LAMP1, a gene transcribed by TFEB, was found to be upregulated in doxorubicin-resistant breast cancer cells [161]. However, we could not observe an upregulation of TFEB itself or the lysosomal housekeeper LAMP1 in VCR-R CEM cells as compared to drug-naïve CCRF-CEM cells.

Therefore, we cannot connect development of chemoresistance to increased TFEB signaling in our cell model. By comparing the expression of several lysosomal genes, we found that TPC2 is most prominently upregulated in the resistant cell line. Concurrently, TPC2 ko caused impaired lysosomal drug sequestration which is most likely attributed to the increased lysosomal pH upon loss-of-TPC2-function. Consequently, TPC2 ko facilitated enhanced accumulation of doxorubicin in the nucleus and increased chemotherapy-induced cell death.

As chemo-resistant cells, including VCR-R CEM cells used in this study, commonly express high levels of P-gp, the question arose whether or not lysosomal drug sequestration is mediated by P-gp-mediated drug influx into lysosomes, which is still debated in the literature. Indeed, Yamagishi et al. found that P-gp is abundant in lysosomes by analyzing the co-localization of P-gp with the lysosomal LAMP2 using confocal microscopy [26]. Of note, P-gp is usually recycled via the endolysosomal pathway [162], suggesting that localization at lysosomes does not necessarily prove functional activity. Gericke et al. shed light on this issue by detecting functional P-gp in LAMP2-positive lysate fractions. This became evident by detecting P-gp-dependent accumulation of the P-gp substrate Rhodamine 123 in P-gp-positive endolysosomes. However, subsequent ultrastructural analyses revealed that P-gp expressed in the endolysosomal system is predominantly found in early endosomes and only rarely in lysosomes [163]. Nevertheless, inhibiting P-gp with specific inhibitors led to impaired lysosomal sequestration of doxorubicin in chemo-resistant cells, resulting in chemosensitization [26]. These data suggest that P-gp localized within lysosomal membranes promotes lysosomal sequestration of weak base drugs, contributing to chemoresistance. In contrast, others reported that P-gp only is only localized within lysosomal membranes in response to nutrient stress, such as glucose or serum starvation [27, 28]. Despite high P-gp expression in VCR-R CEM cells, the observed effect of TPC2-ko-mediated chemosensitization was independent of P-gp activity, as a combination with different model inhibitors did not lead to an alignment in response between TPC2 ko and TPC2 wt cells. In addition, a combination of pharmacological TPC2 inhibitors and weak base cytostatics was also beneficial in drug-naïve leukemia cells as well as in HepG2 and HeLa cells. Based on our results, we hypothesize that increased chemoresponse upon loss-of-TPC2-function is dependent on the physicochemical properties of the drugs – most importantly, they have to be protonatable, as this feature facilitates lysosomal sequestration [29]. Along the line, there were no alterations in sensitivity to the non-basic cytostatics paclitaxel and 5-fluorouracil upon TPC2 ko. This is also supported by Visser et al. who demonstrated that lysosomal alkalinization by V-ATPase inhibition does not sensitize acute myeloid leukemia cells to the non-basic chemotherapeutic cytarabine [164].

The contribution of lysosomes to chemoresistance led to a high interest in treatment strategies focusing on targeting lysosomes to achieve chemosensitization of cancer cells. In this context, the alkalinization of the endolysosomal compartment was identified as a reasonable approach. Of note, one promising study employed lysosomotropic compounds, a class of compounds accumulating in lysosomes and thereby alkalinizing their intraluminal pH, to improve response to commonly used chemotherapeutics. For instance, drug combinations of chloroquine, ammonium chloride, or methylamine with doxorubicin, daunorubicin, or vinblastine, were found to be highly beneficial in chemo-resistant KBV1 cells [26]. This synergism was mediated by impaired sequestration of the chemotherapeutic owing to lysosomal alkalinization [26, 29]. Yet, approaches focusing on distinct lysosomal targets which might provide more cancer-selective effects, are rare or associated with druggability problems. For example, a study revealed the lysosomal V-ATPase as promising target to sensitize doxorubicin-resistant MCF-7 cells to various cytostatics [165]. Yet, hitherto available V-ATPase inhibitors have been reported to be severely toxic, probably impeding a putative clinical application [166, 167]. In contrast, promising inhibitors of TPC2 have recently become available, which is thoroughly discussed in chapter 5.5.

5.3 Induction of lysosomal cell death is a reasonable strategy to improve chemotherapy response

On the one hand, lysosomes apparently exert a protective role upon chemotherapy by lysosomal drug sequestration. On the other hand, damage of lysosomes initiates a special form of cell death, called LCD [18, 29]. This form of cell death results from lysosomal damage and the subsequent release of luminal proteolytic enzymes to the cytosol. Importantly, cells appear to be more susceptible to lysosomal damage upon oncogenic transformation [33], providing a rationale for the induction of lysosomal damage as anticancer strategy, either using drug combinations or monotherapies. For instance, functional inhibitors of the acid sphingomyelinase, a compound class inducing lysosomal damage, caused cancer cell death in monotherapy and increased the sensitivity to paclitaxel [33]. In addition, the lysosome-damaging compound verteporfin potentiated apoptosis induction by sorafenib treatment in hepatocellular carcinoma [168].

Our data underline the suitability of this anti-tumor strategy and further show that targeting TPC2 is a novel approach to provoke lysosomal damage in leukemia cells. This is in line with recent reports which emphasize that manipulation of endolysosomal cation channels may be an effective strategy to modulate susceptibility to lysosomal damage. For instance, it was shown that knockdown of TRPML1 causes lysosomal damage and subsequently apoptosis in

HeLa cells [169], whereas overexpression of the pH-dependent endolysosomal calcium channel RECS1 promoted lysosomal damage which was potentiated by chloroquine-induced lysosomal stress [170]. In our study, we analyzed susceptibility to lysosomal damage in TPC2 ko cells by exposition to phototoxic stress using acridine orange and high-intensity laser light. Furthermore, increased susceptibility to lysosomal damage could also be detected upon doxorubicin treatment, indicating that doxorubicin induces lysosomal damage in cancer cells, which is in agreement with the literature [171]. Importantly, TPC2 ko cells were more prone to doxorubicin-induced lysosomal damage as compared to TPC2 wt cells. Mechanistically, lysosomal damage upon doxorubicin treatment might be connected to ROS formation, which has been previously reported to destabilize the lysosomal membrane [132]. Lysosomal damage then causes the release of cathepsins, including cathepsin B, initiating LCD induction [18]. Accordingly, TPC2 ko cells had increased levels of cytosolic cathepsin B in untreated conditions, whereas cytosolic cathepsin B did not further increase upon doxorubicin treatment. However, measuring cathepsin B proteolytic activity revealed increased activity in TPC2 ko cells treated with doxorubicin, suggesting that the combination of high cytosolic abundance and cathepsin B activation are prerequisites of LCD upon doxorubicin treatment. This was further verified by analysis of the truncation of Bid, a well-known pro-apoptotic target of cathepsin B [18]. In line with these results, inhibition of cathepsin B with CA-074Me decreased doxorubicin-induced cell death in TPC2 ko cells, but not in TPC2 wt cells, pointing to an involvement of LCD in chemotherapy in TPC2 ko cells.

Importantly, lysosomal damage-induced LCD can either occur caspase-dependent or caspase-independent and LCD is deeply connected to apoptotic signaling, which becomes obvious by the involvement of pro- and anti-apoptotic Bcl-2 family proteins in lysosomal damage [18]. We intended to decipher these two pathways by analyzing caspase 3 activation upon doxorubicin treatment and simultaneous cathepsin B inhibition. This revealed reduced caspase 3 activation upon cathepsin B inhibition in TPC2 ko cells, suggesting that cathepsin B activates caspase 3. Concurrently, we are not able to exclude direct execution of LCD via cathepsin B. It has been reported that the direct way of LCD is commonly associated with severe lysosomal damage, which subsequently causes a massive release of cathepsins into the cytosol [172]. From the cytosol, cathepsins can translocate to the nucleus and cleave histone H3 to stimulate cell death signaling [173, 174]. As our results revealed no significant increase of cytosolic cathepsin B in response to doxorubicin treatment, the scenario of enormous, uncontrolled lysosomal damage seems to be implausible in our cell model. Concurrently, caspase 3 is not only activated by cathepsin B, but most prominently via the intrinsic apoptosis pathway via mitochondrial outer membrane permeabilization, resulting in the formation of the apoptosome which consists of cytochrome c, Apaf-1, and caspase 9

upstream of caspase 3 activation [139]. In contrast to several reports that doxorubicin induces mitochondrial apoptosis [175-177], doxorubicin did not trigger mitochondrial apoptosis in VCR-R CEM cells, as there were no alterations in cytosolic cytochrome c or caspase 9 activation observed. This also applied to TPC2 ko cells, even though they showed signs of mitochondrial stress in untreated conditions and had significantly increased levels of truncated Bid upon doxorubicin treatment.

Resistance to apoptotic cell death is an important feature of chemo-resistant cells which is mainly mediated by alterations in mitochondria-associated processes, including energy metabolism, mitochondrial ROS homeostasis, and increased expression of anti-apoptotic Bcl-2 family proteins, preventing mitochondrial outer membrane permeabilization [178]. Therefore, apoptosis resistance is most likely a result of continuous exposition to vincristine during the generation of VCR-R CEM cells and logically goes hand in hand with the chemoresistance phenotype. This further emphasizes that increased cell death induction upon doxorubicin treatment in TPC2 ko cells is predominantly mediated by cathepsin B-dependent caspase 3 cleavage. Thereby, the LCD pathway may compensate for non-occurring intrinsic apoptosis in TPC2 ko cells, suggesting that induction of lysosomal damage is a suitable strategy for chemosensitization, especially in chemo-resistant cells. In addition to the induction of LCD, lysosomal damage may also hinder effective drug sequestration, as trapped cytostatics may diffuse back into the cytosol through the damaged lysosomal membrane. Therefore, we conclude that interfering with TPC2 function may act in a dual, interdependent mode of action amplifying chemoresponse of drug-naïve as well as resistant cells.

5.4 TPC2 and TRPML1 – novel regulators of ferroptosis-associated cellular homeostasis

In the search for innovative anti-cancer treatment strategies, inducing ferroptosis has shown promising results. Evidence suggests that lysosomes are involved in the regulation of ferroptosis sensitivity as they influence major ferroptosis-associated determinants such as intracellular iron levels, redox balance, and lipid homeostasis [97]. Due to many different, significant implications of the endolysosomal system in iron homeostasis, extensive research on that has been conducted in the past. For instance, it has been clarified that lysosomal acidity is indispensable for cellular iron uptake via the endocytic pathway, as it facilitates the dissociation of iron-transferrin complexes [179]. Hence, impairment of lysosomal acidification via V-ATPase inhibition or treatment with ammonium chloride causes iron deficiency [180, 181]. Of note, intracellular iron depletion has also been reported upon loss-of-TPC2-function, as Fernández et al. showed that TPC2-expressing cells have increased free iron levels as

compared to TPC2-deficient cells, which was especially evident upon extracellular iron supplementation. They further confirmed these data using the NAADP-targeting, indirect TPC2 inhibitor Ned-19. Functionally, TPC2 inhibition mitigated ROS generation and subsequently cell death in response to exogenous iron overload [182]. This is in line with the phenotype of TPC2 ko cells obtained in our study, however, mechanistic insights are currently scarce. Grimm et al. reported that TPC2 deficiency in mouse embryonic fibroblast does not lead to impaired transferrin uptake [51], suggesting that the underlying reason is connected to different mechanisms. Our results suggest that iron deficiency in TPC2 ko cells may be mediated by downregulation of STEAP3, a metalloreductase within the endolysosomal system responsible for the enzymatic reduction of ferric to ferrous iron which represents a critical step for the supply of labile ferrous iron [99]. Due to its important role in cellular iron homeostasis, STEAP3 has been previously investigated in terms of regulation of ferroptosis sensitivity. Hitherto, its implication in ferroptosis is unclarified, as Liu et al. showed that knockout of STEAP3 renders cells resistant to ferroptosis [183], contradicting results from Ye et al. who revealed increased ferroptosis sensitivity upon STEAP3 knockdown [184].

Interestingly, unlike TPC2 ko, loss-of-TRPML1-function led to an upregulation of STEAP3. In addition, TRPML1 ko cells had decreased levels of the iron exporter SLC40A1 which is considered to be anti-ferroptotic [185, 186]. This might, in general, point to high iron conditions as pro-ferroptotic mechanism in TRPML1 ko cells since these alterations could cause an excessive ferrous iron supply as well as impaired cellular iron export. However, we did not observe alterations in free ferrous iron levels in TRPML1 ko cells which probably is a result of compensatory upregulation of iron storage proteins, as shown for FTH1. In contrast to our results, Dong et al. found that the absence of TPRML1 causes a decrease in ferrous iron levels in skin fibroblasts. Mechanistically, this was apparently mediated by an impaired release of free ferrous iron from the endolysosomal system, as TRPML1 is permeable for ferrous iron and therefore, might act in a similar way as DMT1. Furthermore, decreased cytosolic ferrous iron levels were accompanied by lysosomal iron accumulation [67]. In conclusion, the role of TRPML1 in cellular iron homeostasis appears to be cell type-dependent and may be dependent on individual expression levels of different endolysosomal iron transporters.

Of note, intracellular labile iron levels strongly influence the generation of reactive oxygen species which need to be detoxified by antioxidant systems by utilizing cellular reducing equivalents, such as glutathione, NADH, or NADPH, to enable cellular survival. Hence, these antioxidant systems are crucial regarding ferroptosis sensitivity [79, 187]. By analyzing total and oxidized glutathione levels, we found that TRPML1 ko cells are oxidatively challenged, as evident by increased levels of oxidized glutathione. Concurrently, increased total glutathione levels pointed to a compensatory mechanism as a response to increased oxidative stress.

These alterations in glutathione metabolism only resulted in a modest decrease of the GSH/GSSG ratio, suggesting that this compensatory mechanism enables proper detoxification of ROS and ensures cellular survival upon TPRML1 ko. In line with that, we detected increased expression levels of the system xc- component SLC7A11, whereas other glutathione metabolism-associated genes were unchanged. Therefore, we hypothesize that system xc- might be the decisive factor for increased glutathione supply as a response to oxidative stress. As TRPML1 ko cells are already challenged by oxidative stress under basal conditions, it seems feasible that they are more susceptible to inhibition of the antioxidative system, i.e. by inhibiting cellular cystine uptake via system xc- or by inhibiting the detoxification of ROS via GPX4. Interestingly, TPRML1 has been reported to regulate autophagy upon exposition to oxidative stress. Zhang et al. demonstrated that TRPML1 is activated by ROS resulting from CCCP treatment, leading to the activation of autophagy which seems to be a homeostatic process to degrade unfunctional, damaged mitochondria [64]. Besides, TRPML1 regulates mitochondrial function in general, as pharmacological activation caused excessive mitochondrial calcium accumulation mediated by lysosome-mitochondria contact sites [66] and increased mitochondrial ROS levels. Concurrently, loss-of-TRPML1-function impairs mitochondrial function as a result of impaired autophagic degradation. This caused a cellular stress response via phosphorylation of eIF2alpha [74] which is commonly known to inhibit global protein synthesis and activate cellular stress responses [188].

Importantly, phosphorylation of eIF2alpha is an early event in the ER stress response [189]. Therefore, we hypothesized that TRPML1 ko causes excessive ER stress. Indeed, loss-of-TRPML1-function led to decreased ER calcium levels which is associated with ER stress in the literature [190]. Hence, this finding is in agreement with data published by Kasitinon et al., showing that loss-of-TRPML1-function leads to impaired protein homeostasis in melanoma owing to excessive protein translation via mTORC1 activation, resulting in accumulation of misfolded proteins [73]. Translating these findings to our model, this putative accumulation of misfolded proteins could cause ER calcium release to initiate calcium-mediated ER stress signaling [191]. Alternatively, depletion of ER calcium could occur via a direct mechanism, as TRPML1 is important for proper calcium homeostasis and lysosomes and the ER are usually in close contact to modulate intracellular calcium distribution [65, 192-194]. Notably, ER stress and oxidative stress are deeply connected to each other since oxidative stress can promote protein misfolding and protein refolding, initiated by oxidation of disulfide bonds, leads to ROS production [195-197]. Indeed, excessive ER stress upon TRPML1 ko was responsible for enhanced oxidative stress in our model, as normal glutathione metabolism could be restored by addition of ER stress inhibitors. Due to the connection between ER stress and ferroptosis, it seems reasonable that ER stress upon TRPML1 ko increases ferroptosis sensitivity. For

example, ER stress caused ferroptosis in an ulcerative colitis model [198]. The implication of ER stress in ferroptosis is furthermore underlined by Xu et al. who showed that ASK1, a kinase important for ER stress propagation [199], is involved in erastin-induced cell death [200]. Furthermore, commonly used ferroptosis inducers caused ER stress [201]. Supporting this theory, the experimental compound tagitinin C induced ferroptosis by induction of ER stress [202].

In addition, the ER and associated calcium signaling are important regulators of lipid homeostasis. In this context, Xin et al. demonstrated that ER calcium depletion by overexpression of MS4A15 or long-term treatment with thapsigargin renders cancer cells resistant to ferroptosis as a result of depletion of polyunsaturated fatty acids [103]. In our cell model, we could not detect significant changes in PUFA-PE levels upon loss-of-TRPML1-function. However, TPC2 ko cells had decreased PUFA-PE levels in favor of MUFA-PE levels which is known to promote resistance to ferroptosis [94]. This was connected to decreased expression of pro-ferroptotic ACSL4, a master regulator of ferroptosis sensitivity that influences the cellular lipid profile in favor of PUFA-containing phospholipids [203]. However, the elucidation of detailed, underlying mechanisms in our model and the exact implication of TPC2 requires further research.

In summary, our data emphasize that TPC2 and TRPML1 differentially modulate ferroptotic cell death. While TPC2 ko causes ferroptosis resistance through alterations in PE lipid composition and ferrous iron depletion, loss-of-TRPML1-function results in increased ferroptosis sensitivity as a consequence of excessive oxidative stress.

5.5 Lysosomal cation channels are promising and druggable targets in cancer and beyond

The results of this study establish the endolysosomal cation channels TPC2 and TRPML1 as promising anti-cancer targets in terms of chemosensitization or modulation of ferroptosis sensitivity. We detected TPC2 in primary ALL PDX cells from clinical patients and demonstrated that TPC2 contributes to chemoresistance, as TPC2 inhibition with tetrandrine increased chemosensitivity. Although analysis of these samples revealed no overexpression in tumor cells as compared to non-cancerous, healthy PBMCs, the combination approach using vincristine and tetrandrine preferentially targeted tumor cells. This is in line with Müller et al. who tested several established and novel TPC2 inhibitors in different cancer cell lines and models of healthy cells. This cancer selectivity was at least partly attributed to increased uptake of these TPC2 inhibitors into tumor cells as compared to healthy cells [45]. Considering

the fact that TPC2 ko mice are viable [51, 146, 204, 205], TPC2 inhibition may be a feasible approach for anti-cancer therapy with tolerable side effects, either in monotherapy or in combination therapies.

Besides chemosensitization by TPC2 ko or pharmacological inhibition, we discovered a novel role of TPC2 in ferroptosis induction, i.e. that targeting TPC2 renders HCC cells resistant to ferroptosis. These findings might be especially valuable – provided that this approach is applicable to other cell types – for diseases whose pathology is connected to ferroptosis induction, such as acute liver failure [206], neurodegenerative diseases [80, 81] or doxorubicin-induced cardiotoxicity [83]. Of note, in the past decade, a lot of effort was put into the identification and development of novel TPC2 inhibitors. Based on the natural product tetrandrine, whose *in vivo* application is limited by toxicity issues [207, 208], novel, easily accessible, less toxic, and more potent truncated analogues have been developed by our group in corporation with the groups of Prof. Dr. Franz Bracher and Prof. Dr. Dr. Christian Grimm (both LMU Munich, Germany) [45]. Similarly, by a screening of many different plant extracts and flavonoids, novel flavonoids were identified as TPC2 inhibitors with around 30-fold increased potency as compared to the established TPC2 inhibitor naringenin [46]. At the same time, drug repurposing approaches led to the identification of approved drugs, such as raloxifene, fluphenazine, or bepridil as TPC2 inhibitors [209].

All the compounds mentioned above are not only valuable tools, but represent lead-like or drug-like molecules in different disease areas related to TPC2. These disease areas include for example viral infection [49, 50], and neurodegenerative disorders for which curative treatments are vastly lacking. For example, TPC2 inhibition with tetrandrine improved cognitive deficits in Alzheimer's disease [52] and other tauopathies [210]. Moreover, TPC2 silencing or pharmacological inhibition with Ned-19 restored lysosomal function in LRRK2-driven Parkinson's disease [53].

Additionally, the concurrent identification and development of novel TPC2 activators advanced the understanding of the cation channel itself. By mimicking the endogenous activators NAADP and $PI(3,5)P_2$ using TPC2-A1-N or TPC2-A1-P, respectively, Gerndt et al. underlined that the ion selectivity of TPC2 is switchable in dependence of the activation mode [42]. In this context, activation with NAADP or TPC2-A1-N predominantly led to calcium permeability, whereas activation with $PI(3,5)P_2$ or TPC2-A1-P facilitated sodium conductance [42]. Of note, ion conductance via TPC2 by pharmacological activation is tunable by a combination of these two mimics [43]. Recently, Scotto Rosato et al. identified activation of TPC2 with TPC2-A1-P as a promising therapeutic strategy for a set of inherited lysosomal storage diseases, including

mucolipidosis type IV, Batten disease, and Niemann-Pick type C1 [211], giving hope for clinical therapeutic approaches in the future.

Similarly, small molecule inhibitors and activators of TRPML1 have been discovered. Exemplarily, by screening a compound library, Rühl et al. found that EDME potently inhibits TRPML1, while inhibition of TRPML2 or TRPML3 as well as other cation channels from the TRP family does only occur at >10-fold higher concentrations, providing a valuable tool to specifically inhibit TRPML1 [75]. Furthermore, by derivatizing ML-SA1, a small molecule activator of TRPML1, TRPML2 and TRPML3, the TRPML1-specific activator ML1-SA1 was discovered [60, 74]. In cancer, targeting TRPML1 is an interesting therapeutic approach. In our study, we discovered that loss-of-TRPML1-function or pharmacological inhibition sensitizes HCC cells to ferroptosis by inducing ER stress. Of note, this feature is not only relevant for drug combinations with recently discovered, pre-clinical ferroptosis inducers, but also for radiation therapy whose efficiency is partly based on ferroptosis induction [212, 213].

The findings presented in our study as well as other recent findings in the field of endolysosomal cation channels will hopefully provide novel approaches for cancer therapy, as well as for therapies in other indications to improve treatment strategies in the future.

6 Summary

In summary, loss-of-TPC2-function sensitizes multidrug-resistant leukemia cells to chemotherapy by a dual mode of action. On the one hand, TPC2 ko leads to lysosomal alkalinization and thereby impairs lysosomal drug sequestration, facilitating increased concentrations of cytostatics at their sites of action. On the other hand, TPC2 ko cells are more susceptible to lysosomal damage, favoring initiation of lysosomal cell death mediated by cathepsin B which amplifies pro-apoptotic signaling. Hence, this work reveals TPC2 as promising, druggable anti-cancer target to sensitize leukemic cells to chemotherapy and moreover gives mechanistic insights into the dual role of lysosomes in chemoresistance and cell death (Fig. 29A).

Secondly, TPC2 and TRPML1 differentially modulate ferroptosis sensitivity by distinct mechanisms. Loss-of-TPC2-function renders HCC cells resistant to ferroptosis mediated by iron depletion and by decreased PUFA-PE levels in favor of MUFA-PEs. Intriguingly, TRPML1 ko cells are more sensitive to ferroptosis induction as compared to wt cells, attributed to the induction of latent ER stress, causing oxidative stress and hence increased demand of reduced glutathione. These data shed light on a novel role of endolysosomal cation channels in ferroptosis and concurrently give insights into the regulation of ferroptosis-associated metabolic processes by channel manipulation (Fig. 29B).

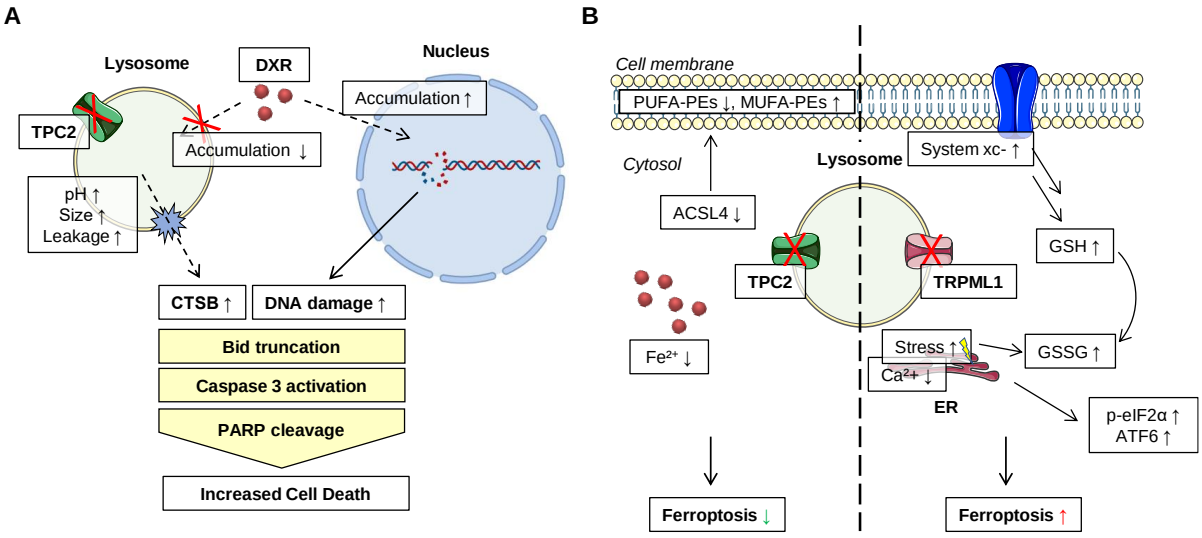

Figure 29. Summary. (Figure legend on next page)

Figure 29. Summary.
A Targeting TPC2 sensitizes ALL cells to chemotherapeutics. Loss-of-TPC2-function causes alkalinization of the lysosomal compartment, hindering lysosomal sequestration of weak base cytostatics. Thereby, instead of accumulating in lysosomes, weak base cytostatics are increasingly abundant at their intracellular targets, causing chemosensitization. Besides, TPC2 ko cells are more susceptible to lysosomal damage, causing cytosolic abundance of cathepsin B which is involved in the activating truncation of Bid as well as caspase 3 activation. This causes a pro-apoptotic milieu which eventually leads to increased cell death upon chemotherapy in TPC2 ko cells. **B** TPC2 and TRPML1 differentially modulate ferroptosis. Loss-of-TPC2-function leads to decreased levels of labile ferrous iron, an important regulator of ferroptosis sensitivity. Besides, TPC2 ko interferes with lipid metabolism mediated by ACSL4 which causes alterations in PUFA-PE and MUFA-PE levels, rendering TPC2 ko cells resistant to ferroptosis. In contrast, loss-of-TRPML1-function promotes ferroptosis sensitivity. This is attributed to increased oxidative stress mediated by the endoplasmic reticulum which influences glutathione metabolism, i.e. increased GSSG levels. Enhanced oxidative stress is compensated by upregulation of the system xc- component SLC7A11, a prominent target of ferroptosis inducers.

7 References

1. Sung, H., et al., *Global Cancer Statistics 2020: GLOBOCAN Estimates of Incidence and Mortality Worldwide for 36 Cancers in 185 Countries.* CA: A Cancer Journal for Clinicians, 2021. **71**(3): p. 209-249.
2. Stankovic, T. and E. Marston, *Molecular mechanisms involved in chemoresistance in paediatric acute lymphoblastic leukaemia.* Srp Arh Celok Lek, 2008. **136**(3-4): p. 187-92.
3. Terwilliger, T. and M. Abdul-Hay, *Acute lymphoblastic leukemia: a comprehensive review and 2017 update.* Blood Cancer Journal, 2017. **7**(6): p. e577-e577.
4. Hoelzer, D., et al., *Acute lymphoblastic leukaemia in adult patients: ESMO Clinical Practice Guidelines for diagnosis, treatment and follow-up.* Ann Oncol, 2016. **27**(suppl 5): p. v69-v82.
5. Oriol, A., et al., *Outcome after relapse of acute lymphoblastic leukemia in adult patients included in four consecutive risk-adapted trials by the PETHEMA Study Group.* Haematologica, 2010. **95**(4): p. 589-96.
6. DuVall, A.S., et al., *Updates in the Management of Relapsed and Refractory Acute Lymphoblastic Leukemia: An Urgent Plea for New Treatments Is Being Answered!* JCO Oncology Practice, 2022. **18**(7): p. 479-487.
7. Mansoori, B., et al., *The Different Mechanisms of Cancer Drug Resistance: A Brief Review.* Adv Pharm Bull, 2017. **7**(3): p. 339-348.
8. Chung, F.S., et al., *Disrupting P-glycoprotein function in clinical settings: what can we learn from the fundamental aspects of this transporter?* Am J Cancer Res, 2016. **6**(8): p. 1583-98.
9. Callaghan, R., F. Luk, and M. Bebawy, *Inhibition of the multidrug resistance P-glycoprotein: time for a change of strategy?* Drug Metab Dispos, 2014. **42**(4): p. 623-31.
10. Ramos, A., S. Sadeghi, and H. Tabatabaeian, *Battling Chemoresistance in Cancer: Root Causes and Strategies to Uproot Them.* Int J Mol Sci, 2021. **22**(17).
11. Tang, T., et al., *The role of lysosomes in cancer development and progression.* Cell & Bioscience, 2020. **10**(1): p. 131.
12. Grimm, C., et al., *Endolysosomal Cation Channels and Cancer-A Link with Great Potential.* Pharmaceuticals (Basel), 2018. **11**(1).
13. Trivedi, P.C., J.J. Bartlett, and T. Pulinilkunnil, *Lysosomal Biology and Function: Modern View of Cellular Debris Bin.* Cells, 2020. **9**(5).
14. De Duve, C., et al., *Tissue fractionation studies. 6. Intracellular distribution patterns of enzymes in rat-liver tissue.* Biochem J, 1955. **60**(4): p. 604-17.
15. Mony, V.K., S. Benjamin, and E.J. O'Rourke, *A lysosome-centered view of nutrient homeostasis.* Autophagy, 2016. **12**(4): p. 619-31.
16. Shin, H.R. and R. Zoncu, *The Lysosome at the Intersection of Cellular Growth and Destruction.* Developmental Cell, 2020. **54**(2): p. 226-238.
17. Dikic, I. and Z. Elazar, *Mechanism and medical implications of mammalian autophagy.* Nature Reviews Molecular Cell Biology, 2018. **19**(6): p. 349-364.
18. Aits, S. and M. Jäättelä, *Lysosomal cell death at a glance.* Journal of Cell Science, 2013. **126**(9): p. 1905-1912.
19. Guicciardi, M.E., M. Leist, and G.J. Gores, *Lysosomes in cell death.* Oncogene, 2004. **23**(16): p. 2881-2890.
20. Lawrence, R.E. and R. Zoncu, *The lysosome as a cellular centre for signalling, metabolism and quality control.* Nature Cell Biology, 2019. **21**(2): p. 133-142.
21. Thelen, A.M. and R. Zoncu, *Emerging Roles for the Lysosome in Lipid Metabolism.* Trends Cell Biol, 2017. **27**(11): p. 833-850.
22. Watts, C., *Lysosomes and lysosome-related organelles in immune responses.* FEBS Open Bio, 2022. **12**(4): p. 678-693.
23. Sun, A., *Lysosomal storage disease overview.* Ann Transl Med, 2018. **6**(24): p. 476.

24. Machado, E.R., et al., *Lysosomes and Cancer Progression: A Malignant Liaison.* Frontiers in Cell and Developmental Biology, 2021. **9**.
25. Zhitomirsky, B. and Y.G. Assaraf, *Lysosomes as mediators of drug resistance in cancer.* Drug Resist Updat, 2016. **24**: p. 23-33.
26. Yamagishi, T., et al., *P-glycoprotein Mediates Drug Resistance via a Novel Mechanism Involving Lysosomal Sequestration*.* The Journal of Biological Chemistry, 2013. **288**: p. 31761 - 31771.
27. Al-Akra, L., et al., *Tumor stressors induce two mechanisms of intracellular P-glycoprotein–mediated resistance that are overcome by lysosomal-targeted thiosemicarbazones.* Journal of Biological Chemistry, 2018. **293**(10): p. 3562-3587.
28. Seebacher, N.A., D.R. Richardson, and P.J. Jansson, *A mechanism for overcoming P-glycoprotein-mediated drug resistance: novel combination therapy that releases stored doxorubicin from lysosomes via lysosomal permeabilization using Dp44mT or DpC.* Cell Death & Disease, 2016. **7**(12): p. e2510-e2510.
29. Geisslinger, F., et al., *Targeting Lysosomes in Cancer as Promising Strategy to Overcome Chemoresistance—A Mini Review.* Frontiers in Oncology, 2020. **10**.
30. Zhitomirsky, B. and Y.G. Assaraf, *The role of cytoplasmic-to-lysosomal pH gradient in hydrophobic weak base drug sequestration in lysosomes.* Cancer Cell & Microenvironment, 2015. **2**.
31. Turk, B. and V. Turk, *Lysosomes as "suicide bags" in cell death: myth or reality?* J Biol Chem, 2009. **284**(33): p. 21783-21787.
32. Gómez-Sintes, R., M.D. Ledesma, and P. Boya, *Lysosomal cell death mechanisms in aging.* Ageing Research Reviews, 2016. **32**: p. 150-168.
33. Petersen, N.H., et al., *Transformation-associated changes in sphingolipid metabolism sensitize cells to lysosomal cell death induced by inhibitors of acid sphingomyelinase.* Cancer Cell, 2013. **24**(3): p. 379-93.
34. Bonam, S.R., F. Wang, and S. Muller, *Lysosomes as a therapeutic target.* Nature Reviews Drug Discovery, 2019. **18**(12): p. 923-948.
35. Chen, C.-C., et al., *Endolysosomal cation channels point the way towards precision medicine of cancer and infectious diseases.* Biomedicine & Pharmacotherapy, 2022. **148**: p. 112751.
36. Grimm, C., et al., *From mucolipidosis type IV to Ebola: TRPML and two-pore channels at the crossroads of endo-lysosomal trafficking and disease.* Cell Calcium, 2017. **67**: p. 148-155.
37. She, J., et al., *Structural mechanisms of phospholipid activation of the human TPC2 channel.* Elife, 2019. **8**.
38. She, J., et al., *Structural insights into the voltage and phospholipid activation of the mammalian TPC1 channel.* Nature, 2018. **556**(7699): p. 130-134.
39. Patel, S., et al., *Electrophysiology of Endolysosomal Two-Pore Channels: A Current Account.* Cells, 2022. **11**(15).
40. Wang, X., et al., *TPC proteins are phosphoinositide- activated sodium-selective ion channels in endosomes and lysosomes.* Cell, 2012. **151**(2): p. 372-83.
41. Calcraft, P.J., et al., *NAADP mobilizes calcium from acidic organelles through two-pore channels.* Nature, 2009. **459**(7246): p. 596-600.
42. Gerndt, S., et al., *Agonist-mediated switching of ion selectivity in TPC2 differentially promotes lysosomal function.* Elife, 2020. **9**.
43. Yuan, Y., et al., *Segregated cation flux by TPC2 biases Ca(2+) signaling through lysosomes.* Nat Commun, 2022. **13**(1): p. 4481.
44. Ogunbayo, O.A., et al., *mTORC1 controls lysosomal Ca²⁺ release through the two-pore channel TPC2.* Science Signaling, 2018. **11**(525): p. eaao5775.
45. Müller, M., et al., *Gene editing and synthetically accessible inhibitors reveal role for TPC2 in HCC cell proliferation and tumor growth.* Cell Chem Biol, 2021. **28**(8): p. 1119-1131.e27.

46. Netcharoensirisuk, P., et al., *Flavonoids increase melanin production and reduce proliferation, migration and invasion of melanoma cells by blocking endolysosomal/melanosomal TPC2.* Scientific Reports, 2021. **11**(1): p. 8515.
47. Sun, W. and J. Yue, *TPC2 mediates autophagy progression and extracellular vesicle secretion in cancer cells.* Exp Cell Res, 2018. **370**(2): p. 478-489.
48. Davis, L.C., A.J. Morgan, and A. Galione, *NAADP-regulated two-pore channels drive phagocytosis through endo-lysosomal Ca2+ nanodomains, calcineurin and dynamin.* The EMBO Journal, 2020. **39**(14): p. e104058.
49. Sakurai, Y., et al., *Two-pore channels control Ebola virus host cell entry and are drug targets for disease treatment.* Science, 2015. **347**(6225): p. 995-998.
50. Ou, X., et al., *Characterization of spike glycoprotein of SARS-CoV-2 on virus entry and its immune cross-reactivity with SARS-CoV.* Nature Communications, 2020. **11**(1): p. 1620.
51. Grimm, C., et al., *High susceptibility to fatty liver disease in two-pore channel 2-deficient mice.* Nature Communications, 2014. **5**(1): p. 4699.
52. Tong, B.C., et al., *Lysosomal TPCN (two pore segment channel) inhibition ameliorates beta-amyloid pathology and mitigates memory impairment in Alzheimer disease.* Autophagy, 2022. **18**(3): p. 624-642.
53. Hockey, L.N., et al., *Dysregulation of lysosomal morphology by pathogenic LRRK2 is corrected by TPC2 inhibition.* J Cell Sci, 2015. **128**(2): p. 232-8.
54. Skelding, K.A., et al., *Targeting the two-pore channel 2 in cancer progression and metastasis.* Exploration of Targeted Anti-tumor Therapy, 2022. **3**(1): p. 62-89.
55. Alharbi, A.F. and J. Parrington, *Endolysosomal Ca2+ Signaling in Cancer: The Role of TPC2, From Tumorigenesis to Metastasis.* Frontiers in Cell and Developmental Biology, 2019. **7**.
56. Faris, P., et al., *Endolysosomal Ca(2+) Signalling and Cancer Hallmarks: Two-Pore Channels on the Move, TRPML1 Lags Behind!* Cancers (Basel), 2018. **11**(1).
57. Li, F., et al., *Identification a novel set of 6 differential expressed genes in prostate cancer that can potentially predict biochemical recurrence after curative surgery.* Clin Transl Oncol, 2019. **21**(8): p. 1067-1075.
58. Nguyen, O.N., et al., *Two-Pore Channel Function Is Crucial for the Migration of Invasive Cancer Cells.* Cancer Res, 2017. **77**(6): p. 1427-1438.
59. Plesch, E., et al., *Selective agonist of TRPML2 reveals direct role in chemokine release from innate immune cells.* eLife, 2018. **7**: p. e39720.
60. Spix, B., et al., *Lung emphysema and impaired macrophage elastase clearance in mucolipin 3 deficient mice.* Nature Communications, 2022. **13**(1): p. 318.
61. Cheng, X., et al., *Mucolipins: Intracellular TRPML1-3 channels.* FEBS Letters, 2010. **584**(10): p. 2013-2021.
62. Chen, Q., et al., *Structure of mammalian endolysosomal TRPML1 channel in nanodiscs.* Nature, 2017. **550**(7676): p. 415-418.
63. Schmiege, P., et al., *Human TRPML1 channel structures in open and closed conformations.* Nature, 2017. **550**(7676): p. 366-370.
64. Zhang, X., et al., *MCOLN1 is a ROS sensor in lysosomes that regulates autophagy.* Nature Communications, 2016. **7**(1): p. 12109.
65. Kilpatrick, B.S., et al., *Endo-lysosomal TRP mucolipin-1 channels trigger global ER Ca2+ release and Ca2+ influx.* Journal of Cell Science, 2016. **129**(20): p. 3859-3867.
66. Peng, W., Y.C. Wong, and D. Krainc, *Mitochondria-lysosome contacts regulate mitochondrial Ca²⁺ dynamics via lysosomal TRPML1.* Proceedings of the National Academy of Sciences, 2020. **117**(32): p. 19266-19275.
67. Dong, X.-P., et al., *The type IV mucolipidosis-associated protein TRPML1 is an endolysosomal iron release channel.* Nature, 2008. **455**(7215): p. 992-996.
68. Fernández, B., et al., *Iron-induced cytotoxicity mediated by endolysosomal TRPML1 channels is reverted by TFEB.* Cell Death & Disease, 2022. **13**(12): p. 1047.

69. Scotto Rosato, A., et al., *TRPML1 links lysosomal calcium to autophagosome biogenesis through the activation of the CaMKKβ/VPS34 pathway.* Nature Communications, 2019. **10**(1): p. 5630.
70. Sun, M., et al., *Mucolipidosis type IV is caused by mutations in a gene encoding a novel transient receptor potential channel.* Human Molecular Genetics, 2000. **9**(17): p. 2471-2478.
71. Vergarajauregui, S. and R. Puertollano, *Mucolipidosis type IV: The importance of functional lysosomes for efficient autophagy.* Autophagy, 2008. **4**(6): p. 832-834.
72. Tedeschi, V., et al., *The activation of Mucolipin TRP channel 1 (TRPML1) protects motor neurons from L-BMAA neurotoxicity by promoting autophagic clearance.* Scientific Reports, 2019. **9**(1): p. 10743.
73. Kasitinon, S.Y., et al., *TRPML1 Promotes Protein Homeostasis in Melanoma Cells by Negatively Regulating MAPK and mTORC1 Signaling.* Cell Rep, 2019. **28**(9): p. 2293-2305.e9.
74. Siow, W.X., et al., *Lysosomal TRPML1 regulates mitochondrial function in hepatocellular carcinoma cells.* J Cell Sci, 2022. **135**(6).
75. Rühl, P., et al., *Estradiol analogs attenuate autophagy, cell migration and invasion by direct and selective inhibition of TRPML1, independent of estrogen receptors.* Scientific Reports, 2021. **11**(1): p. 8313.
76. Jung, J., et al., *HRAS-driven cancer cells are vulnerable to TRPML1 inhibition.* EMBO Rep, 2019. **20**(4).
77. Morelli, M.B., et al., *Transient Receptor Potential Mucolipin-1 Channels in Glioblastoma: Role in Patient's Survival.* Cancers (Basel), 2019. **11**(4).
78. Hu, Z.D., et al., *MCOLN1 Promotes Proliferation and Predicts Poor Survival of Patients with Pancreatic Ductal Adenocarcinoma.* Dis Markers, 2019. **2019**: p. 9436047.
79. Jiang, X., B.R. Stockwell, and M. Conrad, *Ferroptosis: mechanisms, biology and role in disease.* Nature Reviews Molecular Cell Biology, 2021. **22**(4): p. 266-282.
80. Guiney, S.J., et al., *Ferroptosis and cell death mechanisms in Parkinson's disease.* Neurochem Int, 2017. **104**: p. 34-48.
81. Zhang, Y., M. Wang, and W. Chang, *Iron dyshomeostasis and ferroptosis in Alzheimer's disease: Molecular mechanisms of cell death and novel therapeutic drugs and targets for AD.* Frontiers in Pharmacology, 2022. **13**.
82. Zille, M., et al., *Neuronal Death After Hemorrhagic Stroke In Vitro and In Vivo Shares Features of Ferroptosis and Necroptosis.* Stroke, 2017. **48**(4): p. 1033-1043.
83. Abe, K., et al., *Doxorubicin causes ferroptosis and cardiotoxicity by intercalating into mitochondrial DNA and disrupting Alas1-dependent heme synthesis.* Science Signaling, 2022. **15**(758): p. eabn8017.
84. Zhang, C., et al., *Ferroptosis in cancer therapy: a novel approach to reversing drug resistance.* Molecular Cancer, 2022. **21**(1): p. 47.
85. Hangauer, M.J., et al., *Drug-tolerant persister cancer cells are vulnerable to GPX4 inhibition.* Nature, 2017. **551**(7679): p. 247-250.
86. Nie, J., et al., *Role of ferroptosis in hepatocellular carcinoma.* J Cancer Res Clin Oncol, 2018. **144**(12): p. 2329-2337.
87. Pan, F., et al., *The Critical Role of Ferroptosis in Hepatocellular Carcinoma.* Frontiers in Cell and Developmental Biology, 2022. **10**.
88. Dixon, S.J., et al., *Ferroptosis: an iron-dependent form of nonapoptotic cell death.* Cell, 2012. **149**(5): p. 1060-72.
89. Outten, F.W. and E.C. Theil, *Iron-based redox switches in biology.* Antioxid Redox Signal, 2009. **11**(5): p. 1029-46.
90. Dixon, S.J. and B.R. Stockwell, *The role of iron and reactive oxygen species in cell death.* Nature Chemical Biology, 2014. **10**(1): p. 9-17.
91. Bridges, R.J., N.R. Natale, and S.A. Patel, *System xc⁻ cystine/glutamate antiporter: an update on molecular pharmacology and roles within the CNS.* Br J Pharmacol, 2012. **165**(1): p. 20-34.
92. Lu, S.C., *Glutathione synthesis.* Biochim Biophys Acta, 2013. **1830**(5): p. 3143-53.

93. Seibt, T.M., B. Proneth, and M. Conrad, *Role of GPX4 in ferroptosis and its pharmacological implication.* Free Radical Biology and Medicine, 2019. **133**: p. 144-152.
94. Magtanong, L., et al., *Exogenous Monounsaturated Fatty Acids Promote a Ferroptosis-Resistant Cell State.* Cell Chemical Biology, 2019. **26**(3): p. 420-432.e9.
95. Lee, J.-Y., et al., *Polyunsaturated fatty acid biosynthesis pathway determines ferroptosis sensitivity in gastric cancer.* Proceedings of the National Academy of Sciences, 2020. **117**(51): p. 32433-32442.
96. Gao, H., et al., *Ferroptosis is a lysosomal cell death process.* Biochemical and Biophysical Research Communications, 2018. **503**(3): p. 1550-1556.
97. Chen, X., et al., *Organelle-specific regulation of ferroptosis.* Cell Death & Differentiation, 2021. **28**(10): p. 2843-2856.
98. Lee, D.A. and J.M. Goodfellow, *The pH-Induced Release of Iron from Transferrin Investigated with a Continuum Electrostatic Model.* Biophysical Journal, 1998. **74**(6): p. 2747-2759.
99. Bogdan, A.R., et al., *Regulators of Iron Homeostasis: New Players in Metabolism, Cell Death, and Disease.* Trends Biochem Sci, 2016. **41**(3): p. 274-286.
100. Rizzollo, F., et al., *The lysosome as a master regulator of iron metabolism.* Trends Biochem Sci, 2021. **46**(12): p. 960-975.
101. Wu, Z., et al., *Chaperone-mediated autophagy is involved in the execution of ferroptosis.* Proceedings of the National Academy of Sciences, 2019. **116**(8): p. 2996-3005.
102. Singh, R. and A.M. Cuervo, *Lipophagy: connecting autophagy and lipid metabolism.* Int J Cell Biol, 2012. **2012**: p. 282041.
103. Xin, S., et al., *MS4A15 drives ferroptosis resistance through calcium-restricted lipid remodeling.* Cell Death & Differentiation, 2022. **29**(3): p. 670-686.
104. Foley, G.E., et al., *CONTINUOUS CULTURE OF HUMAN LYMPHOBLASTS FROM PERIPHERAL BLOOD OF A CHILD WITH ACUTE LEUKEMIA.* Cancer, 1965. **18**: p. 522-9.
105. Haber, M., et al., *Atypical multidrug resistance in a therapy-induced drug-resistant human leukemia cell line (LALW-2): resistance to Vinca alkaloids independent of P-glycoprotein.* Cancer Res, 1989. **49**(19): p. 5281-7.
106. Müller, M., *Novel chemical tools to target two-pore channel 2, P-glycoprotein and histone deacetylase 6 in cancer*, in *Faculty for Chemistry and Pharmacy*. 2020, Ludwig-Maximilians-University: Munich.
107. Ebinger, S., et al., *Characterization of Rare, Dormant, and Therapy-Resistant Cells in Acute Lymphoblastic Leukemia.* Cancer Cell, 2016. **30**(6): p. 849-862.
108. Nicoletti, I., et al., *A rapid and simple method for measuring thymocyte apoptosis by propidium iodide staining and flow cytometry.* Journal of Immunological Methods, 1991. **139**(2): p. 271-279.
109. Ehrhardt, H., et al., *Optimized anti-tumor effects of anthracyclines plus Vinca alkaloids using a novel, mechanism-based application schedule.* Blood, 2011. **118**(23): p. 6123-31.
110. Zhong, B., et al., *Caspase-8 Induces Lysosome-Associated Cell Death in Cancer Cells.* Mol Ther, 2020. **28**(4): p. 1078-1091.
111. Robey, R.W., et al., *Inhibition of P-glycoprotein (ABCB1)- and multidrug resistance-associated protein 1 (ABCC1)-mediated transport by the orally administered inhibitor, CBT-1((R)).* Biochem Pharmacol, 2008. **75**(6): p. 1302-12.
112. Schieder, M., et al., *Planar patch clamp approach to characterize ionic currents from intact lysosomes.* Sci Signal, 2010. **3**(151): p. pl3.
113. Fleige, S., et al., *Comparison of relative mRNA quantification models and the impact of RNA integrity in quantitative real-time RT-PCR.* Biotechnol Lett, 2006. **28**(19): p. 1601-13.

114. Koeberle, A., et al., *Role of p38 mitogen-activated protein kinase in linking stearoyl-CoA desaturase-1 activity with endoplasmic reticulum homeostasis.* Faseb j, 2015. **29**(6): p. 2439-49.
115. Koeberle, A., et al., *Arachidonoyl-phosphatidylcholine oscillates during the cell cycle and counteracts proliferation by suppressing Akt membrane binding.* Proceedings of the National Academy of Sciences, 2013. **110**(7): p. 2546-2551.
116. Kavallaris, M., et al., *Resistance to tetracycline, a hydrophilic antibiotic, is mediated by P-glycoprotein in human multidrug-resistant cells.* Biochem Biophys Res Commun, 1993. **190**(1): p. 79-85.
117. Kirkegaard, T. and M. Jäättelä, *Lysosomal involvement in cell death and cancer.* Biochimica et Biophysica Acta (BBA) - Molecular Cell Research, 2009. **1793**(4): p. 746-754.
118. Blajeski, A.L., et al., *G1 and G2 cell-cycle arrest following microtubule depolymerization in human breast cancer cells.* The Journal of Clinical Investigation, 2002. **110**(1): p. 91-99.
119. Cliby, W.A., et al., *S Phase and G2 Arrests Induced by Topoisomerase I Poisons Are Dependent on ATR Kinase Function*.* Journal of Biological Chemistry, 2002. **277**(2): p. 1599-1606.
120. Shin, H.-J., et al., *Doxorubicin-induced necrosis is mediated by poly-(ADP-ribose) polymerase 1 (PARP1) but is independent of p53.* Scientific Reports, 2015. **5**(1): p. 15798.
121. Vassileva, K., M. Marsh, and S. Patel, *Two-pore channels as master regulators of membrane trafficking and endocytic well-being.* Curr Opin Physiol, 2020. **17**: p. 163-168.
122. Schütz, R., et al., *Synthesis, biological evaluation and toxicity of novel tetrandrine analogues.* Eur J Med Chem, 2020. **207**: p. 112810.
123. Vick, B., et al., *An advanced preclinical mouse model for acute myeloid leukemia using patients' cells of various genetic subgroups and in vivo bioluminescence imaging.* PLoS One, 2015. **10**(3): p. e0120925.
124. Mlejnek, P., et al., *Lysosomal sequestration of weak base drugs, lysosomal biogenesis, and cell cycle alteration.* Biomedicine & Pharmacotherapy, 2022. **153**: p. 113328.
125. Schmitt, M.V., et al., *Quantitation of Lysosomal Trapping of Basic Lipophilic Compounds Using In Vitro Assays and In Silico Predictions Based on the Determination of the Full pH Profile of the Endo-/Lysosomal System in Rat Hepatocytes.* Drug Metabolism and Disposition, 2019. **47**(1): p. 49-57.
126. Sharma, A., K. Singh, and A. Almasan, *Histone H2AX phosphorylation: a marker for DNA damage.* Methods Mol Biol, 2012. **920**: p. 613-26.
127. Höglinger, D., et al., *Intracellular sphingosine releases calcium from lysosomes.* eLife, 2015. **4**: p. e10616.
128. Brady, O.A., et al., *The transcription factors TFE3 and TFEB amplify p53 dependent transcriptional programs in response to DNA damage.* eLife, 2018. **7**: p. e40856.
129. Ono, K., S.O. Kim, and J. Han, *Susceptibility of lysosomes to rupture is a determinant for plasma membrane disruption in tumor necrosis factor alpha-induced cell death.* Mol Cell Biol, 2003. **23**(2): p. 665-76.
130. Pierzyńska-Mach, A., P.A. Janowski, and J.W. Dobrucki, *Evaluation of acridine orange, LysoTracker Red, and quinacrine as fluorescent probes for long-term tracking of acidic vesicles.* Cytometry Part A, 2014. **85**(8): p. 729-737.
131. Boya, P. and G. Kroemer, *Lysosomal membrane permeabilization in cell death.* Oncogene, 2008. **27**(50): p. 6434-6451.
132. Appelqvist, H., et al., *The lysosome: from waste bag to potential therapeutic target.* J Mol Cell Biol, 2013. **5**(4): p. 214-26.
133. Horváth, I. and L. Vígh, *Stability in times of stress.* Nature, 2010. **463**(7280): p. 436-438.

134. Droga-Mazovec, G., et al., *Cysteine Cathepsins Trigger Caspase-dependent Cell Death through Cleavage of Bid and Antiapoptotic Bcl-2 Homologues*.* Journal of Biological Chemistry, 2008. **283**(27): p. 19140-19150.
135. Kogot-Levin, A., et al., *Upregulation of Mitochondrial Content in Cytochrome c Oxidase Deficient Fibroblasts.* PLOS ONE, 2016. **11**(10): p. e0165417.
136. Leu, J.I., et al., *Inhibition of stress-inducible HSP70 impairs mitochondrial proteostasis and function.* Oncotarget, 2017. **8**(28): p. 45656-45669.
137. Zorova, L.D., et al., *Mitochondrial membrane potential.* Anal Biochem, 2018. **552**: p. 50-59.
138. Rottenberg, H. and S. Wu, *Quantitative assay by flow cytometry of the mitochondrial membrane potential in intact cells.* Biochim Biophys Acta, 1998. **1404**(3): p. 393-404.
139. Jeong, S.Y. and D.W. Seol, *The role of mitochondria in apoptosis.* BMB Rep, 2008. **41**(1): p. 11-22.
140. Geisslinger, F., et al., *Targeting TPC2 sensitizes acute lymphoblastic leukemia cells to chemotherapeutics by impairing lysosomal function.* Cell Death Dis, 2022. **13**(8): p. 668.
141. Medavaram, S. and Y. Zhang, *Emerging therapies in advanced hepatocellular carcinoma.* Experimental Hematology & Oncology, 2018. **7**(1): p. 17.
142. Geng, N., et al., *Knockdown of ferroportin accelerates erastin-induced ferroptosis in neuroblastoma cells.* Eur Rev Med Pharmacol Sci, 2018. **22**(12): p. 3826-3836.
143. Lee, J.Y., et al., *Lipid Metabolism and Ferroptosis.* Biology (Basel), 2021. **10**(3).
144. Kawai, A., et al., *Autophagosome-lysosome fusion depends on the pH in acidic compartments in CHO cells.* Autophagy, 2007. **3**(2): p. 154-7.
145. Cipriano, D.J., et al., *Structure and regulation of the vacuolar ATPases.* Biochim Biophys Acta, 2008. **1777**(7-8): p. 599-604.
146. Lin, P.H., et al., *Lysosomal two-pore channel subtype 2 (TPC2) regulates skeletal muscle autophagic signaling.* J Biol Chem, 2015. **290**(6): p. 3377-89.
147. Ambrosio, A.L., et al., *TPC2 controls pigmentation by regulating melanosome pH and size.* Proceedings of the National Academy of Sciences, 2016. **113**(20): p. 5622-5627.
148. Lu, Y., et al., *NAADP/TPC2/Ca2+ Signaling Inhibits Autophagy.* Communicative & Integrative Biology, 2013. **6**(6): p. e27595.
149. Steinberg, B.E., et al., *A cation counterflux supports lysosomal acidification.* J Cell Biol, 2010. **189**(7): p. 1171-86.
150. Choy, C.H., et al., *Lysosome enlargement during inhibition of the lipid kinase PIKfyve proceeds through lysosome coalescence.* J Cell Sci, 2018. **131**(10).
151. Sharma, G., et al., *A family of PIKFYVE inhibitors with therapeutic potential against autophagy-dependent cancer cells disrupt multiple events in lysosome homeostasis.* Autophagy, 2019. **15**(10): p. 1694-1718.
152. Ponsford, A.H., et al., *Live imaging of intra-lysosome pH in cell lines and primary neuronal culture using a novel genetically encoded biosensor.* Autophagy, 2021. **17**(6): p. 1500-1518.
153. Settembre, C., et al., *A lysosome-to-nucleus signalling mechanism senses and regulates the lysosome via mTOR and TFEB.* The EMBO Journal, 2012. **31**(5): p. 1095-1108.
154. Perera, R.M., C.D. Malta, and A. Ballabio, *MiT/TFE Family of Transcription Factors, Lysosomes, and Cancer.* Annual Review of Cancer Biology, 2019. **3**(1): p. 203-222.
155. Schindler, M., et al., *Defective pH regulation of acidic compartments in human breast cancer cells (MCF-7) is normalized in adriamycin-resistant cells (MCF-7adr).* Biochemistry, 1996. **35**(9): p. 2811-7.
156. Fassl, A., et al., *Increased lysosomal biomass is responsible for the resistance of triple-negative breast cancers to CDK4/6 inhibition.* Science Advances, 2020. **6**(25): p. eabb2210.
157. Sardiello, M., et al., *A Gene Network Regulating Lysosomal Biogenesis and Function.* Science, 2009. **325**(5939): p. 473-477.

158. Napolitano, G. and A. Ballabio, *TFEB at a glance.* Journal of Cell Science, 2016. **129**(13): p. 2475-2481.
159. Fang, L.M., et al., *Transcription factor EB is involved in autophagy-mediated chemoresistance to doxorubicin in human cancer cells.* Acta Pharmacol Sin, 2017. **38**(9): p. 1305-1316.
160. Zhao, B., et al., *TFEB-mediated lysosomal biogenesis and lysosomal drug sequestration confer resistance to MEK inhibition in pancreatic cancer.* Cell Death Discov, 2020. **6**: p. 12.
161. Guo, B., et al., *Role of autophagy and lysosomal drug sequestration in acquired resistance to doxorubicin in MCF-7 cells.* BMC Cancer, 2016. **16**(1): p. 762.
162. Fu, D. and I.M. Arias, *Intracellular trafficking of P-glycoprotein.* Int J Biochem Cell Biol, 2012. **44**(3): p. 461-4.
163. Gericke, B., et al., *Is P-Glycoprotein Functionally Expressed in the Limiting Membrane of Endolysosomes? A Biochemical and Ultrastructural Study in the Rat Liver.* Cells, 2022. **11**(9).
164. Visser, N., et al., *Inhibition of Autophagy Does Not Re-Sensitize Acute Myeloid Leukemia Cells Resistant to Cytarabine.* Int J Mol Sci, 2021. **22**(5).
165. You, H., et al., *Small interfering RNA targeting the subunit ATP6L of proton pump V-ATPase overcomes chemoresistance of breast cancer cells.* Cancer Lett, 2009. **280**(1): p. 110-9.
166. Dröse, S. and K. Altendorf, *Bafilomycins and concanamycins as inhibitors of V-ATPases and P-ATPases.* J Exp Biol, 1997. **200**(Pt 1): p. 1-8.
167. Li, Z., et al., *Complete elucidation of the late steps of bafilomycin biosynthesis in Streptomyces lohii.* J Biol Chem, 2017. **292**(17): p. 7095-7104.
168. Gavini, J., et al., *Verteporfin-induced lysosomal compartment dysregulation potentiates the effect of sorafenib in hepatocellular carcinoma.* Cell Death Dis, 2019. **10**(10): p. 749.
169. Colletti, G.A., et al., *Loss of lysosomal ion channel transient receptor potential channel mucolipin-1 (TRPML1) leads to cathepsin B-dependent apoptosis.* J Biol Chem, 2012. **287**(11): p. 8082-91.
170. Pihán, P., et al., *Control of lysosomal-mediated cell death by the pH-dependent calcium channel RECS1.* Sci Adv, 2021. **7**(46): p. eabe5469.
171. Fehrenbacher, N., et al., *Sensitization to the lysosomal cell death pathway by oncogene-induced down-regulation of lysosome-associated membrane proteins 1 and 2.* Cancer Res, 2008. **68**(16): p. 6623-33.
172. Wang, F., R. Gómez-Sintes, and P. Boya, *Lysosomal membrane permeabilization and cell death.* Traffic, 2018. **19**(12): p. 918-931.
173. Adams-Cioaba, M.A., et al., *Structural basis for the recognition and cleavage of histone H3 by cathepsin L.* Nat Commun, 2011. **2**: p. 197.
174. Nagakannan, P., et al., *Cathepsin B is an executioner of ferroptosis.* Biochimica et Biophysica Acta (BBA) - Molecular Cell Research, 2021. **1868**(3): p. 118928.
175. Childs, A.C., et al., *Doxorubicin treatment in vivo causes cytochrome C release and cardiomyocyte apoptosis, as well as increased mitochondrial efficiency, superoxide dismutase activity, and Bcl-2:Bax ratio.* Cancer Res, 2002. **62**(16): p. 4592-8.
176. Gamen, S., et al., *Doxorubicin treatment activates a Z-VAD-sensitive caspase, which causes deltapsim loss, caspase-9 activity, and apoptosis in Jurkat cells.* Exp Cell Res, 2000. **258**(1): p. 223-35.
177. Tacar, O. and C.R. Dass, *Doxorubicin-induced death in tumour cells and cardiomyocytes: is autophagy the key to improving future clinical outcomes?* Journal of Pharmacy and Pharmacology, 2013. **65**(11): p. 1577-1589.
178. Indran, I.R., et al., *Recent advances in apoptosis, mitochondria and drug resistance in cancer cells.* Biochimica et Biophysica Acta (BBA) - Bioenergetics, 2011. **1807**(6): p. 735-745.
179. Neefjes, J.J., et al., *Intracellular interactions of transferrin and its receptor during biosynthesis.* J Cell Biol, 1990. **111**(4): p. 1383-92.

180. Schneider, L.S., et al., *Vacuolar-ATPase Inhibition Blocks Iron Metabolism to Mediate Therapeutic Effects in Breast Cancer.* Cancer Res, 2015. **75**(14): p. 2863-74.
181. Weber, R.A., et al., *Maintaining Iron Homeostasis Is the Key Role of Lysosomal Acidity for Cell Proliferation.* Mol Cell, 2020. **77**(3): p. 645-655.e7.
182. Fernández, B., et al., *Iron overload causes endolysosomal deficits modulated by NAADP-regulated 2-pore channels and RAB7A.* Autophagy, 2016. **12**(9): p. 1487-506.
183. Liu, J., et al., *NUPR1 is a critical repressor of ferroptosis.* Nature Communications, 2021. **12**(1): p. 647.
184. Ye, C.L., et al., *STEAP3 Affects Ferroptosis and Progression of Renal Cell Carcinoma Through the p53/xCT Pathway.* Technol Cancer Res Treat, 2022. **21**: p. 15330338221078728.
185. Fang, J., et al., *Ferroportin-mediated ferroptosis involved in new-onset atrial fibrillation with LPS-induced endotoxemia.* European Journal of Pharmacology, 2021. **913**: p. 174622.
186. Xu, P., et al., *MicroRNA-147a Targets SLC40A1 to Induce Ferroptosis in Human Glioblastoma.* Analytical Cellular Pathology, 2022. **2022**: p. 2843990.
187. Doll, S., et al., *FSP1 is a glutathione-independent ferroptosis suppressor.* Nature, 2019. **575**(7784): p. 693-698.
188. Boye, E. and B. Grallert, *eIF2α phosphorylation and the regulation of translation.* Curr Genet, 2020. **66**(2): p. 293-297.
189. Donnelly, N., et al., *The eIF2α kinases: their structures and functions.* Cell Mol Life Sci, 2013. **70**(19): p. 3493-511.
190. Groenendyk, J., L.B. Agellon, and M. Michalak, *Calcium signaling and endoplasmic reticulum stress.* Int Rev Cell Mol Biol, 2021. **363**: p. 1-20.
191. Zhang, K. and R.J. Kaufman, *From endoplasmic-reticulum stress to the inflammatory response.* Nature, 2008. **454**(7203): p. 455-462.
192. Atakpa, P., et al., *IP(3) Receptors Preferentially Associate with ER-Lysosome Contact Sites and Selectively Deliver Ca(2+) to Lysosomes.* Cell Rep, 2018. **25**(11): p. 3180-3193.e7.
193. Garrity, A.G., et al., *The endoplasmic reticulum, not the pH gradient, drives calcium refilling of lysosomes.* eLife, 2016. **5**: p. e15887.
194. Lloyd-Evans, E. and H. Waller-Evans, *Lysosomal Ca(2+) Homeostasis and Signaling in Health and Disease.* Cold Spring Harb Perspect Biol, 2020. **12**(6).
195. Bhattarai, K.R., et al., *The aftermath of the interplay between the endoplasmic reticulum stress response and redox signaling.* Experimental & Molecular Medicine, 2021. **53**(2): p. 151-167.
196. Cao, S.S. and R.J. Kaufman, *Endoplasmic reticulum stress and oxidative stress in cell fate decision and human disease.* Antioxid Redox Signal, 2014. **21**(3): p. 396-413.
197. Zeeshan, H.M.A., et al., *Endoplasmic Reticulum Stress and Associated ROS.* International Journal of Molecular Sciences, 2016. **17**(3): p. 327.
198. Xu, M., et al., *Ferroptosis involves in intestinal epithelial cell death in ulcerative colitis.* Cell Death & Disease, 2020. **11**(2): p. 86.
199. Hattori, K., et al., *The roles of ASK family proteins in stress responses and diseases.* Cell Communication and Signaling, 2009. **7**(1): p. 9.
200. Hattori, K., et al., *Cold stress-induced ferroptosis involves the ASK1-p38 pathway.* EMBO reports, 2017. **18**(11): p. 2067-2078.
201. Dixon, S.J., et al., *Pharmacological inhibition of cystine–glutamate exchange induces endoplasmic reticulum stress and ferroptosis.* eLife, 2014. **3**: p. e02523.
202. Wei, R., et al., *Tagitinin C induces ferroptosis through PERK-Nrf2-HO-1 signaling pathway in colorectal cancer cells.* Int J Biol Sci, 2021. **17**(11): p. 2703-2717.
203. Doll, S., et al., *ACSL4 dictates ferroptosis sensitivity by shaping cellular lipid composition.* Nature Chemical Biology, 2017. **13**(1): p. 91-98.
204. Cang, C., et al., *mTOR regulates lysosomal ATP-sensitive two-pore Na(+) channels to adapt to metabolic state.* Cell, 2013. **152**(4): p. 778-790.

205. Favia, A., et al., *VEGF-induced neoangiogenesis is mediated by NAADP and two-pore channel-2-dependent Ca2+ signaling.* Proc Natl Acad Sci U S A, 2014. **111**(44): p. E4706-15.
206. Yamada, N., et al., *Ferroptosis driven by radical oxidation of n-6 polyunsaturated fatty acids mediates acetaminophen-induced acute liver failure.* Cell Death & Disease, 2020. **11**(2): p. 144.
207. Jin, H., et al., *Pulmonary toxicity and metabolic activation of tetrandrine in CD-1 mice.* Chem Res Toxicol, 2011. **24**(12): p. 2142-52.
208. Tainlin, L., et al., *Studies of the chronic toxicity of tetrandrine in dogs: an inhibitor of silicosis.* Ecotoxicol Environ Saf, 1982. **6**(6): p. 528-34.
209. Penny, C.J., et al., *Mining of Ebola virus entry inhibitors identifies approved drugs as two-pore channel pore blockers.* Biochim Biophys Acta Mol Cell Res, 2019. **1866**(7): p. 1151-1161.
210. Tong, B.C.-K., et al., *Tetrandrine ameliorates cognitive deficits and mitigates tau aggregation in cell and animal models of tauopathies.* Journal of Biomedical Science, 2022. **29**(1): p. 85.
211. Scotto Rosato, A., et al., *TPC2 rescues lysosomal storage in mucolipidosis type IV, Niemann–Pick type C1, and Batten disease.* EMBO Molecular Medicine, 2022. **14**(9): p. e15377.
212. Lei, G., et al., *The role of ferroptosis in ionizing radiation-induced cell death and tumor suppression.* Cell Research, 2020. **30**(2): p. 146-162.
213. Ye, L.F., et al., *Radiation-Induced Lipid Peroxidation Triggers Ferroptosis and Synergizes with Ferroptosis Inducers.* ACS Chem Biol, 2020. **15**(2): p. 469-484.

8 Appendix

8.1 Supplementary Figures

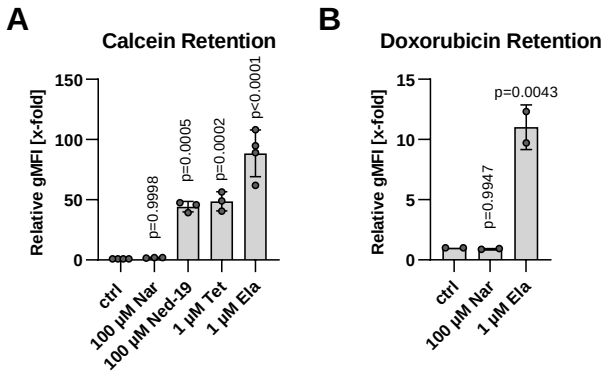

Supplementary Figure S1. P-gp inhibition by TPC2 inhibitors.
The potency of naringenin (Nar), Ned-19 or tetrandrine (Tet) to block P-gp activity in VCR-R CEM TPC2 wt cells was assessed by analyzing P-gp mediated efflux of calcein-AM (**A**) or doxorubicin (**B**). Elacridar (Ela) served as positive control. Data are presented as mean ± SD from three (**A**) or two (**B**) independent experiments. Statistical significance was analyzed by one-way ANOVA with Dunnett's posttest (**A**, **B**).

A

Sample	Type	Subtype	Karyotype/molecular alterations	Disease stage	Age group
ALL-53	ALL	B-ALL	n.d.	relapse	pediatric
ALL-233	ALL	B-ALL	NUTM1 fusions	initial diagnosis	pediatric
ALL-502	ALL	B-ALL	DUX4 fusions	relapse	pediatric
ALL-677	ALL	B-ALL	ZNF846-CRLF2 (Ph like)	unknown	pediatric
ALL-994	ALL	T-ALL	n.d.	relapse	adult
ALL-1124	ALL	B-ALL	complex	initial diagnosis	pediatric

B

Comparison	p-value (PDX)	p-value (PBMC)
ctrl vs. 1 µM Tet	0.9824	>0.9999
ctrl vs. 5 µM Tet	0.2046	0.9418
5 nM VCR vs. 5 nM VCR + 1 µM Tet	0.9976	0.9996
5 nM VCR vs. 5 nM VCR + 5 µM Tet	0.0022	0.8945
10 nM VCR vs. 5 nM VCR + 1 µM Tet	0.9874	0.9999
10 nM VCR vs. 5 nM VCR + 5 µM Tet	<0.0001	0.6564
50 nM VCR vs. 5 nM VCR + 1 µM Tet	0.9808	0.9995
50 nM VCR vs. 5 nM VCR + 5 µM Tet	<0.0001	0.7597

Comparison (PDX vs. PBMC)	p-value
1 µM Tet	0.9667
5 µM Tet	0.8632
5 nM VCR	0.8375
5 nM VCR + 1 µM Tet	0.7916
5 nM VCR + 5 µM Tet	0.0049
10 nM VCR	0.3517
10 nM VCR + 1 µM Tet	0.1917
10 nM VCR + 5 µM Tet	<0.0001
50 nM VCR	<0.0001
50 nM VCR + 1 µM Tet	<0.0001
50 nM VCR + 5 µM Tet	<0.0001

Supplementary Figure S2. Characteristics of PDX ALL cells and expanded statistics corresponding to Figure 12 A. (Figure legend on next page)

Supplementary Figure S2. Characteristics of PDX ALL cells and expanded statistics corresponding to Figure 12 A.
A Information on PDX ALL cells used in this study. **B** Statistical analysis corresponding to Figure 12 A. Statistical significance was analyzed by two-way ANOVA with Sidak's posttest. The left table shows statistical comparisons between different conditions in the group of PDX cells (middle column) and PBMCs (right column). The right table shows statistical comparisons between PDX cells and PBMCs with the same conditions.

A

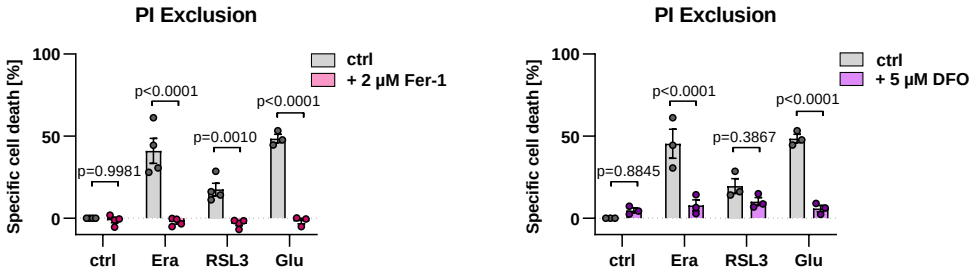

B

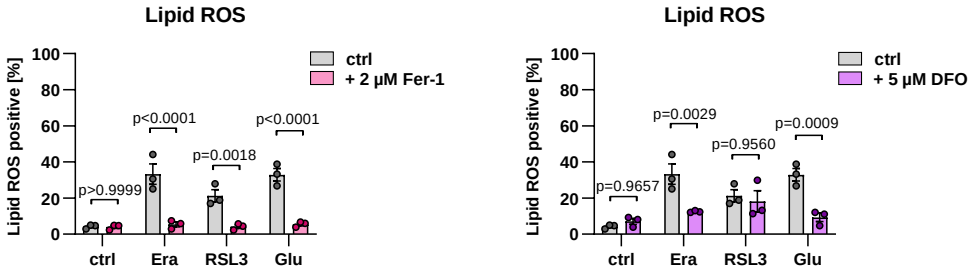

Supplementary Figure S3. Confirmation of ferroptotic cell death upon treatment with erastin, RSL3 and glutamate.
A, **B** RIL175 wt cells were treated with ferroptosis inducers alone or in combination with ferrostatin-1 (Fer-1) or deferoxamine (DFO). **A** Specific cell death was quantified by propidium iodide staining and flow cytometry. **B** Lipid ROS were quantified by C11 Bodipy 581/591 staining and flow cytometry. Data are presented as mean ± SD from three independent experiments. Statistical significance was analyzed by two-way ANOVA with Sidak's posttest (**A**, **B**).

8.2 Abbreviations

Abbreviation	Term
(t)Bid	(truncated) BH3 interacting domain death agonist
4-PBA	4-phenylbutyric acid
5-FU	5-fluorouracil
ABCB1	ATP binding cassette subfamily B member 1
ACSL4	Acyl-CoA synthetase long chain family member 4
ALL	Acute lymphoblastic leukemia
ALOX5	Arachidonate 5-lipoxygenase
ALS	Amyotrophic lateral sclerosis
AM	Acetoxymethyl ester
ANOVA	Analysis of variance
Apaf-1	Apoptotic peptidase activating factor 1
APS	Ammonium persulfate
ASAH1	N-acylsphingosine amidohydrolase/acid ceramidase
ASK1	Apoptosis signaling regulating kinase 1
ASMase	Acid sphingomyelinase
ATF4/6	Activating transcription factor 4/6
ATM	Ataxia telangiectasia mutated
ATP6V0C	ATPase H+ transporting V0 subunit c
AUC	Area under the curve
Bcl-2	B-cell lymphoma 2
Bcl-xL	B-cell lymphoma-extra large
BiP/GRP178	Binding immunoglobulin protein/ 78 kDa glucose-regulated protein
BMAA	Beta-N-methylamino-L-alanine
BSA	Bovine serum albumin
c	Concentration
CCCP	Carbonyl cyanide *m*-chlorophenyl hydrazone
cDNA	Complementary DNA
CLEAR	Coordinated lysosomal expression and regulation
CQ	Chloroquine
CRISPR	Clustered regularly interspaced short palindromic repeats
CRLF2	Cytokine receptor like factor 2
CTSB/D	Cathepsin B/D
DFO	Deferoxamine

DMEM	Dulbecco’s modified eagle medium
DMPE	1,2-dimyristoyl-sn-glycero-3-phosphoethanolamine
DMSO	Dimethyl sulfoxide
DMT1	Divalent metal transporter 1
DNA	Deoxyribonucleic acid
DTT	Dithiothreitol
DUX4	Double homeobox 4
DXR	Doxorubicin
EC50	Half-maximal effective concentration
ECL	Enhanced chemiluminescence
EDME	17β-estradiol methyl ester
EDTA	ethylenediaminetetraacetic acid
EGF(R)	Epidermal growth factor (receptor)
eIF2alpha	Eucaryotic translation initiation factor 2 alpha
Ela	Elacridar
ER	Endoplasmic reticulum
Era	Erastin
ESI	Electrospray ionization
FCS	Fetal calf serum
Fer-1	Ferrostatin-1
FITC	Fluorescein isothiocyanate
FRAP	Fluorescence recovery after photobleaching
FSC	Forward scatter
FTH1	Ferritin heavy chain 1
FTL1	Ferritin light chain 1
GCLC	Glutamate-cysteine ligase catalytic subunit
GCLM	Glutamate-cysteine ligase modifier subunit
Glu	Glutamate
gMFI	Geometric mean fluorescence intensity
GPX4	Glutathione peroxidase 4
GSH	Glutathione
GSSG	Oxidized glutathione
h	Human
HBSS	Hank’s balanced salt solution
HCC	Hepatocellular carcinoma
HRP	Horseradish peroxidase

Hsp70	Heat shock protein 70
HyD	Hybrid detector
IC50	Half-maximal inhibitory concentration
Keto	Ketoconazole
ko	Knockout
LAMP1/2	Lysosome-associated membrane protein ½
LCD	Lysosomal cell death
LLOMe	L-leucyl-L-leucine methyl ester
LPCAT3	Lysophosphatidylcholine acyltransferase
LPL	Lysophospholipids
LRRK2	Leucine rich repeat kinase 2
m	Murine
Me	Methyl ester
MITF	Melanocyte inducing transcription factor
MiT-TFE	Microphthalmia family of transcription factors
mRNA	Messenger RNA
mTORC1	Mammalian target of rapamycin complex 1
MTT	3-(4,5-dimethylthiazol-2-yl)-2,5-dephinyltetrazolium bromide
MUFA	Monounsaturated fatty acid
n.d.	Not determined
NAADP	Nicotinic acid adenine dinucleotide phosphate
NAD^+/NADH	Nicotinamide adenine dinucleotide
$NADP^+$/NADPH	Nicotinamide adenine dinucleotide phosphate
Nar	Naringenin
NCOA4	Nuclear receptor coactivator 4
NEM	N-Ethylmaleimide
NPC1	Niemann-Pick C1 protein
NUTM1	NUT midline carcinoma family member 1
p	phospho
P/S	Penicillin/streptomycin
PAGE	Polyacrylamide gel electrophoresis
PARP	Poly (ADP-ribose) polymerase
PBMC	Peripheral blood mononuclear cells
PBS	Phosphate-buffered saline
PDX	Patient-derived xenograft
PE	phosphatidylethanolamine

P-gp	P-glycoprotein
Ph	Philadelphia chromosome
PI	Propidium iodide
$PI(3,5)P_2$	Phosphatidylinositol 3,5-bisphosphate
PL	Phospholipid
PMT	Photomultiplier
PTX	Paclitaxel
PUFA	Polyunsaturated fatty acid
PVDF	polyvinylidene difluoride
qPCR	Quantitative polymerase chain reaction
RNA	Ribonucleic acid
ROS	Reactive oxygen species
RPMI	Roswell Park Memorial Institute 1640 medium
RSL3	(1S,3R)-RSL3
RT	Room temperature
SCD1	Stearyl-CoA desaturase 1
SD	Standard deviation
SDS	Sodium dodecyl sulfate
Ser	Serine
SFA	Saturated fatty acid
siRNA	Small interfering RNA
SERCA	Sarcoendoplasmic reticulum calcium ATPase
SLC	Solute Carrier Family
SMPD1	Sphingomyelin phosphodiesterase 1/acid sphingomyelinase
SSC	Sideward scatter
STEAP3	Six-transmembrane epithelial antigen of prostate
T/E	Trypsin/ethylenediaminetetraacetic acid
TCE	2,2,2-Trichloroethanol
TEMED	Tetramethylethylenediamine
Tet	Tetrandrine
TF	Transferrin
TFEB	Transcription factor EB
TfR/TFRC	Transferrin receptor
TG	thapsigargin
TM	Transmembrane
TPC	Two-pore channel

TPT	Topotecan
Tris	Tris(hydroxymethyl)aminomethane
TRPML	Transient receptor potential mucolipin
UPLC-MS/MS	Ultra-performance liquid chromatography tandem mass spectrometry
UPR	Unfolded protein response
VCR	Vincristine
VCR-R	Vincristine-resistant
VDAC	Voltage-dependent anion-selective channel
Vera	Verapamil
WC	Whole cell
wt	Wild type
XBP1 (u)/(s)	X-box binding protein 1 (unspliced)/(spliced)
ZNF846	Zinc finger protein 846

Table 9. Abbreviations list.

8.3 List of own publications and conferences

8.3.1 Publications

a. Geisslinger F, Müller M, Chao YK, Grimm C, Vollmar AM, Bartel K. *Targeting TPC2 sensitizes acute lymphoblastic leukemia cells to chemotherapeutics by impairing lysosomal function.* Cell Death Dis. 2022 Aug 1;13(8):668. doi: 10.1038/s41419-022-05105-z.

b. Keller M, Sauvageot-Witzku K, Geisslinger F, Urban N, Schaefer M, Bartel K, Bracher F. *The ethoxycarbonyl group as both activating and protective group in N-acyl-Pictet-Spengler reactions using methoxystyrenes. A short approach to racemic 1-benzyltetrahydroisoquinoline alkaloids.* Beilstein J Org Chem. 2021 Nov 5;17:2716-2725. doi: 10.3762/bjoc.17.183.

c. Müller M, Gerndt S, Chao YK, Zisis T, Nguyen ONP, Gerwien A, Urban N, Müller C, Gegenfurtner FA, Geisslinger F, Ortler C, Chen CC, Zahler S, Biel M, Schaefer M, Grimm C, Bracher F, Vollmar AM, Bartel K. *Gene editing and synthetically accessible inhibitors reveal role for TPC2 in HCC cell proliferation and tumor growth.* Cell Chem Biol. 2021 Aug 19;28(8):1119-1131.e27. doi: 10.1016/j.chembiol.2021.01.023.

d. von Schirnding C, Giopanou I, Hermawan A, Wehl L, Ntaliarda G, Illes B, Datz S, Geisslinger F, Bartel K, Sommer AK, Lianou M, Weiß V, Feckl J, Vollmar AM, Bräuchle C, Stathopoulos GT, Wagner E, Roidl A, Bein T, Engelke H. *Synergistic Combination of Calcium and Citrate in Mesoporous Nanoparticles Targets Pleural Tumors.* Chem. 2021 Feb 11;7(2):480-494. doi: 10.1016/j.chempr.2020.11.021.

e. Schütz R, Müller M, Geisslinger F, Vollmar A, Bartel K, Bracher F. *Synthesis, biological evaluation and toxicity of novel tetrandrine analogues.* Eur J Med Chem. 2020 Dec 1;207:112810. doi: 10.1016/j.ejmech.2020.112810.

f. Geisslinger F, Müller M, Vollmar AM, Bartel K. *Targeting Lysosomes in Cancer as Promising Strategy to Overcome Chemoresistance-A Mini Review.* Front Oncol. 2020 Jul 9;10:1156. doi: 10.3389/fonc.2020.01156.

g. Geisslinger F, Vollmar AM, Bartel K. *Cancer Patients Have a Higher Risk Regarding COVID-19 - and Vice Versa?* Pharmaceuticals (Basel). 2020 Jul 6;13(7):143. doi: 10.3390/ph13070143.

8.3.2 Conferences

a. **DPhG Annual Meeting 2022, Marburg, Germany (September 2022)**
   Poster: Geisslinger F, Vollmar AM, Bartel K. *Endolysosomal TPC2 and TRPML1 differentially modulate ferroptosis sensitivity in HCC.*
b. **71st Lindau Nobel Laureate Meeting 2022, Lindau, Germany (June and July 2022)**
   Funded by the Bayer Foundation
c. **FOR 2625 symposium: Lysosomes and Autophagy, Berlin, Germany (May 2022)**
   Poster: Geisslinger F, Müller M, Chao YK, Grimm C, Vollmar AM, Bartel K. *Lysosomal Two-Pore Channel 2 as novel target to improve chemotherapy response.*
d. **7th German Pharm-Tox Summit, Digital (March 2022)**
   Oral Presentation: Geisslinger F, Müller M, Vick B, Chao YK, Bracher F, Grimm C, Jeremias I, Vollmar AM, Bartel K. *Manipulating lysosomal function to improve chemotherapy response – Targeting lysosomal Two-Pore Channel 2 as novel strategy*
e. **DPhG Annual Meeting 2021, Digital (September and October 2021)**.
   Poster: Geisslinger F, Müller M, Vick B, Chao YK, Bracher F, Grimm C, Jeremias I, Vollmar AM, Bartel K. *Targeting Two-Pore Channel 2 Sensitizes Leukemia Cells to Chemotherapy.*

8.4 Acknowledgements

Zu allererst möchte ich meiner Doktormutter Frau Prof. Dr. Vollmar danken. Vielen Dank, dass Sie mir ermöglicht haben, nach meiner Bachelorarbeit und Masterarbeit auch meine Dissertation an Ihrem Lehrstuhl anzufertigen. Ich weiß es sehr zu schätzen, dass ich im Rahmen dieser Arbeit eigene Ideen verfolgen und umsetzen konnte. In Kombination mit anregenden Diskussionen und Ihren guten Ratschlägen, vor allem in den regelmäßigen Achievement Meetings, habe ich das immer als gute Mischung für meine wissenschaftliche Entwicklung empfunden. Außerdem bin ich dankbar, dass ich während meiner Doktorandenzeit zahlreiche Konferenzen besuchen durfte, besonders herausstehend meine Teilnahme am Lindau Nobel Laureate Meeting 2022 (vielen Dank auch an die Bayer Foundation für die finanzielle Unterstützung), die ohne Ihre Unterstützung nicht möglich gewesen wäre.

Ebenso danke ich Dr. Karin Bartel für die Betreuung meiner Promotion. Danke Karin für deine Hilfe bei allen möglichen Problemen, für konstruktive Diskussionen und, dass du generell immer mit Rat zur Seite standest.

Mein Dank gilt auch Herrn Prof. Dr. Zahler für die Erstellung des Zweitgutachtens, sowie den weiteren Mitgliedern des Prüfungskomitees Herrn Prof. Dr. Wagner, Frau Prof. Dr. Merkel, Frau Prof. Dr. Koch und Herrn Prof. Dr. Frieß.

Außerdem möchte ich bei den Kooperationspartnern bedanken: Ich danke Dr. Yu-Kai Chao und Prof. Dr. Dr. Grimm für das Durchführen der Patch-Clamp-Experimente, Dr. Binje Vick und Prof. Dr. Irmela Jeremias für die Bereitstellung der PDX Zellen, Finja Witt und Prof. Dr. Andreas Koeberle für die Lipid-Messungen, sowie Prof. Dr. Franz Bracher, Dr. Marco Keller und Dr. Ramona Schütz für erfolgreiche, gemeinsame Projekte.

Weiterhin möchte ich mich bei allen aktuellen und ehemaligen Mitarbeitern unseres Arbeitskreises bedanken. Vielen Dank für das freundschaftliche Verhältnis, die gegenseitige Unterstützung bei Problemen und für viele schöne Momente sowohl während der Arbeit als auch außerhalb des Labors. Vielen Dank an Sylvia Schnegg für unzählige Western Blots und Bernadette Grohs für die Unterstützung bei Experimenten. Außerdem danke ich Lina Ouologuem für die hervorragende Arbeit während ihrer Bachelorarbeit im Rahmen meiner Arbeit. 3

Zu guter Letzt möchte ich mich bei meinen Eltern bedanken. Liebe Mama, lieber Papa, vielen Dank für eure bedingungslose, immer da gewesene Unterstützung und eure Hilfe bei Problemen jeglicher Art.